LAWRENCE
LIVERMORE
NATIONAL
LABORATORY

LLNL-JRNL-830603

Theory of Nuclear Fission

N. Schunck, D. Regnier

January 7, 2022

Progress in Particle and Nuclear Physics

Disclaimer

Theory of Nuclear Fission

LLNL-JRNL-830603

Nicolas Schunck*

Nuclear and Chemical Sciences Division, Lawrence Livermore National Laboratory, Livermore, California 94551, USA

David Regnier

CEA, DAM, DIF, 91297 Arpajon, France

Université Paris-Saclay, CEA, Laboratoire Matière en Conditions Extrêmes, 91680 Bruyères-le-Châtel, France

Abstract

Atomic nuclei are quantum many-body systems of protons and neutrons held together by strong nuclear forces. Under the proper conditions, nuclei can break into two (sometimes three) fragments which will subsequently decay by emitting particles. This phenomenon is called nuclear fission. Since different fission events may produce different fragmentations, the end-products of all fissions that occurred in a small chemical sample of matter comprise hundreds of different isotopes, including α particles, together with a large number of emitted neutrons, photons, electrons and antineutrinos. The extraordinary complexity of this process, which happens at length scales of the order of a femtometer, mostly takes less than a femtosecond but is not entirely over until all the lingering β decays have completed – which can take years – is a fascinating window into the physics of atomic nuclei. While fission may be more naturally known in the context of its technological applications, it also plays a crucial role in the synthesis of heavy elements in astrophysical environments. In both cases, simulations are needed for the many systems or energies inaccessible to experiments in the laboratory. In this context, the level of accuracy and precision required poses formidable challenges to nuclear theory. The goal of this article is to provide a comprehensive overview of the theoretical methods employed in the description of nuclear fission.

Keywords: Fission, Fission fragment yields, Cross sections, Prompt fission spectrum, Delayed spectrum, Large-amplitude collective motion, Energy density functional theory, Time-dependent density functional theory

2010 MSC: 00-01, 99-00

Contents

*Corresponding author

Email addresses: schunck1@llnl.gov (Nicolas Schunck), david.regnier@cea.fr (David Regnier)

1. Introduction

?⟨sec:intro⟩?

The first experimental evidence of nuclear fission was obtained in late 1938 by German scientists Hahn and Strassman [1, 2], who observed that "*isotopes of Barium ($Z = 56$) are formed as a consequence of the bombardment of Uranium ($Z = 92$) with neutrons*" [excerpt from [3]]. The first theoretical interpretation of this phenomenon was given shortly thereafter by Meitner and was based on the liquid drop model of the atomic nucleus [3]. Only a few months later, Bohr and Wheeler published the first comprehensive theoretical study of the process [4]. These initial discoveries pertained to what we now call neutron-induced fission; Flerov and Petrzhak separately discovered the spontaneous fission of Uranium isotopes in 1941 [5, 6].

In simple terms, nuclear fission is the process by which a heavy atomic nucleus divides into two (binary) or three (ternary) fragments. Although there is no formal definition for it, the usual consensus is that any nuclide bigger than an α particle ($Z = 2, N = 2$) formed by the breaking up of a heavy nucleus is considered a fission fragment; anything smaller would be considered as particle emission or radioactivity. For a given sample of fissioning material, not all nuclei fission identically: the relative proportion of each isotope is called the **primary fission fragments distribution**. Fission fragments are always in an excited state. Therefore, as soon as they are formed, they undergo a sequence of decays. Initially, this decay proceeds mainly through neutron emission. When the energy of the fragment becomes smaller than the separation energy S_n of a single neutron, photon emission becomes the dominant mode of deexcitation. This initial phase of the decay process is very rapid, of the order of $\tau \lesssim 10^{-13}$s and defines what is called the **prompt particle emission**. Since neutron emission changes the isotopic composition of the sample, it is customary to refer to the distribution of fission fragments after prompt emission as the **independent fission yields**. After neutron and photon emission, many fragments may be unstable against β decay – the conversion of a neutron into a proton with the emission of an electron and antineutrino. Beta decay takes place over time scales ranging from a few picoseconds up to years. Since the daughter nuclei produced in the decay may also be excited, β decay is often followed by photon and sometimes neutron emission. This phase of the decay of the fission fragments is called **delayed emission**. At the end of all emissions, both the isotopic and elemental composition of the sample have changed. The relative proportion of each isotope is encoded in what is called the **cumulative fission product yields** [7]. Figure 1 gives a qualitative representation of the entire process.

From a theoretical perspective, nuclear fission is a striking example of large-amplitude collective motion for a quantum many-body system. In other words, it results, or emerges, from the quantum many-body effects induced by in-medium nuclear forces. The characteristic features of atomic nuclei, e.g., the competition between individual and collective behavior, their self-bound nature and the fact that they are open quantum systems, all play a role in our understanding of the various phases of the fission process. Finally, fission is intrinsically a time-dependent process that eventually populates a huge number of output channels. This short enumeration should already suggest to the informed reader that the theoretical description of nuclear fission poses enormous challenges by itself. In addition, fission plays a major role in understanding the limits of nuclear stability, especially concerning superheavy elements [8, 9, 10, 11, 12, 13, 14, 15, 16, 17, 18, 19]. Partly for this reason, fission is one of the main mechanisms that limits the formation of heavy and superheavy elements in astrophysical environments, especially in the rapid-neutron capture

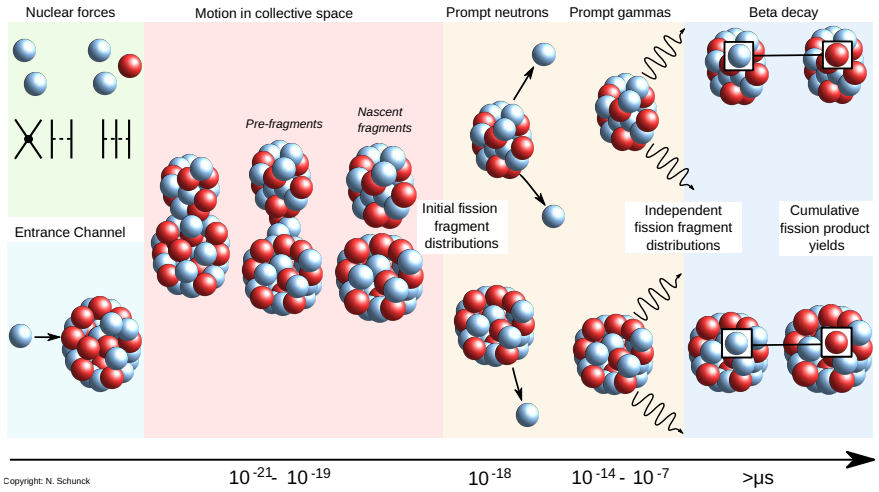

Figure 1: Schematic representation of the fission process. A heavy atomic nucleus, possibly formed in a nuclear reaction, deforms until it divides into two (sometimes three) fragments, thereby releasing a large amount of energy of the order of about 200 MeV for actinide nuclei. The excited fission fragments rapidly emit neutrons followed by photons (prompt fission spectrum). About a few picoseconds after the scission of the original nucleus, many of the resulting fission fragments undergo a sequence of β decays in competition with additional photon and or neutron emission (delayed emission).

⟨fig:schematic⟩

process (r process) [20, 21, 22, 23]. Last but not least, the fission mechanism is at the heart of nuclear technology. Apart from the standard example of nuclear energy [24, 25], details of the fission process are also important for nuclear forensics [26] and international non-proliferation efforts and safeguards by the international community. Knowledge about the physics of the fission process is summarized in evaluated nuclear data libraries such as JEFF [27] and ENDF [28], which list the cross sections of a large range of nuclear reactions along with the fission yields, or ENSDF [29], which is more oriented toward nuclear structure data.

Whether one is interested in the fundamental description of fission or its applications in other scientific or technological disciplines, the recent years have brought many interesting developments. The rapid and sustained increase in computational capabilities has rejuvenated fission theory by enabling simultaneously realistic large-scale simulations of fission properties [22, 30] and more fundamental descriptions of the process [31, 32]. Figure 2 schematically illustrates the chronology of various theoretical methods that will be discussed in this review as well as their approximate computational cost in million core hours. Many of these most recent results and methods are not yet employed to build nuclear data libraries, which – as far as fission is concerned – often rely on very phenomenological models and concepts from the 1950's or 1960's. At the same time, the quality and robustness of these libraries keeps improving partly thanks to the introduction of novel techniques from artificial intelligence and machine learning to evaluate and verify nuclear data [33, 34, 35].

Surprisingly there are only a few textbooks providing a comprehensive introduction to nuclear fission, especially fission theory, and they are just a few years old [36, 37, 38]. In the past five years, three review articles have been published covering either microscopic methods [31], experimental results [39] or phenomenology [40], while the

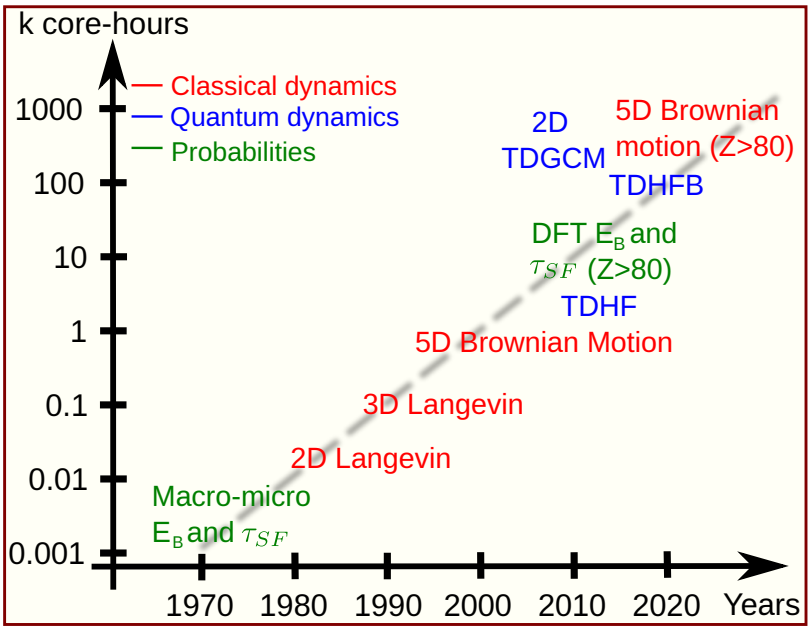

Figure 2: Approximate computational cost in thousand core-hours (k core-hours) of various theoretical methods as a function of the date they became standard in realistic simulations. The notation 2D, 3D or 5D refer to the number of collective variables; the notation $Z > 80$ refers to calculations performed for all nuclei with $Z > 80$.

⟨fig:flops⟩

recent whitepaper [32] offers a consensual view of the major challenges and expected future developments related to fission theory. While these papers have provided a welcome update of recent results, their focus is mostly on the chain of events leading to the divide of the nucleus and not so much on the probability that this process takes place nor on the decay of the fragments, even though nearly all experimental information on fission is collected, directly or indirectly, during this decay phase. We also feel that there is a disconnect between the basic nuclear science community, the goal of which is to understand the basic mechanisms at play in fission, and the specialized user communities where fission data is employed. For example, the producers and users of global nuclear data libraries may not always be aware of the most recent developments in nuclear theory that could impact the evaluation process; conversely, nuclear scientists may not always be aware of the possible impact of their work nor of the constraints (especially in terms of precision) imposed by applications. The goal of this review is to try to provide an overview of fission theory that could be beneficial to both types of communities.

Our presentation is organized to follow the chronology of the fission process. Following Bohr [4, 41, 42], one still thinks of fission as a deformation process. In Section 2, we will therefore discuss in details how the qualitative concept of deformation emerges from the nuclear mean field theory, and how fission fragments are mapped to specific, deformed configurations of the fissioning nucleus at the point of scission. This section has some overlap with [31], but it is necessary to introduce some very basic concepts that will be used throughout this review. Section 3 deals with the probability that fission occurs. In the case of spontaneous fission, this probability is in fact the main quantity that must be computed to determine the fission half-life; in induced fission, it is related to the very challenging problem of computing the fission cross section, namely the probability (per unit area) that fission takes place relatively to

other possible mode of decay such as neutron scattering, evaporation, photoemission, etc. The mechanisms by which the nucleus will change its deformation and reach the point of scission are described in Section 4. In the past two or three decades, this is perhaps the area where the most progress has been made. The static models of fission en vogue from the 1950's to the 1990's have been replaced by explicit time-dependent descriptions, either semi-classical or full quantum-mechanical. As mentioned earlier, the decay of fission fragments has been seldom addressed in a review. It will be presented in Section 5. This decay leads to the emission of neutrons and photons and to a series of β decays. Some fundamental problems in basic science such as the role of fission in nucleosynthesis mechanisms [43, 44, 45, 23, 46, 47] or what has been dubbed the antineutrino reactor anomaly [48, 49, 50, 51, 52, 53, 54, 55] cannot be properly understood without invoking fission fragment deexcitation. Finally, Section 6 will review some of the most recent attempts at predicting the properties of the primary fission fragments after the point of scission with microscopic methods. By connecting the physics of large amplitude collective motion with the statistical decay of the fragments, these efforts offer the prospect of building a consistent and comprehensive theory of fission in the near future. Figure 3 illustrates the chronology of the many theoretical approaches discussed in this review.

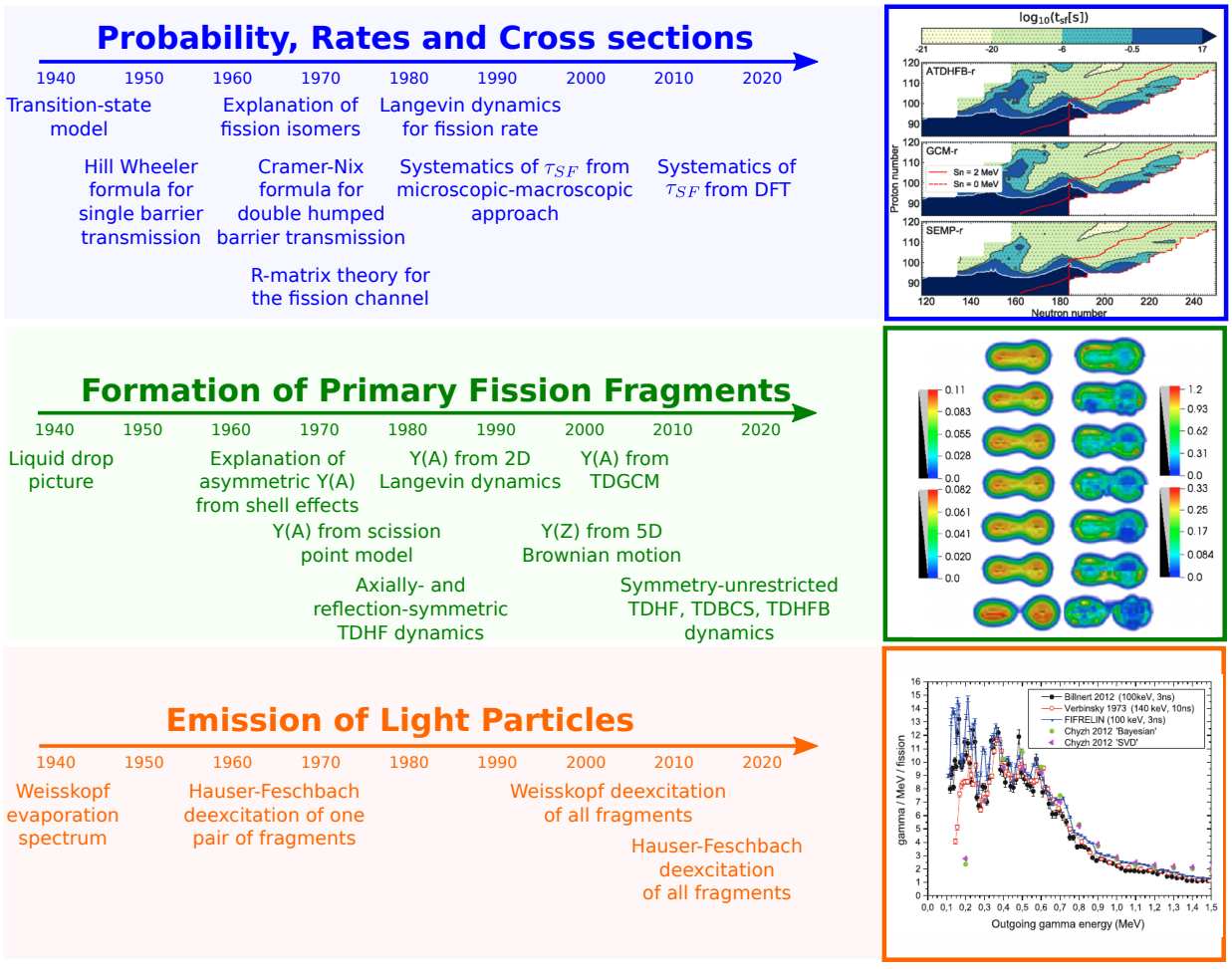

Figure 3: Schematic representation of some of the most noticeable developments in fission theory as a function of time, which this review will discuss in more details. Right hand side figures reproduced with permission from [22, 56, 57].

⟨fig:history⟩

2. Nuclear Deformation

ec:deformation⟩

The concept of nuclear deformation is a phenomenological one. The nuclear Hamiltonian $\hat{H}$ that determines, in principle, all nuclear properties, is rotationally invariant [58, 59]. Theories that attempt to solve directly the many-body Schrödinger equation, such as the no-core shell model [60] or the nuclear shell model [61] never need consider deformation: the eigenvectors of $\hat{H}$ are always rotationally-invariant. This observation also applies to the other types of many-body methods that give approximations to the true eigenvectors of $\hat{H}$ [62, 63, 64].

However, it was discovered already in the 1950's that one could describe, qualitatively and quantitatively, many important nuclear properties such as, e.g., the value of nuclear quadrupole moments, the strength of electromagnetic transitions between excited states or the particular distribution of discrete energy levels, by invoking collective behaviors associated with a deformed average nuclear potential in which nucleons move independently [65, 66, 67]. While originally introduced in a phenomenological manner, the concept of deformation can be formalized as a spontaneous symmetry breaking of the nuclear mean field: the average potential is not invariant under rotation [68]. Deformation is a very pervasive concept in fission theory. Potential energy surfaces, i.e., the potential energy as a function of nuclear deformation, determine fission paths and the large-amplitude dynamics of the nucleus. The number of particles in fission fragments is typically mapped onto the deformation of the fissioning nucleus at the point of scission. The overlap, in the quantum mechanical sense, between the nuclear wave functions at different deformations is directly related to the calculation of fission probabilities. For these reasons, models to compute deformed nuclei are the cornerstones of any fission theory.

Before the 1980's, such models were based on phenomenological mean-field approaches, where the average nuclear potential is parametrized directly with an appropriate mathematical function. Examples of such phenomenological potentials include the Nilsson, Woods-Saxon, and Folded-Yukawa potentials. Within this framework, some of the most comprehensive studies of fission were reported already in the 1970's [69, 70]. In recent years, this phenomenology has also been used to provide large-scale, systematic surveys of nuclear properties [71, 72, 73, 74, 75]. We briefly review this approach in Section 2.1. Nuclear energy density functional theory provides a more fundamental description of nuclear deformation, since it basically relates the average potential to an energy density functional or an effective pseudo-potential that describes effective interactions between nucleons [68]. The theory can be viewed as a (considerable) extension of the self-consistent Hartree-Fock theory [76, 77, 78] and is inspired in part by the density functional theory of electrons in atoms [79]. As mentioned above, nuclear deformation emerges when the density of particles breaks some of the symmetries of the nuclear Hamiltonian [80]. While computationally more involved, the advantage of EDF methods is that they provide (effective) Hamiltonians and an arsenal of many-body techniques to compute quantum numbers. While there were pioneering applications of EDF to fission in the 1970's [81, 82], it is fair to say that self-consistent calculations of fission properties contained too many approximations until the late 1980's and 1990's. In the past two decades, these methods have now become really competitive with more phenomenological ones thanks to advances in computing capabilities [31]. We will summarize the most relevant notions of the EDF approach in Section 2.2. Finally, we will discuss in Section 2.3 how to infer from potential energy surfaces the points at which the nucleus breaks into two fragments.

2.1. *Phenomenological Nuclear Mean Field*

⟨subsec:micmac⟩

What is known as the macroscopic-microscopic approach to nuclear structure is at the heart of nuclear phenomenology. It relies on modeling the atomic nucleus as a classical, charged liquid drop with additional corrective terms that account for quantum many-body effects. In the language of modern many-body theory, one would call such an approach a 0-body theory with corrective terms of 1- and 2-body origin. In this picture, fission is the extreme distortion of the droplet that leads to its breakup. In more details, the total energy of the atomic nucleus is written as the sum of several contributions: (i) the macroscopic energy $E_{\rm mac}(\boldsymbol{q})$, typically represented by the liquid drop or droplet model, (ii) a shell correction $\delta E_{\rm shell}(\boldsymbol{q})$ originating from the single-particle degrees of freedom and (iii) a pairing correction $\delta E_{\rm pair}(\boldsymbol{q})$ to account for nuclear superfluidity. Each of these three terms parametrically depends on the underlying deformation $\boldsymbol{q} = (q_1, \cdots, q_N)$ of the nuclear shape,

$$E(\boldsymbol{q}) = E_{\rm mac}(\boldsymbol{q}) + \delta E_{\rm shell}(\boldsymbol{q}) + \delta E_{\rm pair}(\boldsymbol{q}) \tag{1}$$ eq:micmac

The leading term in this expression is the macroscopic energy which is computed as the energy of a charge drop of nuclear matter in the liquid drop model (LDM). This finite piece of nuclear matter can also be expressed as a series of powers of Z and A – the lepdotermous expansion [83, 84] – and be related to predictions from more microscopic theories [85, 86, 87]. Initial parameterizations of the liquid drop were relatively simple [88]; more recent models have included additional terms to mock up various effects (charge asymmetry, odd-even effect of pairing, proton form factors, etc.) that vary smoothly with Z and N [71, 72, 75]. In the 1940's, the LDM provided the theoretical basis for the first explanation of fission by Meitner, Bohr and Wheeler [3, 4]. The stability of a liquid drop against fission is captured in the dimensionless fissility parameter x, which is the ratio of the Coulomb to the surface energy of the drop [4, 41]. Empirically, the fissility parameter can be approximated as

$$x \approx \frac{Z^2}{47A(1-\eta I^2)}, \tag{2}$$?eq:fissility?

with $I = (N-Z)/A$ and $\eta = -a_{\rm ssym}/a_{\rm surf}$ is the ratio of the surface-symmetry to surface coefficients of the leptodermous expansion of the nuclear energy. These two terms are proportional to $I^2A^{2/3}$ and $A^{2/3}$, respectively. They can be either fitted to reproduce average properties of nuclei [83], or computed from a model of nuclear matter.

Even if the macroscopic energy represents nearly 99% of the total binding of a heavy atomic nucleus such as an actinide, corrective terms must be added to obtain a more precise estimate of the total energy. The shell correction effectively simulates the fact that neutrons and protons are quantum-mechanical particles occupying single-particle levels, the distribution of which impacts the stability of the nucleus, hence its binding energy [89, 90]. Generically, it reads

$$\delta E = \sum_{k\in\mathcal{S}} e_k - \left\langle \sum_{k\in\mathcal{S}} e_k \right\rangle \tag{3}$$ {?}

where $\mathcal{E} = \{e_k\}_{k=1,\ldots,p}$ refers to a full set of single-particle (s.p.) energies and $\mathcal{S}$ is a subset of $\mathcal{E}$. To extract the energy for the lowest configuration at deformation $\boldsymbol{q}$, $\mathcal{S}$ would simply contain the Z and N lowest energies; any other combination of s.p. levels would yield the energy of an excited state. The symbol $\langle\cdots\rangle$ refers to the Strutinsky averaging procedure to produce the "smooth" energy. Full details about how to compute this term are given

in [70]; variants of the standard Strutinsky procedure to remove the spurious effect of continuum or pairing effects are discussed in [91, 92, 93, 94]. The introduction of the shell correction was key to explain two major features of the fission process: (i) the energy threshold at which fission takes place is nearly constant for actinides, contrary to LDM predictions; (ii) the LDM cannot account for the existence of fission isomers [95, 96]. These meta-stable states are more deformed than the ground state thanks to the stabilizing effect of the shell correction.

The shell correction can be interpreted as having a one-body origin: it is associated with an independent-particle model of the nucleus, where each nucleon moves, independently of one another, in the average mean field. In the language of second quantization, the resulting Hamiltonian operator only contains one-body operators. To describe the different energy spectra between even-even and odd nuclei, pairing correlations must be taken into account explicitly; see [97] for a comprehensive introduction to nuclear pairing. The effect of pairing on the total energy was first quantified by introducing a pairing correction $\delta E_{\rm pair}$ akin to the shell correction. In most applications of the macroscopic-microscopic model, this pairing correction is computed from the BCS solution and can thus be interpreted as a corrective term of two-body origin. All three terms of (1) can be modified to describe nuclei at finite angular momentum or finite temperature [98, 99, 100, 101, 102, 103, 104, 105]; see also the textbook [106].

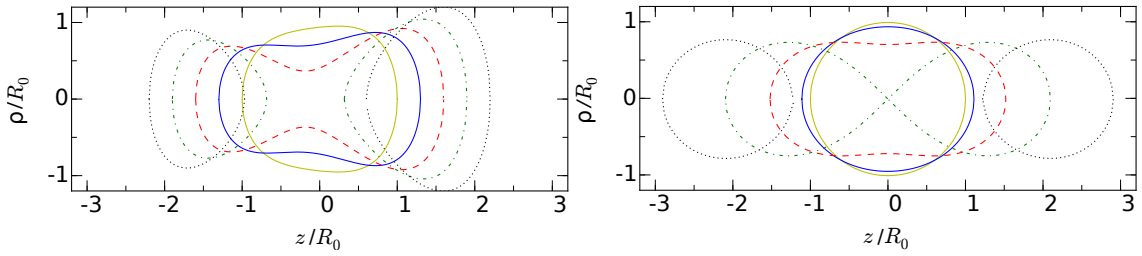

Figure 4: Left: Funny Hills parameterization [69] of the nuclear shape for $(h, \alpha) = (0.2, 0.3)$ with c varying from 1.0 to 2.2 by steps of 0.3. Right: Axial shapes with the Cassini oval parameterization [107] for $u = 0.0, 0.4, 0.8, 1.0, 1.2$. The value $u = 0$ corresponds to the sphere, the value $u = 1.0$ to the point of scission and the value $u = 1.2$ to separated fragments. Figures reproduced with permission from [31] courtesy of Schunck; copyright 2016 by Institute of Physics.

⟨fig:shapes⟩

All terms in the decomposition (1) of the total energy depend on the deformation of the nuclear shape which, in this approach, is an *input* to the calculation. The determination of a suitable parameterization of the nuclear shape is in fact a challenging problem. Given a parameterization $\mathcal{P}$ and a set of shape parameters $\boldsymbol{q} = (q_1, \cdots, q_N)$, the following criteria should be met: (i) there should be a one-to-one correspondence between any vector $\boldsymbol{q}$ and the actual shape; (ii) since the shape parameterization is an input to any calculation, the number N of components of $\boldsymbol{q}$, i.e., the number of shape parameters, should be as small as possible (iii) the parameterization must be capable of describing weakly-deformed, compact shapes, extremely elongated shapes and even disjoint shapes representing the separated fragments. The standard multipole expansion of the nuclear radius [108], for example, does not meet any of these criteria: it is not bijective [109, 110], the number of parameters needed to describe well-deformed shapes increases with deformation, and it cannot characterize separated fragments. Parametrizations more adapted to describing fission include the Funny-Hills parameterization [69], the Los Alamos parameterization [42], Cassini ovals [107], Fourier series [111] or Legendre polynomials [112]; see also [31] for an explicit summary of some of these parameterizations.

Figure 4 shows an example of the Funny Hills and Cassini ovals parameterization.

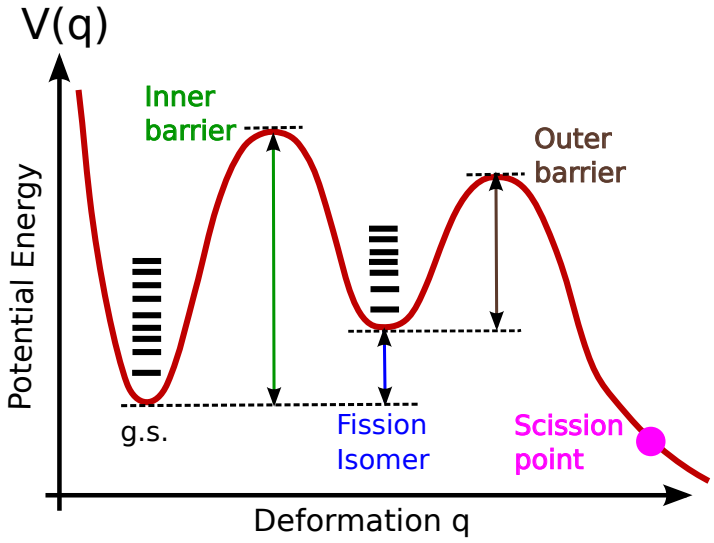

Figure 5: One-dimensional representation of fission barriers in actinide nuclei. Note that the scission point is not represented at scale: in practice, it is "far" from the outer barrier. The distance in the deformation space between the location of the scission point and that of the fission isomer may be four to five times larger than the distance between the fission isomer and the ground state.

iers_actinides⟩

This nuclear phenomenology based on the macroscopic-microscopic model has been extremely successful in predicting many facets of nuclear properties [71, 72, 73, 75, 104, 113]. In the context of fission, this approach provides a computationally efficient, realistic method to perform large-scale calculations of deformation properties, namely **potential energy surfaces (PES)**. In many actinides, there is empirical evidence that the PES require several deformation degrees of freedom to adequately capture the full dynamics of fission: elongation of the whole nucleus, reflection asymmetry of the shape, triaxiality parameters, but also deformation parameters characterizing the fragments themselves [114]. Investigations performed in the 2010's emphasize the importance of reflection asymmetric shapes of the fragments, which would require at least another two parameters to describe the shape asymmetry for each fragment [115, 116]. Such multi-dimensional PES cannot be visualized, but a lot of important information can be extracted by projecting them onto a one-dimensional subspace of lowest energy: the **fission path**. In actinide nuclei, this fission path is typically characterized by a deformed potential minimum (i.e. the classical ground state) and an additional, meta-stable minimum at larger deformations: the **fission isomer**. Both minima are separated by potential energy **barriers**: the inner barrier, between the ground state and the fission isomer, and the outer barrier, between the fission isomer and regions corresponding to ever larger deformations. Precise calculations of these fission barriers are especially important for estimating spontaneous fission half-lives and fission cross sections, as will be presented in Section 3. Figure 5 shows a typical, schematic representation of the one-dimensional fission path in actinide nuclei. In such one-dimensional representations, the **saddle point** is simply the point on the fission path that has the highest energy (here: the top of the inner barrier).

In the 1970's, the prediction of fission isomeric states and "double-humped" fission barriers was a major success of

the macroscopic-microscopic approach [69, 70, 117, 118], as was the explanation of asymmetric fission by reflection-asymmetric shapes stabilized by the shell correction [107]. Refinements in the models combined with modern computational capabilities have led to global predictions of static fission barriers [119, 120, 121, 122, 123, 124, 125]. Such calculations are necessary, since as we go away from the valley of stability, the topology of the potential energy surfaces may change quite dramatically and the traditional features of fission barriers in actinides may not apply anymore. Figure 6 shows a systematics of fission barrier heights (more precisely, the highest fission barrier) in heavy and superheavy nuclei taken from [22]. It is clear from these results that uncertainties from nuclear models alone can reach a few MeV, which corresponds to dozens of orders of magnitude in spontaneous fission half-lives; see Section 3.1.

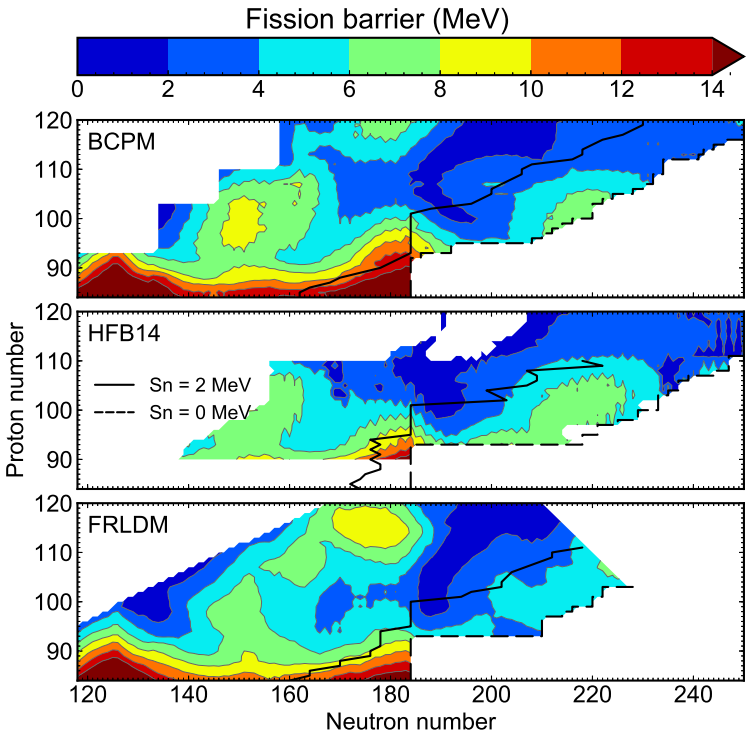

Figure 6: Highest fission barrier heights for heavy and superheavy elements with $84 \leq Z \leq 120$ and $118 \leq N \leq 250$ for three different models of nuclear deformation: FRLDM corresponds to the macroscopic-microscopic calculation of [120] while the BPCM [126] and HFB14 [127] are two different versions of energy density functionals; see discussion in Section 2.2. Figures reproduced with permission from [22] courtesy of Giuliani; copyright 2018 by The American Physical Society.

⟨fig:barriers⟩

2.2. *Energy Density Functional Theory*

⟨subsec:EDF⟩

The EDF approach is the modern name for what was known for a long time as the self-consistent mean field theory. Its root can be found both in the generalized Hartree-Fock theory, which was formalized in a few seminal papers in the early 1960's [128, 129], as well as in the density functional theory for electrons [79, 130]. In a nutshell, the basic idea of the EDF approach is to compute the nuclear mean field from a suitable model of nuclear forces among nucleons rather than parameterizing it as in the macroscopic-microscopic approach. In practice, this calculation is often based on a model for in-medium, two-body effective nuclear interactions (or pseudo-potentials) such as the Skyrme [131]

or Gogny [132] force. When computing the expectation value of such pseudo-potentials on a many-body product state of single-particle wave functions (Slater determinant), both the resulting energy and the nuclear mean field become functionals of the density of particles [133]. Direct parameterizations of the energy density have also been proposed, with varying success [134, 135, 136, 126, 137]. Note that the effective potentials need not be restricted to two-body terms only: three- and higher-order many-body interactions could be included as well [138, 139]. The EDF approach comprises a full hierarchy of approximations and methods yielding increasing accuracy and precision in the determination of nuclear properties. One may consider two main categories: single-reference energy density functional (SR-EDF) and multi-reference energy density functional (MR-EDF). Both types are used mostly to compute static properties of the nucleus but could also be implemented in a time-dependent formalism. The EDF approach has a decade-old rich history and it would go far beyond the scope of this review to describe it in too many details. We refer the interested reader to [68, 133, 140, 141, 142, 143, 144]. Below, we will only summarize the essential concepts and formulas most relevant to fission theory.

2.2.1. *Single-Reference Energy Density Functional Theory: Self-Consistent Mean Field*

subsec:SR-EDF⟩?

Today, the single-reference EDF approach is largely built on the Hartree-Fock-Bogoliubov (HFB) theory, where the nuclear many-body wave function is approximated by a generalized product of quasiparticle wave functions [133, 59, 68]. In the formalism of second quantization, these quasiparticles (q.p.) are associated with annihilation and creation operators $(\beta_\mu, \beta_\mu^\dagger)$ and the many-body wave function reads

$$|\Phi\rangle = \prod_\mu \beta_\mu \, |0\rangle \,, \tag{4}$$ eq:HFB_ansatz

where $|0\rangle$ is the particle vacuum. The q.p. operators are themselves related to the annihilation and creation operators $(c_k, c_k^\dagger)$ of an arbitrary single-particle basis by the Bogoliubov transformation [129]

$$\beta_\mu = \sum_m \left[U_{\mu m}^\dagger \, c_m + V_{\mu m}^\dagger \, c_m^\dagger \right] , \tag{5a}$$ {?}

$$\beta_\mu^\dagger = \sum_m \left[V_{\mu m}^T \, c_m + U_{\mu m}^T \, c_m^\dagger \right] . \tag{5b}$$ {?}

Let us consider an effective two-body pseudo-potential $\hat{V}$ characterized by the matrix elements $v_{ijkl} \equiv \langle ij|\hat{V}|kl\rangle$ in the single-particle basis, with $\bar{v}_{ijkl}$ the anti-symmetrized version of these matrix elements ($\bar{v}_{ijkl} = v_{ijkl} - v_{ijlk}$). The HFB energy reads

$$E[\rho, \kappa, \kappa^*] = \sum_{ij} t_{ij} \rho_{ji} + \frac{1}{2} \sum_{ijkl} \bar{v}_{ijkl} \rho_{lj} \rho_{ki} + \frac{1}{4} \sum_{ijkl} \bar{v}_{ijkl} \kappa_{ij}^* \kappa_{kl} . \tag{6}$$ eq:HFB_energy

where t_{ij} are the matrix elements of the kinetic energy operator, ρ is the one-body density matrix and κ the pairing tensor. These two quantities encode the basic degrees of freedom of the HFB theory. They can be expressed in terms of the matrices of the Bogoliubov transformation as $\rho = V^* V^T$ and $\kappa = V^* U^T$. The main idea of the HFB theory is to minimize the energy (6) with respect to the matrix elements of U and V. This results in the HFB equation

$$\left[\mathcal{H}, \mathcal{R} \right] = 0, \tag{7}$$ eq:HFB_equ

where $\mathcal{H}$ is the HFB matrix and $\mathcal{R}$ the generalized density, respectively given by

$$\mathcal{H} = \begin{pmatrix} h & \Delta \\ -\Delta^* & -h^* \end{pmatrix}, \qquad \mathcal{R} = \begin{pmatrix} \rho & \kappa \\ -\kappa^* & 1-\rho^* \end{pmatrix}. \tag{8}$$

eq:HFB_matrices

In these expressions, $h = t + \Gamma$ is the mean field, t is the single-particle kinetic energy potential and $\Gamma \equiv \Gamma_{ik} = \sum_{jl} \bar{v}_{ijkl}\rho_{lj}$ the mean field potential, and $\Delta \equiv \Delta_{ij} = \frac{1}{2}\sum_{kl} \bar{v}_{ijkl}\kappa_{kl}$ is the pairing field. Both objects are functionals of ρ and κ.

Applications of the formalism rely on effective two-body potentials $\hat{V}$ such as the Skyrme or Gogny interactions; see [133, 145, 146] for recent reviews. There is also a relativistic version of the EDF approach based on solving a self-consistent Dirac equation [147, 148, 68]. Both non-relativistic and relativistic EDFs depend on a small set of adjustable parameters that must be calibrated on data. In practice, this amounts typically to 10-20 free parameters that are adjusted mostly on some known nuclear masses and radii. The calibration may also be guided and/or constrained by infinite nuclear matter properties and may include phenomenological information about fission barrier heights. The most commonly used parameterizations in fission studies are the SkM* [149] and UNEDF1 [150] Skyrme EDFs, the D1S parameterization of the Gogny force [151], and the DD-PC1 [152], DD-ME2 [153] and DD-K1 [154] parameterizations of relativistic Lagrangians. Pairing correlations are central to the HFB theory. As can be seen from (6), the same effective pseudo-potential $\hat{V}$ should be at the origin of all components of the energy: the particle-hole part proportional to ρ and the particle-particle one proportional to κ. This requirement is enforced only in the case of the Gogny force. In practice, users of the Skyrme and relativistic EDFs adopt a different effective potential in the pairing channel based, e.g., on simple density-dependent forces [155], separable finite-range interactions [156], or even non-empirical pairing forces built out of chiral effective field theory [157, 158, 159]. Such choices are largely motivated by pragmatic reasons such as the divergences induced by zero-range effective potentials, which require a regularization procedure [160, 161] or/and the difficulty in efficiently probing the pairing channel when fitting the parameters of the EDF [68].

The HFB approach works best when the symmetries of the nuclear Hamiltonian are broken. For example, the minimization of the HFB energy may lead to solutions where both densities ρ and κ are not rotationally-invariant. These symmetries are not restricted to spatial ones such as translational and rotational invariance, axial symmetry or reflection symmetry: they also include time-reversal or isospin symmetry [162, 163, 164]. In fact the ansatz (4) by itself breaks a fundamental symmetry of the nuclear Hamiltonian: particle number. Therefore, HFB solutions, strictly speaking, correspond to wave packets of Slater determinants with different particle numbers [59].

The SR-EDF framework based on *deformed* HFB solutions is thus the direct, "microscopic" equivalent of the macroscopic-microscopic approach and can in fact be viewed as its theoretical justification [165]. Qualitatively, the main difference between the two is how the average nuclear potential is determined: it is approximated by a suitable mathematical function in the macroscopic-microscopic approach and computed self-consistently from a model of nuclear forces in the HFB theory. Potential energy surfaces can be constructed by imposing various constraints on the HFB solutions. For example, the expectation value of the multipole moment operators $\hat{Q}_{\lambda\mu}(\boldsymbol{r}) = r^\lambda Y_{\lambda\mu}(\theta,\varphi)$, where

$Y_{\lambda\mu}(\theta,\varphi)$ are the spherical harmonics [166], is given by

$$\langle \hat{Q}_{\lambda\mu} \rangle = \int d^3\boldsymbol{r}\, \hat{Q}_{\lambda\mu}(\boldsymbol{r})\rho(\boldsymbol{r}), \tag{9}$$

eq:multipoles

where $\rho(\boldsymbol{r})$ is the total density of particles. These moments have a straightforward physics interpretation: $\hat{Q}_{20}$ quantifies the degree of elongation of the shape, $\hat{Q}_{30}$ the degree of left-right asymmetry, $\hat{Q}_{40}$ the bulging around the mid-point of the shape, etc.. By solving the HFB equation (7) with constraints on the values $\langle \hat{Q}_{\lambda\mu} \rangle$ as given by (9), we can generate a manifold of HFB solutions representing many different shapes. Figure 7 shows a simple example of such a potential energy surface in the case where only two constraints were imposed on $\langle \hat{Q}_{20} \rangle$ and $\langle \hat{Q}_{30} \rangle$.

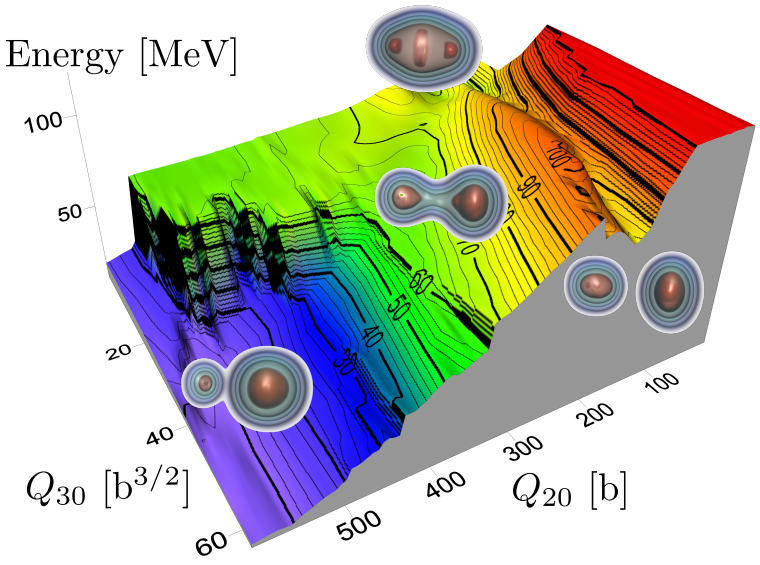

Figure 7: Potential energy surface of ^{240}Pu in the (Q_{20}, Q_{30}) collective space. The four volume renderings give a visual representation of the nuclear shape at various locations on the PES. The calculation was performed for the SkM* parameterization of the Skyrme functional and corresponds to Fig. 3 of [167].

fig:PES_HFB

2.2.2. *Multi-Reference Energy Density Functional Theory: Configuration Mixing*

subsec:MR-EDF

While the SR-EDF approach introduces symmetry-breaking as a means to build more correlations in what would be otherwise a very simplified nuclear wave function, the multi-reference EDF ansatz takes these deformed solutions and combines them [168]. Schematically, this mixing takes the form

$$|\Psi\rangle = \int d\boldsymbol{q}\, f(\boldsymbol{q})\, |\Phi(\boldsymbol{q})\rangle\,, \tag{10}$$

eq:MREDF_ansat

where $\boldsymbol{q}$ is a generic label for the HFB solutions $|\Phi(\boldsymbol{q})\rangle$ given by (4) and $f(\boldsymbol{q})$ are some weight functions to be determined [169]. This quantum configuration mixing can be used, in particular, to restore all the broken symmetries and therefore recover the quantum numbers that were lost during the symmetry breaking [170]. In this case, the labels $\boldsymbol{q}$ correspond to the parameters of the symmetry group, the basis states $|\Phi(\boldsymbol{q})\rangle$ are typically given by $|\Phi(\boldsymbol{q})\rangle \equiv \hat{R}(\boldsymbol{q})\,|\Phi\rangle$

where $\hat{R}(\boldsymbol{q})$ is the generator of the relevant symmetry group, and $f(\boldsymbol{q})$ is an appropriate weight function. In the simplest case of particle-number projection, which is associated with the $U(1)$ symmetry group, the ansatz (10) thus becomes

$$|\Psi\rangle = \int d\varphi \left(\frac{1}{2\pi} e^{-i\varphi N}\right) e^{i\varphi\hat{N}} |\Phi\rangle = \frac{1}{2\pi} \int_0^{2\pi} d\varphi \, e^{i\varphi(\hat{N}-N)} |\Phi\rangle \,. \tag{11}$$ {?}

The most relevant symmetries for fission include parity [171], particle number [172, 173] and angular momentum [174]. MR-EDF techniques also provide a powerful way to improve the ansatz for the nuclear wave function by adding yet another layer of correlations that could not be captured at the SR-EDF level [175]. One of the most standard techniques of MR-EDF is the generator coordinate method (GCM) [176, 177]. The GCM is especially well adapted to describing collective correlations that involve all nucleonic degrees of freedom and play such a central role in understanding fission. In such a case, the labels $\boldsymbol{q}$ correspond to different values of some constraint operators $\hat{Q}$ and the basis states are the constrained HFB solutions. In fact, GCM-based techniques can be used to extract a purely collective Hamiltonian called the Bohr Hamiltonian that is somewhat reminiscent of a quantized version of the deformed liquid drop, in the sense that it depends on global, collective coordinates that typically represent nuclear deformation [178, 179, 180].

2.3. Scission Configurations and Fission Fragments

ubsec:scission⟩

Qualitatively, the moment when the two fragments just separate and the whole nucleus breaks apart is called the **scission point**. This picture results from the analogy of the fission process with the deformation of a charged liquid drop that overcomes surface tension [3]. Within the macroscopic-microscopic model of Section 2.1, such a naive concept of scission can still make sense: in all the parameterizations of the nuclear shape specifically designed to describe very elongated shapes, there always exists a set of parameter values for which the neck between the two prefragments reduces to a single point – the scission point [42, 107, 181].

One may thus be tempted to simply define scission as the locations on the potential energy surfaces where the two fragments are fully formed and well separated. However, when determining the solutions to the nuclear mean field, whether semi-phenomenologically as in Section 2.1 or self-consistently as in Section 2.2, the obtained wave functions correspond to for the whole nucleus: if only because of the Pauli principle, some of the single-particle wave functions spread over each of the two prefragments. In other words, the system is (heavily) entangled [182]. In fact, it remains entangled even when the two fragments are far apart from one another. These difficulties are compounded by the use of a variational principle (in the EDF approach) or by the naive filling of orbits (in the macroscopic-microscopic approach). For nuclear shapes corresponding to well-separated fragments – such configurations are sometimes called the asymptotic conditions – the total energy computed in both frameworks is, in practice, the one that minimizes the energy of each fragment. As a result, calculations of fission fragments properties for such configurations are highly non-physical: against all experimental evidence, fragments have no excitation energy.

To mitigate these problems, one is thus forced to resort to phenomenological criteria to define scission *before* the nuclear shape truly corresponds to two fragments. The simplest of these criteria involve setting a critical value for the density of particles in the neck region between the prefragments [183] or for the number of particles in that same region

[167]. Random neck rupture models provide an additional layer of refinement to such approaches [184, 185, 186]. Since fission in general, and scission in particular, is the result of a competition between attractive nuclear forces and repulsive Coulomb forces, one may define scission as the point where the nuclear interaction energy between the two prefragments is smaller than the Coulomb repulsion between them [187]. However, as mentioned above, the two prefragments are entangled and the very notion of a nuclear and Coulomb energy for a prefragment is ambiguous at best. In fact, it was shown that such quantities are not invariant under unitary transformations of the whole fissioning nucleus [182]. It is possible to design specific transformations that maximize the localizations of quasiparticles in each prefragment and minimize their interaction energy and, as a consequence, change the definition of scission [167]. More recently, there have been a few attempts to better understand the physics of scission by borrowing from configuration-interaction and reaction theory techniques, the goal being to establish a continuous pathway between pre- and post-scission configurations [188, 189, 190].

From these remarks, it should be clear that there is no unique definition of scission and that predictions of fission fragment properties, including their initial conditions in terms of numbers of particle, excitation energy, spin and parity, are highly model-dependent. This has a significant impact on the modeling of the deexcitation of the fission fragments, which is largely determined by these initial conditions as will be discussed in Section 5. Furthermore, the class of fission models called the scission-point models are based on using the hypothesis of statistical equilibrium at scission to determine fission fragment properties [191, 192]. The predictions of such models are contingent on what definitions of scission they adopt.

3. Probabilities, Rates and Cross Sections

⟨sec:proba⟩

The previous section summarized the various theoretical methods used to compute the properties of deformed atomic nuclei – including the extreme deformations characteristic of the point of scission. This prologue was necessary to introduce the basic concepts of fission theory: deformation (or symmetry breaking), collective space, potential energy surfaces, fission barriers, scission point, etc. The next three sections will build upon these notions to address the three most fundamental problems in fission theory: computing the probability that fission takes place – possibly in competition with other decay modes, characterizing the evolution of the nucleus from a near ground-state configuration to the point of scission and predicting the outcome of the overall process, namely all the particles emitted and the fission products. This section is focused on fission probabilities.

In nuclear physics jargon, fission probabilities are related to what is called the entrance channel, which we can define here as the mechanism that produces the proper conditions for an atomic nucleus (Z, N) to undergo fission. Many of the elements heavier than Lead have in fact a significant probability of undergoing fission simply as a consequence of the large number of protons they contain. The spontaneous fission half-life $\tau_{\rm sf}$ is the key quantity that theorists must compute and compare with experimental measurements. This is in fact very challenging since the experimental values of spontaneous fission half-lives cover about 30 orders of magnitude, from about $\tau_{\rm sf} \approx 4.1\mu$s for ^{250}No to $\tau_{\rm sf} > 14$ billions years for ^{232}Th [36].

The case of induced fission is even more complex. By definition, the fissioning nucleus is formed in a nuclear

reaction involving a projectile, a target and a set of initial conditions: type of incoming particle, beam energy, impact parameter. While neutron-induced and photofission (fission induced by photons) are the most common and most important cases, other scenarii such as β-delayed fission (where fission follows the β decay of an isotope), proton-induced fission or fission in heavy-ion collisions are also important, especially in nucleosynthesis or superheavy science. It is often assumed that fission takes place after the equilibration of all degrees of freedom that follows the reaction, resulting in what is called the compound nucleus [4, 193]. The validity of this approximation depends on how typical fission times compare with the relaxation time of the various degrees of freedom including single-particle, collective vibrations such as the Giant Dipole Resonance (GDR) or neutron emission [194]. Estimates of these various timescales suggest that the notion of a compound nucleus is valid for up to several dozens of MeV of excitation energy [194, 195, 196]. In such cases, the main challenge for nuclear theory becomes describing the exact structure of this compound nucleus. There are also instances where fission takes place before full equilibration. This is the quasifission, that is especially important in heavy ion collisions [197].

3.1. Spontaneous Fission

⟨subsec:sf⟩

As discussed earlier in Section 2.1, fission results from the competition between Coulomb repulsion and surface tension. This mechanism is encoded either directly, in the values of the liquid drop parameters, or indirectly in the parameters of the energy functional, and is best understood as a deformation process. This process itself depends on the variations of the potential energy as a function of the deformation of the nuclear shape – the potential energy surface (PES). If first-year students of quantum mechanics were to look at an example of a one-dimensional PES such as Fig. 5, they would be immediately reminisced of quantum tunneling. Indeed, spontaneous fission is most conveniently described as quantum tunnelling through a (multi-dimensional) potential energy barrier. Qualitatively, the problem thus posed is quite simple: initially, the nucleus is in its ground state. The probability of fission is simply related to the probability of tunneling from this initial condition to a deformed shape outside the barrier. Such a probability is often computed semi-classically with the Wentzel-Kramers-Brillouin (WKB) approximation [198] and it is given by the following formula

$$\tau_{1/2}^{\mathrm{SF}} = \frac{1}{\nu} \exp\left(\frac{2}{\hbar} \int_a^b ds \sqrt{2B(s)(V(s) - E_0)} \right), \tag{12}$$

eq:t_sf

where s is the curvilinear abscissa along the most likely fission path, i.e., the trajectory in the N-dimensional collective space spanned by the collective variables $\boldsymbol{q} = (q_1, \ldots, q_N)$ that minimizes the classical action [36]. The nuclear potential energy along this path is noted $V(s)$ and $B(s)$ is the collective inertia. ν is the number of assaults to the barrier per unit time [69]. The ground-state energy is noted E_0 and the points a and b are referred to as the inner and outer turning points, respectively.

While qualitatively simple, the devil hides in the details. Firstly, in addition to involving the introduction of a set of collective variables $\boldsymbol{q}$, the derivation leading to (12) also relies on an explicit decoupling between these collective variables and the other nuclear degrees of freedom, which expresses the fact that the collective motion is confined within the space spanned by the variables $\boldsymbol{q}$ [199, 200, 201, 202, 180, 144]. As a result, the potential energy cannot be taken directly as either the macroscopic-microscopic potential energy (1) or the HFB energy (6). Instead, these values

are modified by zero-point energy corrections, the specifics of which depend on the nature of the collective variables and of the theoretical framework used to express the decoupling. Most of the time, these zero-point energy corrections are computed with the GCM [177]. Importantly, their values do not only affect the overall potential energy surface $V(\boldsymbol{q})$, but also the initial energy of the nucleus E_0: in principle, the latter should correspond to the lowest eigenstate of the collective Hamiltonian. In practice, most calculations treat the value of E_0 as an adjustable parameter to reproduce existing data.

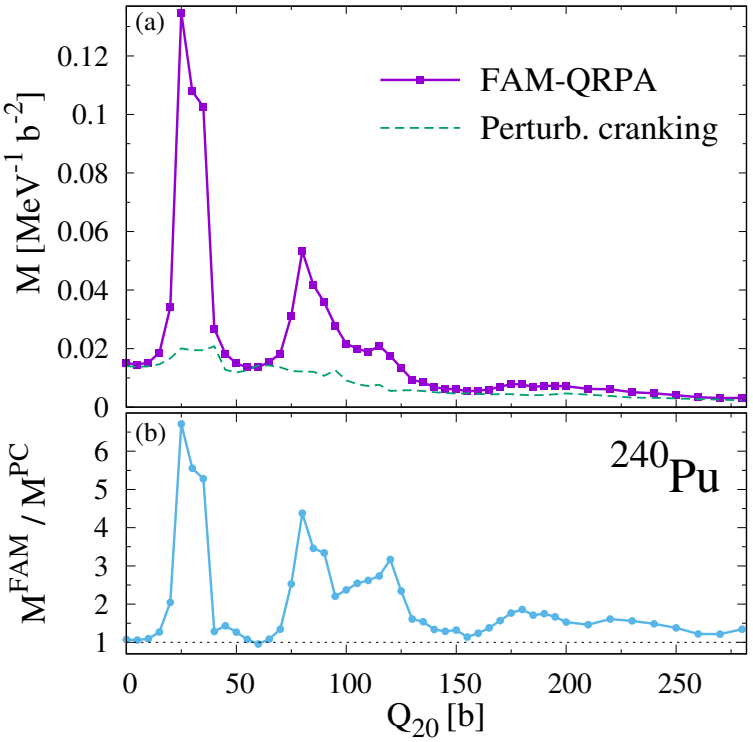

Figure 8: Top panel: Comparison between the perturbative cranking approximation to the collective mass tensor $\mathsf{M} = \mathsf{B}^{-1}$ and the exact calculation along the symmetric fission path of ^{240}Pu. Bottom panel: ratio between the exact and perturbative cranking inertia. Figures reproduced with permission from [203] courtesy of Washiyama; copyright 2021 by The American Physical Society.
⟨fig:coll_mass⟩

Secondly, in contrast to textbook examples of tunnelling, the potential energy surface is defined in the abstract space that represents deformation. In practice the set of collective coordinates $\boldsymbol{q}$ can be either the deformations of the nuclear surface, see Section 2.1, or the expectation value of other relevant observables, see Section 2.2. This means that the term B in the WKB formula is not related to the mass of the nucleus, but is a more abstract object called the collective inertia tensor. It is in fact a rank-2 tensor $\mathsf{B}(\boldsymbol{q}) \equiv B_{ij}(\boldsymbol{q})$ with $i, j = 1, \ldots, N$ where N is the number of collective variables. The calculation of this object is far from simple. Traditional formulas rely on the GCM or the adiabatic time-dependent HFB (ATDHFB) approximation; see [31] for a summary of the relevant formulas. Most practical implementations of these methods neglect the effect of velocity, time-odd terms induced by the generalized momenta $\boldsymbol{p}$ associated with the collective variables $\boldsymbol{q}$, both in the GCM where these momenta should be introduced explicitly and would double the number of collective variables [204], or in the ATDHFB formulas where their effect

is simply neglected [205, 206]. Both the GCM and ATDHFB collective inertia involve the inverse of a large matrix related to the Quasiparticle Random Phase Approximation (QRPA) matrix [31]: the latter is often approximated by its diagonal form as the sum of pairs of quasiparticle energies – the cranking approximation. In addition, the formulas for the inertia tensor involve the derivative operators $\partial/\partial q_i, i = 1, \ldots, N$. These operators are often reduced to a local approximation: this perturbative cranking approximation has been shown to give rather different results from the non-perturbative cranking approximation [207, 208, 209] and to have a large impact on half-lives [210]. Because of these limitations, other methods have been proposed to compute the collective inertia, including "dynamic" path calculations [211] and the adiabatic self-consistent collective coordinate method [212, 213]. In the last few years, there have been very promising attempts to perform "exact" ATDHFB calculation of the collective inertia tensor by inverting the full QRPA inertia [203]. Results of these exact calculations also suggest rather large differences with the standard perturbative cranking approximation as seen in Fig. 8.

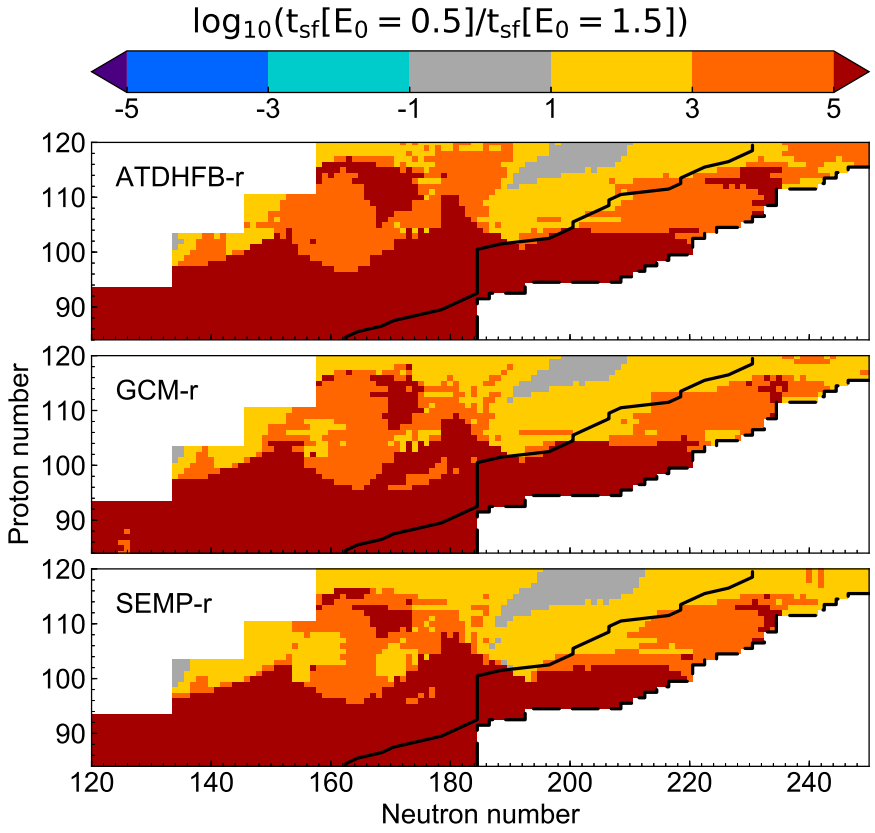

Figure 9: Sensitivity of the spontaneous fission lifetimes to different values of the ground-state energy $\log_{10}[\tau_{\rm sf}(E_0 = 0.5\,{\rm MeV})/\tau_{\rm sf}(E_0 = 1.5\,{\rm MeV})]$ computed with different collective inertias: ATDHFB (top panels), GCM (middle panels), and semi-empirical inertia formula (bottom panels). Figures reproduced with permission from [22] courtesy of Giuliani; copyright 2018 by The American Physical Society.

⟨fig:t_sf_E0⟩

Spontaneous fission half-lives depend very sensitively on each of these ingredients. Because of the exponential factor, small variations in the value of the potential energy, zero-point energy or collective inertia can change the half

life by orders of magnitude [12, 214, 210]. Large-scale surveys of fission modes in heavy nuclei have attempted in the 2010's to systematically probe the influence of these model parameters. For example, Fig. 9 shows how the spontaneous fission half-life varies depending on the total value E_0 of the ground-state energy. Because of the exponential factor in (12), a variation of the ground-state energy of only 1 MeV can change half-lives by up to 5 order of magnitude [22]. Such large effects are typical of spontaneous fission calculations. Similar variations can be the indirect result of which theory is used to compute the collective inertia tensor [210] or of the number of collective variables [215, 216, 217]. In the EDF framework, both the potential energy surface and inertia tensor are directly impacted by both the form and the parameters of the energy functional, and so do the spontaneous fission half-lives [17]. There were a few studies where the statistical uncertainties coming from the calibration of energy functionals were propagated to the prediction of fission barriers [218, 17, 219]. Results suggest uncertainties of at least 1–2 MeV on fission barrier heights, which could lead to changes in $\tau_{\rm SF}$ of up to a dozen orders of magnitude. Similar remarks apply to whether the potential energy surface is computed at the HFB level or with additional corrections, e.g., coming from the restoration of broken symmetries [220].

Among the quantities that can impact the final result are the number and type of collective variables $\boldsymbol{q}$ that define the PES. It has been known for a long time, for example, that pairing correlations can have a dramatic impact on $\tau_{\rm sf}$, largely by reducing the collective inertia which, in a simple solvable one-dimensional model scales like $B \propto 1/\Delta^2$ where Δ is the pairing gap [221, 222, 223, 224, 225]. This observation was an incentive to take collective variables associated with pairing correlations, such as the constraint on the particle-number fluctuations $\langle \Delta \hat{N}^2 \rangle = \langle \hat{N}^2 \rangle - \langle \hat{N} \rangle^2$ or the pairing gap Δ [210, 215, 216, 217, 220, 226].

A global analysis of spontaneous fission half-lives in heavy nuclei, based on quantum tunnelling through one-dimensional potentials including triaxiality and reflection-asymmetry, can be found in [17]. Earlier results were largely focused on superheavy elements with either macroscopic-microscopic methods [227, 228, 8], Gogny HFB [15, 229], Skyrme Hartree-Fock+BCS [12] or Skyrme HFB [16]. Figure 10 shows an example of self-consistent calculation of fission barriers, spontaneous fission and α-decay half-lives in superheavy elements. Results suggest that in superheavy neutron-rich nuclei, spontaneous fission is the dominant channel of decay. This is especially important to properly model the r process [21].

Over the years, there have been several attempts to go beyond the semi-classical WKB approximation for spontaneous fission rates. Functional-integral methods are, formally, the most developed alternatives [230, 231, 232, 233]. They lead to an imaginary-time evolution equation for the nucleus under the barrier, the solutions of which are called instantons. This theory has been tested in a few semi-realistic cases [234, 235]. Other more recent approaches include solving directly the time-dependent Schrödinger with a complex absorbing potential [236], and using a configuration-interaction approach (similar to the nuclear shell model) to test the validity of the adiabatic hypothesis, namely the fact that the potential energy surface is precomputed [237, 238]. Although most of these attempts have been tested with toy-model Hamiltonians and sometimes involved important numerical simplifications, they clearly suggest that the adiabatic approximation may overestimate the spontaneous fission half-life significantly.

To finish this section, we should mention a particularly exotic spontaneous fission mode called "cluster" radioac-

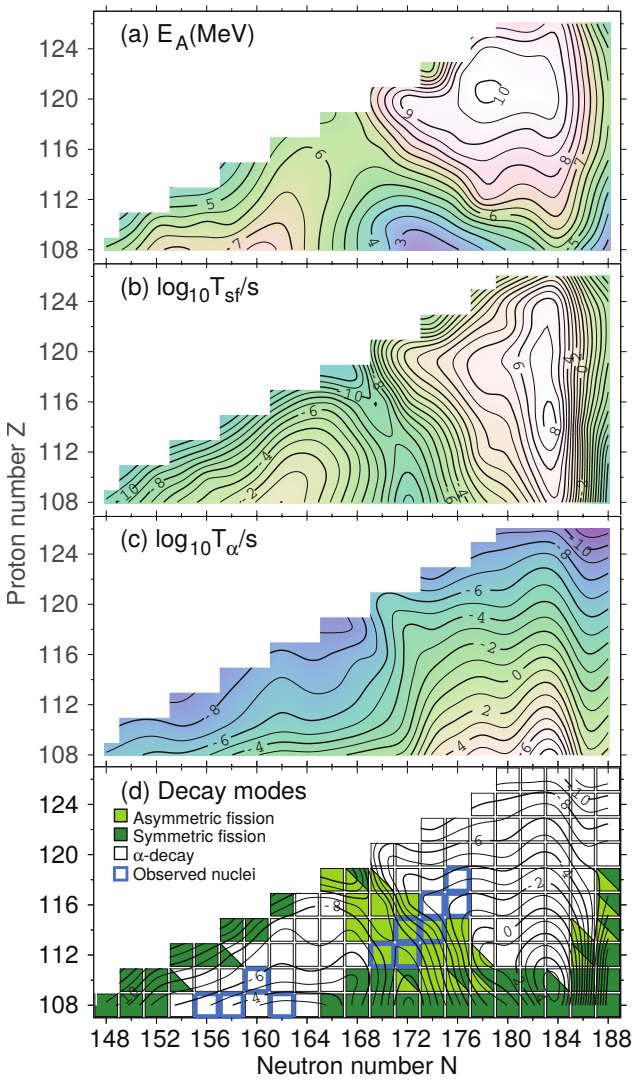

Figure 10: Summary of spontaneous fission calculations with the SkM* EDF for even-even super-heavy nuclei. (a) Inner fission barrier heights E_A (in MeV); (b) SF half-lives $\log_{10}\,\tau_{\rm SF}$ (in seconds); (c) α-decay half-lives $\log_{10}\,\tau_\alpha$ (in seconds); (d) Dominant decay modes. If two modes compete, this is marked by coexisting triangles. Figures reproduced with permission from [16] courtesy of Staszczak; copyright 2013 by The American Physical Society.

⟨fig:t_sf⟩

tivity, where one of the fragments is a small nucleus of up to mass $A \approx 20$ that is much smaller than its partner [239]. While initial descriptions of this decay mode were based on extrapolating the α-decay model of Gamow [240], it was shown early on that standard fission model techniques based on computing tunneling probabilities across multi-dimensional potential energy surfaces could be very successful [241, 242]. The main difference is that these PES must probe extremely asymmetric shapes with, e.g., a much larger ratio $\langle\hat{Q}_{30}\rangle$ / $\langle\hat{Q}_{20}\rangle$ than for traditional fission modes. This phenomenon was studied extensively in the framework of the SR-EDF approach [243, 18] and was suggested as the primary decay mode of Oganesson ($Z = 118$) isotopes [19, 244].

3.2. Neutron-Induced Fission

ubsec:induced⟩?

Neutron-induced fission plays a special role both in basic science and in technological applications of fission. As the name indicates, it is a special case of fission that is triggered when a neutron interacts with a (heavy) target (Z, N) of binding energy $B(Z, N)$. Assuming for now that the neutron is absorbed by the target, the energy of the resulting nucleus is then $B(Z, N) + E_n$: this nucleus is thus in an highly excited state of energy $E = B(Z, N) + E_n - B(Z, N + 1)$ (binding energies are negative). In the case of the ^{235}U(n,f) reaction, for example, the binding energies of ^{235}U and ^{236}U are $B(^{235}\mathrm{U}) = -1783.102$ MeV and $B(^{236}\mathrm{U}) = -1789.648$ MeV leading to an excitation energy of $E = E_n + 6.546$ MeV. In the standard view of fission as a deformation process, neutron-induced fission occurs or, more precisely, has a large probability to occur whenever E (in the compound nucleus) exceeds the height of the highest fission barrier. For some naturally-occurring elements such as ^{235}U, this happens regardless of the energy E_n of the incident neutron: these elements are called fissile. Odd-mass nuclei are a lot more likely to be fissile than even-even ones: pairing correlations induce an additional gain in binding energy after the absorption of the neutron, which increases the chance for the compound nucleus to be at an energy above the fission barrier. Elements where fission can be triggered by higher-energy neutrons, with $E_n > 1$ MeV, are called fissionable or fertile and a typical case of interest for nuclear technology is ^{238}U.

Qualitatively, the fission cross section σ_{nf} can be thought of as the probability (expressed as a surface area) that an incoming beam's neutron is captured by the target and that the resulting nucleus decays through fission. It is obviously a function of the energy of the incident neutron. A very pedagogical introduction to this topic can be found in [38]. In practice, the theoretical treatment of neutron-induced fission is thus markedly more complex than that of spontaneous fission. Because of the substantial amount of excitation energy in the fissioning nucleus many decay channels such as neutron emission (n, xn), radiative capture (n, γ), etc. can be open. Crucially, the fission cross section also depends on the entrance channel, i.e., the probability that the neutron is absorbed in the first place – a process that competes with scattering, both elastic (n, el) and inelastic (n, n'). Therefore, the variations of the fission cross section with the nucleus (Z, N) or the energy E_n of the incident neutron depend not only on how the characteristics of the fission process itself vary with these quantities, but also on how every other channel is affected. For example, neutron emission from an excited nucleus cannot occur if the energy is lower than the neutron separation energy S_n. This channel is thus entirely closed for all $E < S_n$ (the cross section is zero), a situation that can happen for instance in low energy gamma-induced fission. This will in turn impact in a non-trivial way how the fission cross section will change as a function of E.

Figure 11 lists some of the various channels that should typically be considered in a heavy nucleus such as actinides and transactinides. It is important to mention that the various output channels may be populated by processes with very different time scales. In short-time processes, the neutron may simply scatter without interacting with the internal region of the target nucleus. This corresponds to what is called direct reactions, which contributes to the elastic scattering channel and possibly the inelastic one when low-energy vibrational/rotational modes of the target are excited. In intermediate-time processes at higher energies, the neutron can lead to successive excitations/deexcitations of single-particles degrees of freedom (DoFs) of the target with not enough time for the whole system to thermalize.

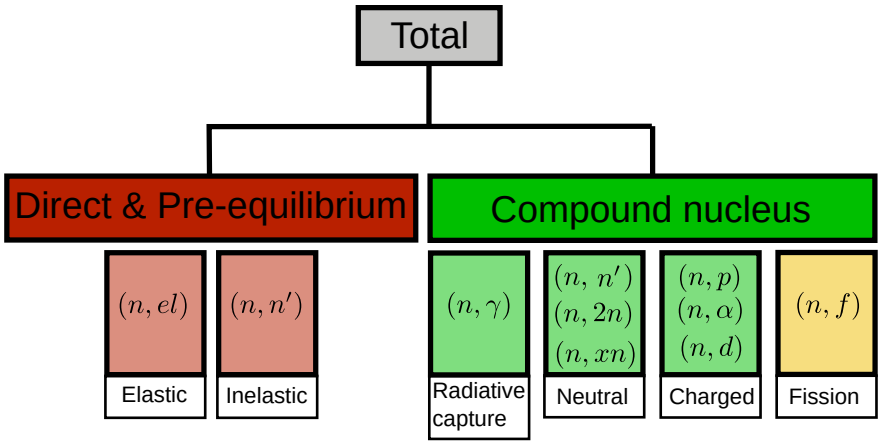

Figure 11: Overview of some of the most relevant reaction channels for the compound nucleus. Depending on the energy of the incident neutron, many reaction mechanisms may be competing. These include direct reactions, where the incoming particle interacts with specific rotational/vibrational modes of the target, and pre-equilibrium reactions, where several single-particle excitations/deexcitations take place without a complete thermalization of the compound system. The total cross section is the sum of the cross sections of each process.

⟨fig:reactions⟩

This is the pre-equilibrium part of the cross section [245], which populates mostly the inelastic scattering channel. Finally, the longer-time processes consist in the absorption of the neutron leading to a thermalized compound nucleus. In this case, one assumes that the compound nucleus is in a strongly-damped regime [246, 247, 248, 249, 250]: its wave function is a very complex, incoherent linear superposition of many different types of intrinsic, collective and coupled wave functions. The compound nucleus itself emits particles and populates a variety of output channels. Due to its typically large time scale, neutron-induced fission falls into this category of compound nucleus processes.

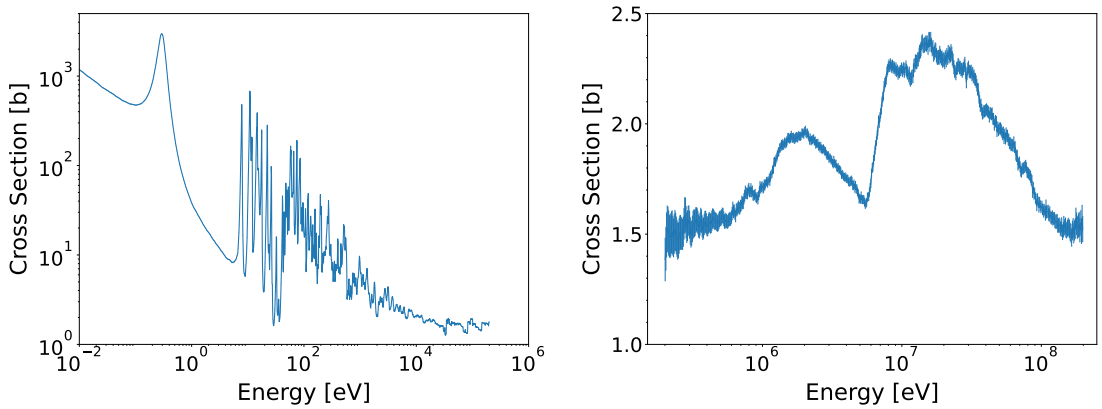

Figure 12: Fission cross sections in the reaction ^{239}Pu(n,f) as a function of the energy of the incident neutron. Data taken from the EXFOR database [251, 252]; measurements from [253]. Left: thermal and resonance region $E_n < 0.1$ MeV; both axes are in log scale. Right: fast region $E_n > 0.1$ MeV; the y-axis is in linear scale while the x-axis is in log scale.

cross_sections⟩

As an example, Fig. 12 shows the variations of the fission cross section as a function of the incident neutron energy for the case of ^{239}Pu(n,f). At very low energies $E_n < 0.1$ eV (the *thermal* regime), the cross section varies smoothly

with the energy and is roughly proportional to the time spent in the vicinity of the nucleus, hence to the inverse of the neutron velocity. At such low energies, the (n, n') and (n, xn) channels are closed and the fission cross section results from the competition between elastic scattering, photodeexcitation and actual fission. In fact, the smoothly decreasing trend mostly reflects the fact that the probability of absorption decreases with neutron energy (or equivalently: the scattering probability increases). The epithermal or resolved resonance region ranges from 1 to about 10^4 eV. In this range of neutron energies, the resonances associated with the capture of the neutron by the target can be resolved experimentally. In this maze of resonances, only a few actually corresponds to resonances in the fission output channel from a compound nucleus. Most of them are in fact related to the probability of capturing the neutron, i.e. the input channel. Finally, the region of $E_n > 100$ keV corresponds to what is defined as fast neutrons. At such energies, most decay channels are open: (n, γ), (n, n') and (n, xn). The rapid increase of σ_{nf} at around 5-6 MeV corresponds to second-chance fission, i.e., a neutron is emitted from ^{240}Pu but leaves enough energy in the ^{239}Pu daughter that this nucleus fissions. Note that several features of the resonance and fast-neutron region are markedly different in fissile and fissionable (or fertile) elements, as illustrated in Figure 15 page 31.

As this introduction may already suggest, accurate predictions of fission cross sections are extraordinarily challenging. The large number of reaction mechanisms that must be taken into account, the range of time or energy scales involved and the need for high-precision calculations imply that several models, each characterized by some free parameters, have to be carefully stitched together. Evaluations of fission cross sections thus typically involve of the order of a few dozens of parameters for each nucleus involved in the reaction process [254, 28]. Thanks to Bayesian statistical techniques and careful accounting for sources of theoretical and experimental uncertainties [255, 256, 257], fission cross sections can typically be reproduced within a few percents of experimental values [254, 28]. However, these uncertainties may be underestimated because of missing experimental information and unknown model biases [258].

3.2.1. Fission Rates at High Energy

bsubsec:rates⟩?

One of the earliest theories attempting to compute the probability of induced fission was proposed by Kramers [259]. The main hypothesis is to assume that the fission *rate* can be obtained by computing the flux of a current of probability $\boldsymbol{j}(\boldsymbol{q}, \boldsymbol{p}, t)$ through the saddle point. This semi-classical and statistical model depicts the nucleus as a few shape collective coordinates $\boldsymbol{q}$ and their associated momenta $\boldsymbol{p}$ interacting with a thermal bath of residual DoFs. The current $\boldsymbol{j}(\boldsymbol{q}, \boldsymbol{p}, t)$ is computed from the probability distribution function $f(\boldsymbol{q}, \boldsymbol{p}, t)$ representing the probability for the nucleus to be at point $(\boldsymbol{q}, \boldsymbol{p})$ at time t. The equation of motion for this quantity is the Kramers equation [260],

$$\frac{\partial f}{\partial t}(\boldsymbol{q}, \boldsymbol{p}, t) = \sum_{\alpha\beta} \left[-B_{\alpha\beta} p_\beta \frac{\partial}{\partial q_\alpha} + \left(\frac{\partial V}{\partial q_\alpha} + \sum_\delta \frac{1}{2} \frac{\partial B_{\beta\gamma}}{\partial q_\alpha} p_\beta p_\delta \right) \frac{\partial}{\partial p_\alpha} + \sum_\gamma \Gamma_{\alpha\beta} B_{\beta\gamma} \frac{\partial}{\partial p_\alpha} p_\delta + D_{\alpha\beta} \frac{\partial^2}{\partial p_\alpha \partial p_\beta} \right] f(\boldsymbol{q}, \boldsymbol{p}, t), \tag{13}$$

eq:kramers

where $D_{\alpha\beta}(\boldsymbol{q}) = \Gamma_{\alpha\beta}(\boldsymbol{q}) T$ is the dissipation tensor, T the temperature of the bath, $\Gamma_{\alpha\beta}$ the friction tensor and $B_{\alpha\beta}(\boldsymbol{q})$ the collective inertia tensor. We define the reduced friction tensor $\boldsymbol{\beta} = \Gamma\mathsf{B}$, that is, $\boldsymbol{\beta} \equiv \beta_{\alpha\gamma} = \sum_\delta \Gamma_{\alpha\delta} B_{\delta\gamma}$. The

Kramers equation is the extension of the Fokker-Planck equation in presence of a potential $V(\boldsymbol{q})$ [261, 262, 263]. In addition to not assuming a stationary process, the advantage of such approaches based on diffusion is that they include a mechanism to couple intrinsic excitations to collective motion through the dissipation tensor $D_{\alpha\beta}$.

In its original formulation, Kramers used a one-dimensional version of (13) where he further assumed that the potential well near the ground state was approximately parabolic with a frequency ω' and that the top of the barrier was also well described by an inverted parabola of frequency ω_0. In such a case, he obtained the following fission rate λ_f in the limit of large dissipation,

$$\lambda_f = \frac{\omega'}{2\pi\omega_0}\left(\sqrt{\frac{\beta^2}{4}+\omega'^2}-\frac{\beta}{2}\right)e^{-E_{\rm B}/kT}, \tag{14}$$ {?}

where $E_{\rm B}$ is the height of the fission barrier, T is the nuclear temperature, which is given (approximately) by $T \approx \sqrt{E/a}$ with a the level-density parameter, E the excitation energy, and β is the one-dimensional version of the reduced friction tensor introduced earlier. This approach was later generalized in multi-dimensional cases [264, 265, 266, 267, 268]. In this case, assuming that the local minimum of the potential $V(\boldsymbol{q})$ characterizing the ground state is at $\boldsymbol{q}_{\rm gs}$ and the saddle point at $\boldsymbol{q}_{\rm B}$, the formula for the fission rate becomes

$$\lambda_f = \frac{1}{2\pi}e^{-V(\boldsymbol{q}_{\rm B})/kT}\left(\frac{\det W^{(\rm gs)}}{|\det W^{(\rm B)}|}\right)^{1/2}\Lambda, \tag{15}$$ {?}

with

$$W^{(\rm gs)}_{\alpha\beta} = \left.\frac{\partial^2 V}{\partial q_\alpha q_\beta}\right|_{\boldsymbol{q}=\boldsymbol{q}_{\rm gs}}, \qquad W^{(\rm B)}_{\alpha\beta} = \left.\frac{\partial^2 V}{\partial q_\alpha q_\beta}\right|_{\boldsymbol{q}=\boldsymbol{q}_{\rm B}}, \tag{16}$$ {?}

and Λ given by the only positive eigenvalue of the matrix equation $\det|\mathsf{M}\Lambda^2+\boldsymbol{\beta}\Lambda+\mathsf{W}^{(\rm B)}|=0$, where M is the collective mass tensor, $\mathsf{M}=\mathsf{B}^{-1}$. Projecting such multi-dimensional calculations on one-dimensional trajectories is equivalent to introducing a mass correction and an additional friction term [269].

Early studies of fission rates were limited since numerically solving the Kramers equation (13) is notoriously difficult [271]. However, the solutions to this equation, which are probability distribution functions, can also be sampled by solving the stochastic Langevin equation (26). Given a large enough number of full Langevin trajectories, the time-dependent fission rate is given by $\lambda_f(t) = -1/N(t)dN/dt$ where $N(t)$ is the number of trajectories that did not escape the saddle point at time t [272, 270]. At small t, this fission rate is nearly 0, while at larger t calculations show that the rate converges to a nearly constant, quasistationary value [273, 274, 270] that matches what one would obtain from the solution of the Kramers equation [275], as illustrated in Fig. 13. The transient time needed for the system to reach quasistationary flow plays an important role when other decay channels such as neutron or γ emission are taken into account: during that time, fission plays a relatively smaller role compared with these other processes, and this can affect, e.g., the number of pre-scission neutrons [276]. As shown in Fig. 13, the fission rate is very sensitive to the size of the collective space and the excitation energy, but it also depends strongly on the value of the dissipation coefficient [277]. Further analysis based on generalized Langevin equation allowing for non-Markovian dynamics suggested that memory effects could be relatively strong [278]. Note that because of its classical character, this approach cannot describe lower-energy effects related to resonances or even tunneling. Until now, it has therefore mostly been applied to calculations of fission rates at very high energies such as encountered in heavy-ion collisions.

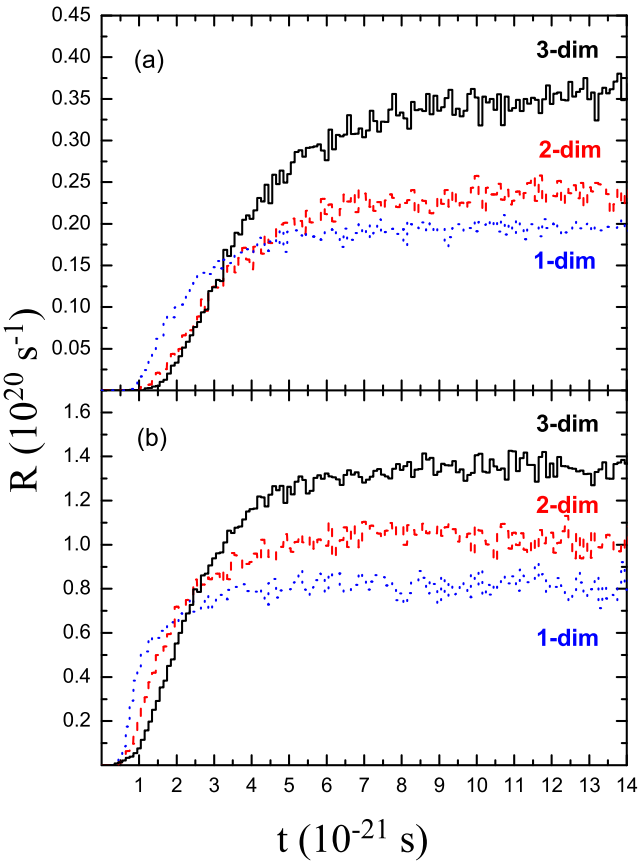

Figure 13: Fission rate calculated for the nucleus ^{248}Cf in the case of two-body dissipation for excitation energy $E = 30$ MeV (a) and $E = 1500$ MeV (b). The solid, dashed, and dotted curves correspond to the Langevin calculations in three-, two-, and one-dimensional collective potential energy surfaces, respectively. Figures reproduced with permission from [270] courtesy of Nadtochy; copyright 2007 by The American Physical Society.

⟨fig:rate⟩

3.2.2. Fission Cross Sections for Fast Neutrons

:fast_neutrons⟩

The approach presented above allows computing fission rates (or probabilities) but has not been used to the calculation of fission cross sections yet. Predicting a fission cross section is actually more demanding as it requires the proper description of both the input channel and of the competition mechanism between all the possible output channels such as, e.g., γ and neutron emission. In the fast-neutron range ($E_n \gtrsim 100$ keV), such calculations are usually performed within the Hauser-Feshbach theory [279] and relies on a statistical picture of nuclear structure.

General Theoretical Framework. In the high-energy range the density of resonances is so high that it is impossible to resolve them experimentally. As a consequence, theoretical approaches focus on estimating the average cross sections over a small sliding window in energy. The standard theory to describe the average cross section for compound-nucleus processes in this energy range is the Hauser-Feshbach theory. A pedagogical review of this approach can be found

in [193]. The Hauser-Feschbach framework relies heavily on the Bohr hypothesis stating that the probability for an output channel depends only on the energy, spin and parity of the compound nucleus and is independent of the details of its formation process [280, 281, 282, 283, 193, 194]. Its goal is to compute the average cross section $\sigma_{\alpha\beta}(E, J, \pi)$ that describes the formation through an entrance channel generically noted α of a compound nucleus of energy E, spin J and parity π that subsequently decays through a channel β. Channels refer both to a certain combination of projectile and targets, e.g., $\alpha \equiv n + ^{239}$ Pu, but also to specific combinations of quantum numbers for each of the constituents. In this context, fission is depicted by one macroscopic channel without details about the exact fragmentations. For example both the ^{138}Te+^{102}Mo and ^{140}Ba+^{100}Sr mass splits will be part of what is considered the fission channel of ^{240}Pu. Given an entrance channel $\alpha = a+A$ corresponding to an incident particle a and a target A, and an exit channel β (e.g. neutron or gamma emission), the cross section for the process, assuming no width fluctuations, reads [193]

$$\sigma_{\alpha\beta}(E, J, \pi) = \pi\lambda\!\!\!^{-2} \sum_{J\pi} \frac{2J+1}{(2j_a+1)(2J_A+1)} \sum_{l_\alpha j_\alpha l_\beta j_\beta} \frac{T^{J\pi}_{\alpha l_\alpha j_\alpha}(E) T^{J\pi}_{\beta l_\beta j_\beta}(E)}{\sum_\delta T_\delta(E)}, \tag{17}$$

eq:hauser-feshb

where j_a and J_A are the total angular momentum of the incident and target nuclei, J is the total compound-nucleus angular momentum, l_α, j_α and l_β, j_β are the orbital and angular momentum coupling in the channels α and β, and $\lambda\!\!\!^{-}$ is the reduced wavelength of the incident particle a.

The coefficients $T_\alpha(E) \equiv T^{J\pi}_{\alpha l_\alpha j_\alpha}(E)$ are the transmission coefficients for the channel α at energy E. In neutron-induced fission, the typical decay channels involve neutron emission, γ emission, and actual fission, while the entrance channel is neutron absorption. In the case of resolved resonances, $T_\alpha(E) = 2\pi\Gamma_\alpha/D$ where Γ_α is called the width of the channel α, which is inversely proportional to the lifetime τ of the state through $\Gamma_\alpha = \hbar/\tau_\alpha$, and D is the level spacing at energy E [284]. In practice, the partial widths fluctuate rapidly with the energy. The average cross section is obtained by averaging (17) over a small energy window centered on E by using the relation

$$\left\langle \frac{\Gamma_\alpha(E)\Gamma_\beta(E)}{\sum_\delta \Gamma_\delta(E)} \right\rangle = W_{\alpha\beta} \frac{\langle\Gamma_\alpha(E)\rangle \langle\Gamma_\beta(E)\rangle}{\sum_\delta \langle\Gamma_\delta(E)\rangle}, \tag{18}$$

{?}

where $\langle \ldots \rangle$ refers to the energy averaging. The actual transmission coefficients used in (17) are thus defined as the *average* quantities $T_\alpha(E) = 2\pi \langle\Gamma_\alpha\rangle / D$ and $W_{\alpha\beta}$ is called the width-fluctuation correction. If $\langle\Gamma\rangle / D \ll 1$, then this correction can be calculated semi-analytically [285]. Let us emphasize that we have discussed here only the simplest version of the Hauser-Feshbach theory and have restricted ourselves to the formula most relevant for fission. In-depth discussions and additional references can be found in several review articles [286, 193]. One of the main limitations of Hauser-Feshbach theory is its assumption that channels do not interfere, i.e., direct interactions cannot take place. Several extensions of the theory were developed in the 1970's to address these issues but they are not applied very frequently [287, 288, 289].

From a practical perspective, the application of Hauser-Feshbach theory to fission implies that we "only" have to determine the transmission coefficients of all the relevant processes. Their expression depends on the type of channel involved, e.g., the neutron optical model gives the neutron transmission $T_n(E)$. In this review, we are only going to discuss the calculation of $T_f(E)$; see [290] and references therein for additional details about the neutron-capture,

neutron-emission and γ transmission coefficients.

Calculation of Transmission Coefficients. The standard method to determine fission transmission coefficients $T_f(E)$ consists in computing the penetrability through a one-dimensional fission barrier [291]. This involves first the construction of a collective potential and inertia as a function of a single collective coordinate associated with the elongation of the fissioning system. The probability that the compound nucleus decays through fission derives from the transmission of a collective plane wave from the low-deformations to the high-deformation domain. In other words, the transmission coefficient is extracted from the solution of a stationary version of an equation of the type (31); see Section 4.4. It is important to realize that such a wave equation is not the Schrödinger equation for a particle, but the equation of motion for a collective wave packet traveling through the collective space (=deformation space) characterizing the fission process. Although this approach could in principle be rooted in first-principle theories [291] it is still mostly guided by phenomenological considerations. When the energy of the system lies above the fission barrier, this approach is often combined with the transition-state model [292]: at the top of each barrier are a sequence of discrete excited states of energies ϵ_k. For each such state, there is an associated transmission coefficient (20) determined from a collective potential up-shifted by an energy ϵ_k. These states are typically modeled as members of collective rotational bands built on top of vibrational bandheads. The total fission transmission coefficient thus becomes

$$T_f(E) = \sum_k f_k T_f(E - \epsilon_k), \tag{19}$$ eq:Tf_total

where $f_k = 1$ if the spin and parity of the transition state equals that of the compound nucleus, and is zero otherwise. Note that (19) can be extended by additionally considering a continuum of excited states [293].

The main ingredients of this approach are the collective potential and the associated inertia. For fissile nuclei such as ^{239}Pu and ^{235}U, the energy E of the compound nucleus always exceeds the highest fission barrier irrespective of the energy of the incident neutron. In this regime, transmission coefficients are most of the time determined from the formula given by Hill and Wheeler [294]. It is obtained by assuming that the collective potential is an inverted parabola of frequency ω_0 and height E_f. If we work within a one-dimensional collective space and further assume that the collective inertia does not depend on the collective variable, then the wave equation can be solved analytically and yields the following Hill-Wheeler formula for the transmission coefficient,

$$T_f(E) = \frac{1}{1 + \exp\left[2\pi(E_f - E)/\hbar\omega_0\right]}. \tag{20}$$ eq:Tf

Note that the resulting transmission coefficient is independent of the collective inertia. In practice, (20) is often applied by using semi-realistic estimates of the fission barrier height E_f from either macroscopic-microscopic [295, 296] or fully microscopic calculations [127] and by choosing ω_0 as an adjustable parameter. There have been some attempts to modify the Hill and Wheeler formula to account for the dependence of fission barriers on excitation energy [297]. In the case of the double-humped fission barrier typical of actinide nuclei, the full transmission coefficient is computed by coupling the coefficients of the first (T_A) and second (T_B) barriers according to

$$T_f = \frac{T_A T_B}{T_A + T_B}, \tag{21}$$ eq:tatb

if we assume no decay from either the first or second potential wells [298].

Equation (20) could in principle be generalized to a more realistic collective space. Along this line, we can mention the early work of Cramer and Nix solving the case of two inverted parabola on a finite support connected by a parabolic shape [299]. The subsequent description of quasi-bound states in the outer potential qualitatively explains the presence of resonances in the fission cross section at energies below the barrier height; see Fig.14. Similar studies are performed in [300]. Going even further, one can add an imaginary part to the collective potential, typically in the second well, to account for the damping of collective vibrations. This idea leads to the fission optical model and is for instance discussed in [301, 302]. As shown in the right panel of Fig.14, such an approach well reproduces the large (few 100 keV) resonances just below the fission threshold.

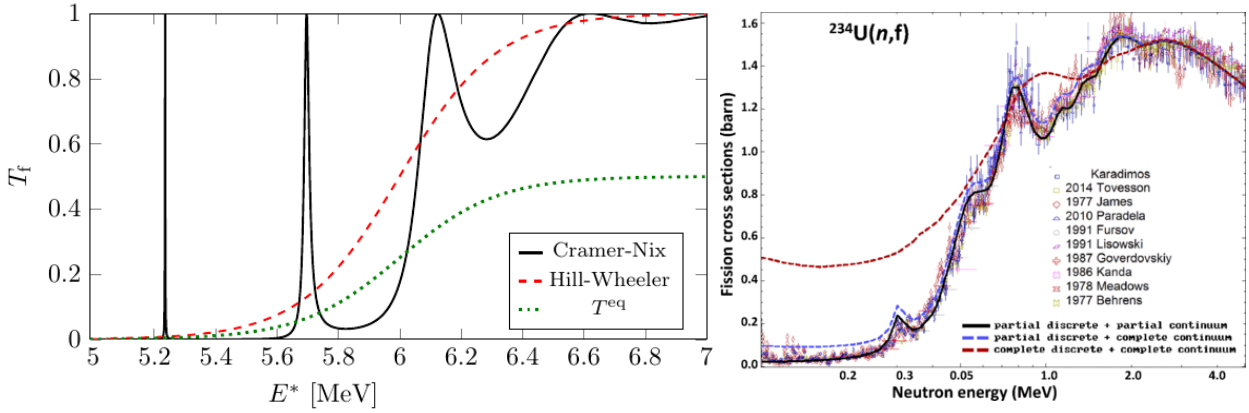

Figure 14: Left: Fission transmission coefficient as a function of the excitation energy of the fissioning system. The one humped Hill-Wheeler estimation (red curve) is compared to its counterpart when coupling two barriers as in (21) (green dotted line) as well as the one obtained from a Cramer-Nix potential (full black line). While the Hill-Wheeler formula gives a smooth evolution with energy, the Cramer-Nix approach predicts resonances in qualitative agreement with experiment. Courtesy of P. Tamagno [298]. Right: ^{234}U cross section predicted by the extended optical model for fission (full black line) compared to various experimental data. Figure reproduced with permission from [301] courtesy of M. Sin; copyright 2016 by The American Physical Society.

n_transmission⟩

It could also be possible to solve (20) numerically for an arbitrary potential and inertia functions. Doing so still poses a number of practical challenges. Encoding the physics of fission requires collective spaces with more than one deformation degree of freedom. Most importantly, the Hill-wheeler equation was obtained by neglecting the deformation dependence of the collective inertia: in this case, the final formula is independent of it. In a more realistic calculation, the transmission coefficient would most certainly depend on it – like the spontaneous fission rate (12). The problem of which boundary conditions to adopt is also not trivial. Finally, the extreme sensitivity of the fission cross section to the barrier height as well as to the fine structure of the resonant states in the secondary potential well makes such approaches highly challenging.

3.2.3. Resolved Resonance Region: the R-matrix Formalism

sec:resonances⟩

When the energy of the compound nucleus becomes close to the top of the fission barrier, or is even lower than it, the situation becomes more complex as both the level structure of the two potential wells and their coupling begin

playing a role [303, 304]. In particular, the excited states associated with the second potential well, which correspond to more elongated shapes and have a higher probability to fission, play the role of *doorway states* for the fission exit channel [305, 306, 307]. The presence of such intermediate structures – states that are neither continuum states with a very broad width nor are pure single-particle or collective states with a very narrow width – in the cross sections partly explains the structure of the resolved resonance region at $10\,\mathrm{eV} < E_n < 10\,\mathrm{keV}$ in Fig. 12, together with the resonances that come from the entrance channel and reflect an enhanced probability that the neutron is absorbed.

While the Hauser-Feschbach theory captures well the smooth-energy trends of the cross sections, it is, by design, not able to describe the narrow resonances observed in the intermediate-energy range. The description of these fine structures relies on another formalism: the R-matrix theory. The R-matrix theory is a general, multi-channel approach especially designed to handle resonances [308, 309]. More specifically, it is the reference method used for evaluating the neutron cross sections in the resolved resonance region (RRR) and is extensively used to fit experimental cross section data [310, 311].

We recall that in the standard R-matrix theory of a reaction between a projectile and a target, space is divided into two regions, the interaction (or internal) and asymptotic regions, and the system target+projectile is also divided into two subsystems with different numbers of particles and quantum numbers (=the channels α) [308, 309]. The wave function in the external region is the product of the intrinsic wave functions of each subsystem and an asymptotic wave function for the relative motion of the center of mass; in the internal region, it is a many-body wave function. The actual R matrix is a mathematical object that connects the wave functions of all possible output channels at the boundary between the internal and external regions.

Fission requires a special treatment in the context of the R-matrix due to the fact that it is not by itself a well defined output channel but can actually lead to a large number of different fragmentations. The extension of the R-matrix formalism to the case of fission was first formalized by Lynn [312, 313, 314]; a comprehensive and pedagogical presentation of his model can also be found in [315]. The basic idea is to identify a set of collective variables $\boldsymbol{\eta}$ that defines the fission channel and separate it from all the other degrees of freedom $\boldsymbol{\xi}$ of the nucleus. In all applications of this formalism, the vector $\boldsymbol{\eta}$ has only one component η that typically coincides with the axial quadrupole deformation β of the nucleus – which is also one of the collective variables used to define PES; see Section 2. The associated collective motion will only include the corresponding β-vibrational modes, i.e., the shapes vibrations of the axial quadrupole moment of the nucleus. In this approach the many-body Hamiltonian is expanded as [315]

$$\hat{H} = \hat{H}_{\mathrm{vib}}(\boldsymbol{\eta}) + \hat{H}_{\mathrm{int}}(\boldsymbol{\xi}) + \hat{H}_c(\boldsymbol{\eta}, \boldsymbol{\xi}), \tag{22}$$ eq:H_rmatrix

where the collective Hamiltonian $\hat{H}_{\mathrm{vib}}(\boldsymbol{\eta})$ acts only on the fission mode variables $\boldsymbol{\eta}$. The intrinsic Hamiltonian operator $\hat{H}_{\mathrm{int}}(\boldsymbol{\xi})$ acts only on the intrinsic variables $\boldsymbol{\xi}$, which includes single- or quasi-particle degrees of freedom, rotational modes and any non-β-vibrational mode. The term $\hat{H}_c(\boldsymbol{\eta}, \boldsymbol{\xi})$ encodes the coupling between the fission modes and all intrinsic excitations. In analogy to standard R-matrix theory, the total space, here the collective space of deformations $\boldsymbol{\eta}$, is divided into two regions, internal and external. Traditionally, the fission channel "radius" that defines the boundary is put near, or at the outer barrier denoted $\boldsymbol{\eta}_0$ [314].

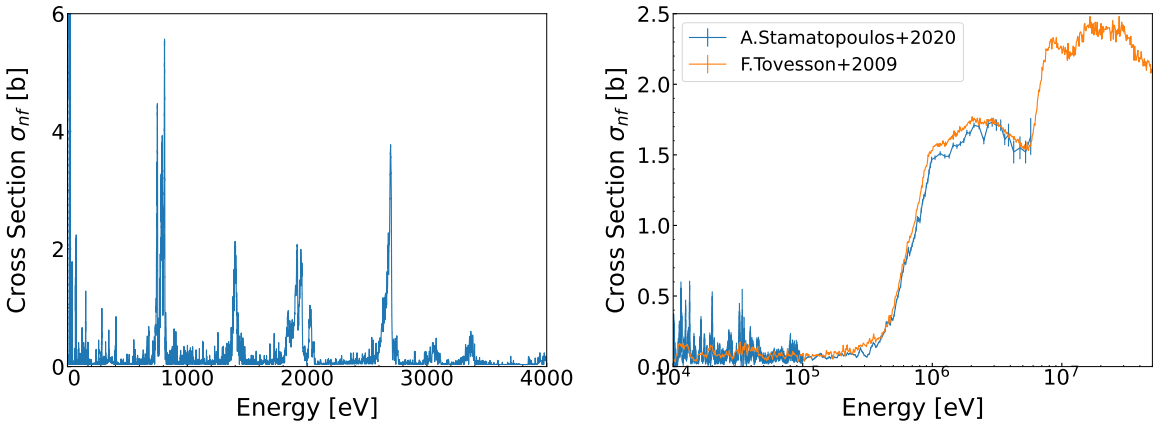

Figure 15: Left: Fission cross section for the ^{240}Pu(n,f) reaction in the resonance region for $0 \leq E_n \leq 4$ keV. The data is taken from [316]. Right: Same quantity for neutrons energies $10\,\text{keV} \leq E_n \leq 50\,\text{MeV}$. Data taken from [316, 317].

oss_sections_1⟩

In the internal region, the eigenstates X_λ of the complete Hamiltonian (22) are expanded as

$$X_\lambda = \sum_n \sum_\nu C^\lambda_{n\nu}(\boldsymbol{\eta}_0)\Phi^{\boldsymbol{\eta}_0}_n(\boldsymbol{\eta})\chi_\nu(\boldsymbol{\xi}), \tag{23}$$

eq:expand_inte

where the basis wave functions of the vibrational modes are denoted by $\Phi^{\boldsymbol{\eta}_0}_n(\boldsymbol{\eta})$. The notation indicates that these are eigenfunctions of the collective, vibrational Hamiltonian that only depend on $\boldsymbol{\eta}$ but with specific boundary conditions set at $\boldsymbol{\eta} = \boldsymbol{\eta}_0$. The basis wave functions for the intrinsic excitations are $\chi_\nu(\boldsymbol{\xi})$ and correspond to eigenstates of the intrinsic Hamiltonian. They define the Bohr fission channels. For the double-humped barrier typical of actinides, collective vibrational states can only be built inside the two potential wells corresponding to the ground state and the fission isomer. Therefore, one can adapt the expansion (23) as follows,

$$X_\lambda = \sum_n \sum_\nu C^{\lambda;\mathrm{I}}_{n\nu}(\boldsymbol{\eta}_0)\Phi^{\boldsymbol{\eta}_0;\mathrm{I}}_n(\boldsymbol{\eta})\chi_\nu(\boldsymbol{\xi}) + \sum_n \sum_\nu C^{\lambda;\mathrm{II}}_{n\nu}(\boldsymbol{\eta}_0)\Phi^{\boldsymbol{\eta}_0;\mathrm{II}}_n(\boldsymbol{\eta})\chi_\nu(\boldsymbol{\xi}), \tag{24}$$

eq:expand_inte

where the additional labels I and II refer to states that localized primarily in the first and second well respectively. These are referred to as class-I and class-II states. The computation of the matrix elements of the total Hamiltonian with the ansatz (24) makes manifest the potential couplings between the two wells. Different regimes of coupling (weak coupling, uniform mixing) lead ultimately to different resonant structures in the fission cross section which are presented in great details in [291]. It includes phenomena going from the large (100 keV) sub-barrier vibrational resonances observed for instance in ^{230}Th(n,f) to the clusters of low-energy (a few keV) fission resonances illustrated in Fig. 15. In this formalism it is possible to interpret such structures as the interplay between class I and class II states. Upon formation, the nucleus has some probability (and associated width) to pass the first fission barrier and to exit in the second potential well. In that second well, the system has a (much higher) probability of fissioning. The amount of couplings depends on the energy of the nucleus and on all other possible decay modes inside the two wells.

The final product of the formal R-matrix theory is a link between the scattering matrix, hence the cross section, and a set of parameters related to the internal wave functions X_λ. The theory was initially successful at explaining qualitatively the large number of narrow resonances (intermediate structures) in the fission sub-barrier cross sections

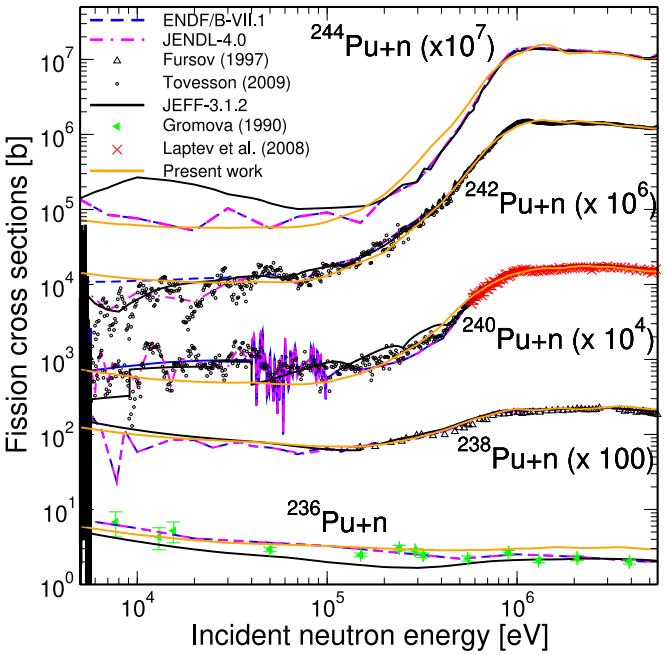

Figure 16: Fission cross-sections as a function of the energy of the incident neutron for a chain of Plutonium isotopes. Calculations were performed using R-matrix theory for sub-barrier fission and are compared to experimental measurements and reference evaluations. Figures reproduced with permission from [318] courtesy of Bouland; copyright 2013 by The American Physical Society.
⟨fig:pu_cs⟩

[312, 313, 314, 306, 319]. It is now used routinely as an advanced theoretical framework in the context of cross section evaluation to fit existing measurements [320, 321]. To our knowledge, the R-matrix formalism has not yet been used to predict (instead of fitting or analyzing) features of resonances starting from a first-principle Hamiltonian. Although possible in principle, such predictions would require the knowledge of the internal region at a level of precision that is most likely beyond what is possible with state-of-the-art many-body theories.

In recent years, the focus of such approaches has also shifted to the prediction of the average fission cross section in the continuum energy range [318, 322, 323]. Figure 16 shows an example of the fission cross sections in several Plutonium isotopes obtained within this formalism. The idea is to consider a stochastic ensemble of realistic R-matrices that account for a statistical ensemble of resonances. One then determines the cross section as an average over all the cross sections obtained with the R-matrix samples. This kind of approach bridges the R-matrix formalism with the Hauser-Feshbach approach. In the latter, the optical potential phenomenologically accounts for the averaging over resonances.

4. Formation of Primary Fission Fragments
⟨sec:lacm⟩

In the previous two sections, we have described how the concept of nuclear fission emerges naturally from a description of the atomic nucleus in a symmetry-breaking mean field, where fission probabilities are related to quantum tunnelling through a multi-dimensional potential energy surface and fission cross sections to the presence and structure

of deformed excited states. In this section, we assume that fission is happening and we review the methods capable of predicting the primary fragments properties. One may distinguish two classes of theoretical approaches. The first one relies on defining an ensemble of scission configurations and populating them according to a statistical distribution. The so-called scission point models that we discuss in Section 4.1 are prime examples of this class of methods. A second option is to describe explicitly the dynamics of the process as the nucleus evolves from its weakly-deformed initial state toward configurations where two primary fragments can be identified. Such models of fission dynamics can be further subdivided into two sub-categories:

- Real-time, time-dependent calculations simulate a *single fission event*, that is, the evolution in time of a single configuration of the fissioning nucleus. A single solution of the Langevin equation or a single random walk (Section 4.2) or a fully self-consistent time-dependent Hartree-Fock (TDHF) or time-dependent Hartree-Fock-Bogoliubov (TDHFB) trajectory (Section 4.3) are examples of such techniques;
- Time-dependent collective models simulate the time-dependent evolution of the *probability distribution* of populating a specific configuration. The most common example of such an approach is the quantum-mechanical time-dependent generator coordinate method (TDGCM) presented in Section 4.4 [324]. Although it has been applied very rarely in practical calculations, its classical equivalent would be the Kramers equation [260].

The two classes of methods are obviously related. For example, sampling many different single-configuration trajectories allows reconstructing probability distributions: this is how fission fragment distributions can be extracted from Langevin or random walks simulations and could, in principle, be compared with the equivalent time-dependent collective model. As we will discuss in more details in Section 6, the main goal of time-dependent models of fission dynamics is to predict actual observables related to the primary fission fragments such as their distribution in charge and mass as well as their **total kinetic energy** (TKE) distribution. These initial conditions are important inputs to be used in fission event generators to simulate the deexcitation of the fragments and compare with experimental measurements (cf. Section 5).

4.1. Statistical Models for Fission Fragment Distributions

ec:statistical⟩

Before the 1980's, solving explicitly time-dependent differential equations to directly simulate fission dynamics often exceeded the available computational resources. At the same time, there was a consensus that the characteristics of the potential energy surface of the fissioning nucleus at scission played a key role in determining the fission fragment mass and charge distributions. In particular, it had become clear that the nuclear shell structure and, more generally, the deformation properties of the fission fragments were important drivers in setting their relative abundance [191, 192]. What is known as the scission-point model is an attempt to take advantage of these observations to obtain realistic estimates of the primary fission fragment distributions without simulating the dynamics explicitly. Scission-point models rely on the hypothesis of quasi-statistical equilibrium at scission: it is assumed that the dynamics of fission populates scission configurations in a statistical manner. Scission-point models have been relatively successful and have the clear advantage of being computationally rather cheap (cf. Fig 2) since all that is needed is a "good" potential energy surface: it entirely avoids simulating fission dynamics.

In most implementations of scission-point models, the PES is not computed from the potential energy of the fissioning nucleus, but instead defined as the sum of the potential energy of each fragment $V_i(\boldsymbol{q}_i)$, $i = 1, 2$ and of the interaction between them, which depends mostly on their relative distance d_{12}. The latter term contains both a Coulomb and nuclear component,

$$\begin{aligned} V(\boldsymbol{q}) =& V_1(Z_1, N_1, \boldsymbol{q}_1) + V_2(Z_2, N_2, \boldsymbol{q}_2) \\ &+ V_{\rm Coul}(Z_1, N_1, \boldsymbol{q}_1, Z_2, N_2, \boldsymbol{q}_2, d_{12}) + V_{\rm nucl}(Z_1, N_1, \boldsymbol{q}_1, Z_2, N_2, \boldsymbol{q}_2, d_{12}). \end{aligned} \quad (25)$$

eq:SPM_potenti

After the total potential energy $V(\boldsymbol{q})$ of the system at scission has been tabulated, the probability of populating a given fragment at a given excitation energy E^* can be computed in several ways. One option is to relate it to a statistical Boltzman factor, i.e. $\propto e^{-V(\boldsymbol{q})/T}$ where T is a "collective temperature", which can be either a parameter of the model or related to excitation energy via the usual $E^* \approx aT^2$ expression [192, 325]. Another option consists in relating it to the level density in each fragment at the current excitation energy E^* [326, 327]. This latter prescription requires introducing a mechanism to share the **total excitation energy** (TXE) available among the fragments; see discussion in Section 6.4. Obviously, different assumptions can be made about the ingredients of the calculation, such as the size of the deformation space for each fragment, the specific model of the interaction between the fragments, and the method used to populate each fragmentation. Overall, scission-point models reproduce fairly well the mass yields, for example in the neutron-induced fission of major actinides [325], or the transition between symmetric and asymmetric fission in heavy actinides such as Fm isotopes [328, 329]. The models can be extended to predict other important observables such as the TKE of the reaction and the neutron emission in actinides [330].

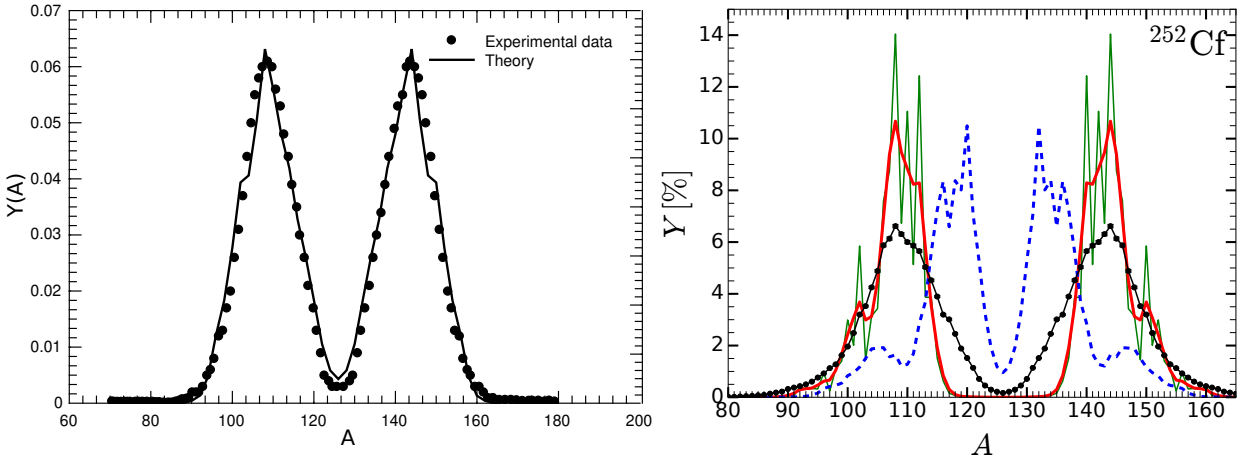

Figure 17: Primary fragments mass distribution for the spontaneous fission of ^{252}Cf. Left: Comparison of the scission point model of [331] (full line) to experimental data (black dots). Figure reproduced with permission from [331] courtesy of H. Pasca; copyright 2019 by The American Physical Society. Right: Comparison of the scission point model SPY-2 with a smoothing (full red line) to experimental data (black dotted line). The raw predictions of SPY-2 (green full line) along with the predictions of SPY-1 (blue dotted line) are also plotted for the record. Figures reproduced with permission from [327] courtesy of J.-F. Lemaitre; copyright 2019 by The American Physical Society.

_prc_2019_fig1⟩

The low computational cost of scission-point models makes systematic studies over a large range of fissioning sys-

tems possible; see, e.g., [327]. Key ingredients of these approaches include the ensemble of configurations considered in the neighborhood of scission and the details of the potential energy (25). The ensemble of scission configurations is inevitably chosen in a somewhat arbitrary way since the very concept of scission remains ill defined, as mentioned in Section 2.3. As for the nuclear potential energy, it was historically computed in the macroscopic-microscopic approach outlined in Sec. 2.1 [192, 325, 328, 328, 330] while recent versions have also relied on HFB potential energy [326, 327]. In both cases, there have been not systematic studies to propagate the uncertainties associated with either the parameters of the liquid drop model and average nuclear potential or the parameters of the energy functionals on the predictions from scission-point models. As a result, different scission-point models may predict significantly different primary fragments distributions as illustrated in the right panel of Fig. 17.

4.2. Classical Dynamics

ec:t_classical⟩

Fission is by nature a time-dependent process and one would be forgiven to think that static approaches such as the scission-point model may not capture all facets of the phenomena. Going beyond such models therefore requires describing the time evolution of the nucleus starting from its nearly spherical shape up to well-separated primary fragments. A fully microscopic theory of this process involves a quantum and real-time evolution of more than 200 nucleons characterized by their position and spin/isospin quantum numbers. The complexity of this task scales exponentially with the number of DoFs and makes it impossible to solve exactly the associated Schrödinger equation even on state-of-the-art supercomputers. A long-term goal of fission theory is thus to find reliable approximations, or reductions, of this quantum many-body dynamics that capture the physics of fission while staying computationally tractable (cf. Fig. 2).

The first possible level of approximation is based on a classical and statistical picture of the dynamics, which leads to the well-known Langevin equations. These equations have a long history in physics and we refer to the review articles [260, 332] for a detailed discussion of their various forms in the context of nuclear physics. In this section, we simply want to recall the basic form of the Langevin equations and highlight some of the results that have been obtained from their application to fission.

The Langevin equations originate from a transformation of the classical nucleonic degrees of freedom into (i) a few collective coordinates $\boldsymbol{q}(t) = (q_1(t), \dots, q_N(t))$ and their associated momenta $\boldsymbol{p}(t) = (p_1(t), \dots, p_N(t))$ (ii) the set of all remaining degrees of freedom usually dubbed intrinsic DoFs. The idea is to choose properly the collective variables such that the formation of the primary fragments is mostly independent of the detailed characteristics of the intrinsic DoFs. With this in mind, the intrinsic DoFs are often interpreted as a thermal bath interacting with the collective DoFs. The resulting Langevin equations of the system describe the dynamics of the collective DoFs and read

$$\dot{q}_\alpha = \sum_\beta B_{\alpha\beta} p_\beta, \tag{26a}$$

$$\dot{p}_\alpha = -\frac{1}{2}\sum_{\beta\gamma} \frac{\partial B_{\beta\gamma}}{\partial q_\alpha} p_\beta p_\gamma - \frac{\partial V}{\partial q_\alpha} - \sum_{\beta\gamma} \Gamma_{\alpha\beta} B_{\beta\gamma} p_\gamma + \sum_\beta \Theta_{\alpha\beta} \xi_\beta(t). \tag{26b}$$

The scalar field $V(\boldsymbol{q})$ is the potential energy, $\mathsf{B}(\boldsymbol{q}) \equiv B_{\alpha\beta}$ is the collective inertia tensor and $\Gamma(\boldsymbol{q}) \equiv \Gamma_{\alpha\beta}(\boldsymbol{q})$ the coordinate-dependent friction tensor. A dissipation term is encoded in the random force $\boldsymbol{\xi}(t)$. Its strength $\Theta \equiv \Theta_{\alpha\beta}$ is related to the friction tensor through the fluctuation-dissipation theorem, $\sum_\beta \Theta_{\alpha\beta}\Theta_{\beta\gamma} = \Gamma_{\alpha\gamma}T$, with $T \equiv T(\boldsymbol{q})$ the local temperature of the bath of intrinsic DoFs at point $\boldsymbol{q}$.

There are many different ways to compute the ingredients entering (26), that is, the fields $V(\boldsymbol{q})$, $\mathsf{B}(\boldsymbol{q})$, and $\Gamma(\boldsymbol{q})$. These quantities must be pre-computed by a nuclear model capable of giving realistic estimates of nuclear deformation properties. Traditional applications of the Langevin equation often rely on the macroscopic-microscopic model described in Section 2.1 to compute them. In addition, a popular way to determine the friction tensor is the wall-and-window formula, which describes the energy exchange between collective and microscopic DoFs in the framework of classical thermodynamics [333, 334]. All in all, these ingredients rely on 10-20 parameters typically calibrated on ground-state properties of nuclei across the whole nuclear chart [71, 72], together with a few additional parameters per fissioning system [335]. With such parameterization, the predictions typically match our experimental knowledge for the primary mass distribution of actinides within 20% at the peaks. The actual uncertainties on, e.g., the mass distributions, that result from propagating the uncertainties resulting from the calibration of the model parameters have not been rigorously quantified yet.

There have been recently a few attempts to couple microscopic inputs computed from the EDF approach with the semi-classical dynamics given by the Langevin equation [336, 337, 244, 338, 339]. In this case, $V(\boldsymbol{q})$ is the HFB energy and $\mathsf{B}(\boldsymbol{q})$ the collective inertia tensor briefly discussed in Section 3.1. Note that the friction tensor can also be computed from a microscopic approach as for instance in [340]. Along the same lines, it is very important to keep in mind that the formal and technical difficulties in determining the scission configurations discussed in Section 2.3 will be relevant when solving the Langevin equation since the end-point of Langevin trajectories typically correspond to scissionned configurations.

To obtain meaningful estimates of fission observables, the equations (26) must be solved many times, possibly with different initial conditions. These statistical fluctuations of the initial state mimic here the quantum fluctuations of the system. Because of the stochastic nature of the equation of motion, each trajectory is unique. If sufficiently many trajectories are sampled, probability distributions can be reconstructed. The full Langevin equations have thus been applied to studies of fission rates [270], to the determination of the charge and mass distribution of fission fragments [341, 335, 342], and to the evaluation of the TKE [340, 335, 343, 344, 345]. Figure 18 shows an example of the latter calculations. Finally, it is possible to include into the Langevin framework the competition between fission and the emission of light particles such as neutrons or γ rays. This is of particular interest to study multi-chance fission at high energies [346].

If the motion across the potential is strongly dissipative, it makes sense to assume that collective velocities are very small. In this case, we can neglect terms proportional to the square of the velocities as well as the acceleration terms [347, 348]. The Langevin equation takes the much simpler form of the Smoluchowski equation

$$\sum_{\beta\gamma} \Gamma_{\alpha\beta}\dot{q}_\beta = -\frac{\partial V}{\partial q_\alpha} + \sum_\beta \Theta_{\alpha\beta}\xi_\beta(t). \tag{27}$$

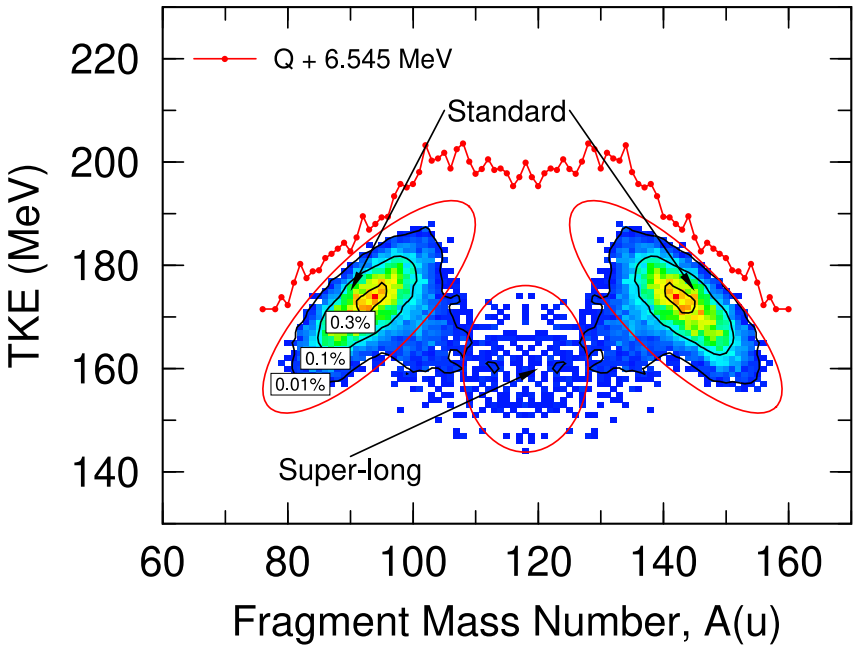

Figure 18: Distribution of TKE as a function of the fragment mass number for the fission of ^{236}U at excitation energy $E = 6.545$ MeV. The red curve represents the kinematically allowed maximal value of TKE given by $Q + E$, where Q is the Q-value of the reaction ^{235}U(n,f). Figures reproduced with permission from [343] courtesy of Usang; copyright 2017 by The American Physical Society.

⟨fig:TKE_A⟩

The Smoluchowski equation (27) was used to compute estimates of primary fission fragment distributions [347, 348, 349, 350, 351, 30]. The formalism was extended in [350] to describe fission dynamics at higher excitation energies. In the case of the macroscopic-microscopic model, the main effect of increasing excitation energy is to destroy shell corrections [99, 352, 103], although the macroscopic energy should in principle also be modified [100]. One can incorporate this effect by computing, at each deformation point $\boldsymbol{q}$ of the standard macroscopic-microscopic PES, a local temperature $T(\boldsymbol{q})$ based on the value of the relative excitation energy at this point. This local temperature can then be used to modify the Strutinsky shell correction and generate PES at finite excitation energy; see examples in [103, 353]. This approach was used in [340, 343] to analyze the impact of excitation energy on dissipation. A simplified version of temperature-dependent shell corrections consists in multiplying the shell correction by a phenomenological damping factor. Figure 19 shows the impact of the PES underpinning the random walk calculations at finite excitation energies. At temperatures $T > 1$ MeV, such an approximation works rather well and has been used in large-scale calculations in [350], but it fails to account for the more complex dependency of the yields at low excitation energies. In this regime, an alternative to temperature-dependent shell correction is to use level densities to guide the evolution of the Metropolis walk on the surface [354].

The hypothesis of strongly-damped motion was originally introduced with semi-phenomenological arguments based on the wall-and-window model for dissipation [333, 356]. Early attempts at verifying this hypothesis from more microscopic arguments related to the nuclear shell structure suggested that dissipation may be even stronger than

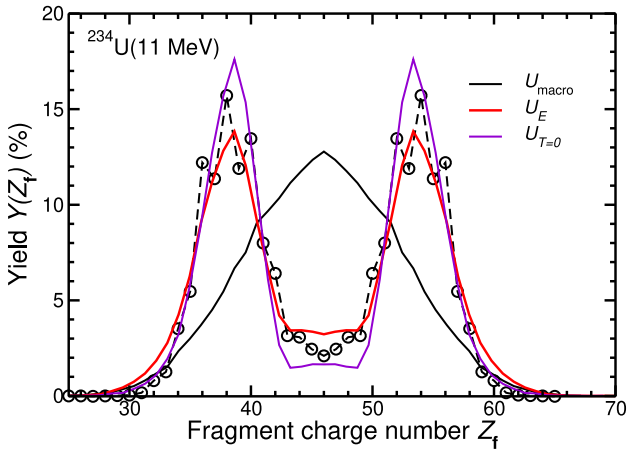

Figure 19: Relative fragment charge distribution fo the fission of ^{234}U at $E = 11$ MeV excitation energy. Each curve was obtained by solving (27) with different prescriptions for the PES: a pure liquid drop formula ($U_{\rm macro}$), the standard macroscopic-microscopic potential defined by (1) ($U_{T=0}$) and a modified version of the latter where the shell correction is multiplied by a damping factor $S(E)$ (U_E). Figures reproduced with permission from [350] courtesy of Randrup; copyright 2013 by The American Physical Society.

⟨fig:damping⟩

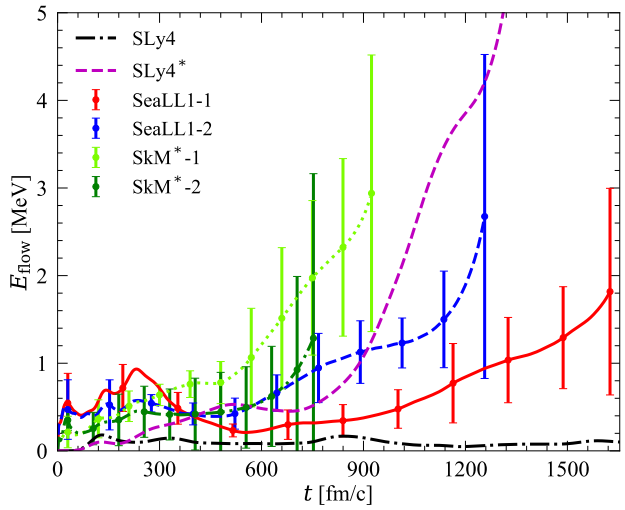

Figure 20: Collective flow energy $E_{\rm flow}(t)$ as a function of time in the fission of ^{240}Pu. Each curve correspond to a simulation with different energy functional and/or pairing characteristics. Error bars indicate variations with respect to different initial conditions. Figures reproduced with permission from [355] courtesy of Shi; copyright 2019 by The American Physical Society.

ig:dissipation⟩

anticipated [357]. Theories of dissipation based on transport models were introduced to provide a better description of the dissipation tensor in either the Langevin or Smoluchowski equations [200, 358, 359]. In recent years, fully microscopic simulations of fission based on TDHF+BCS and TDHFB also predict a strongly dissipative dynamics along with very small velocities of the one-body-density multipole moments [360, 56, 355]. This is illustrated in

Fig. 20, which shows the collective kinetic energy

$$E_{\rm flow}(t) = \frac{1}{2}\int d^3\boldsymbol{r}\, m\boldsymbol{v}^2(\boldsymbol{r},t)\rho(\boldsymbol{r},t), \tag{28}$$ {?}

in the descent from saddle to scission in the real-time simulation of ^{240}Pu. Here the local collective velocity $\boldsymbol{v}(\boldsymbol{r},t)$ is given by $\boldsymbol{v}(\boldsymbol{r},t) = \boldsymbol{j}(\boldsymbol{r},t)/\rho(\boldsymbol{r},t)$ with $\boldsymbol{j}(\boldsymbol{r},t)$ the usual current density $\boldsymbol{j}(\boldsymbol{r},t) = \frac{1}{2i}\,(\boldsymbol{\nabla}-\boldsymbol{\nabla}')\rho(\boldsymbol{r},\boldsymbol{r}',t)\big|_{\boldsymbol{r}'=\boldsymbol{r}}$ [68]. For most of the evolution, this collective energy is of the order of 1-2 MeV, which is less than 10% of the variations in potential energy and less than 1% of total energy released at scission.

4.3. Time-Dependent Density Functional Theory

sec:t_diabatic⟩

The Langevin equations and their different variants provide a computationally tractable method (cf. Fig. 2) to study the real-time evolution of a fissioning nucleus in presence of dissipation and fluctuations but they present a few limitations. For instance, a classical treatment of dynamics cannot account for tunneling effects, which is crucial for spontaneous fission. In addition, going beyond a thermal bath description of the intrinsic DoFs is necessary if one wants to predict detailed properties of the emerging fragments such as, e.g. the energy or spin of primary fragments. The goal of microscopic approaches is to overcome these limitations by describing the quantum dynamics of the many-body wave function associated with all the nucleonic DoFs. A reduction in complexity is enforced by a variational principle that limits the possible many-body wave functions to a subspace of the complete Hilbert space. Assuming that the many-body wave function remains a product state at all times leads to the time-dependent density functional theory (TDDFT). In this article, we include under the label TDDFT an arsenal of different methods including TDHF, THDF+BCS, TDHFB. A detailed discussion of how these methods are related can be found, e.g. in [141, 361]. Several important aspects of the general formalism have been presented in review articles and textbooks; see [362, 363, 364, 365, 202, 144, 68]. A more succinct presentation of the theory specifically geared toward fission theory can be found in [366].

Time-dependent density functional theory is especially relevant for fission: given an initial state, which is typically a deformed, SR-EDF solution, TDDFT describes the real-time evolution of the nucleus as it deforms all the way until the point of scission and even beyond; see Fig. 21. For instance, in [367] the dynamics is simulated up to fragments separated by a distance of 30 fm. At this stage the nuclear interaction between the fragments is negligible and the properties of the primary fragments such as their excitation energy and spin can be reliably estimated. The simplest version of TDDFT is the time-dependent Hartree-Fock (TDHF) theory which leads to the equation of motion

$$i\hbar\frac{\partial\rho}{\partial t} = \big[h[\rho(t)],\rho(t)\big], \tag{29}$$ eq:tdhf

where $\rho(t)$ is the time-dependent one-body density matrix and $h[\rho(t)]$ the Hartree-Fock mean field – the time-dependent version of the mean field h in (8). The time-dependent Hartree-Fock-Bogoliubov (TDHFB), which includes the pairing degrees of freedom in the dynamics, is obtained from (29) by doing the substitutions $\rho(t) \to \mathcal{R}(t)$ and $h[\rho(t)] \to \mathcal{H}[\mathcal{R}(t)]$; see (8). Note that practical implementations of these theories in nuclear physics always rely on an energy density functional to encode the nucleon-nucleon interaction. The predictive power of such theoretical

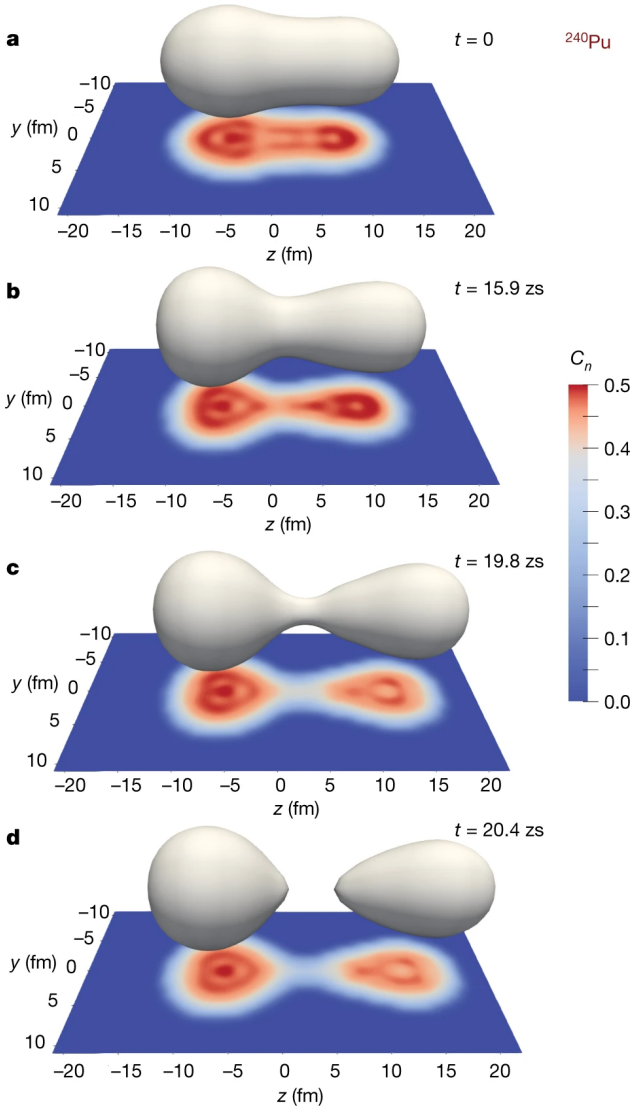

Figure 21: Real-time evolution of the one-body density in the asymmetric fission of ^{240}Pu. The predictions are obtained from a TDHF+BCS calculation. The 3D surface highlights the half-saturation density (0.08 fm^{-3}) isosurface whereas the projected color map corresponds to a localization function of the nucleons. Figures reproduced with permission from [116] courtesy of Scamps; copyright 2018 by Nature.

ture_2018_fig1⟩

approaches therefore depends on the 10 to 20 parameters associated with the energy density functional, as already mentioned in the context of spontaneous fission in Sec. 3.1.

Negele and collaborators reported the first application of the TDHF formalism to fission back in 1978 [82]. However, these initial simulations included a large number of rather strong simplifications; the earliest realistic application of TDHF to fission can probably be attributed to Simenel and Umar [368]. One important result of their work was the quantitative prediction of vibrational modes in the fission fragments (see also [369]) and the determination of a mechanism to estimate the TKE of the reaction and the excitation energy of the fragments. The implementation and release of efficient TDDFT codes without symmetry assumptions [370, 371, 372] together with the inclusion of su-

perfluidity at the BCS [373] and full HFB level [56] were key to popularize this approach. Among the most important early results was the confirmation that pairing degrees of freedom are indispensable to reach the point of scission: pure TDHF calculations initialized around the saddle point of the fission barrier in actinides failed to reach that point unless a significant boost in energy was imparted to the system [374, 375]. Including pairing degrees of freedom, even at the TDHF+BCS approximation with BCS occupation frozen after a given time, completely removed the need to introduce such boosts [373]. This mechanism naturally results from the ability of pairing correlations to pass through single-particle level crossings, as schematically depicted in Figure 22. For this reason, pairing has been dubbed the "fission lubricant". The TDDFT approach successfully predicts many properties of the average primary fission fragments such as their kinetic energy, with a precision of a few percents [56], their deformation close to scission [116], and more recently the spin of the fragments [367].

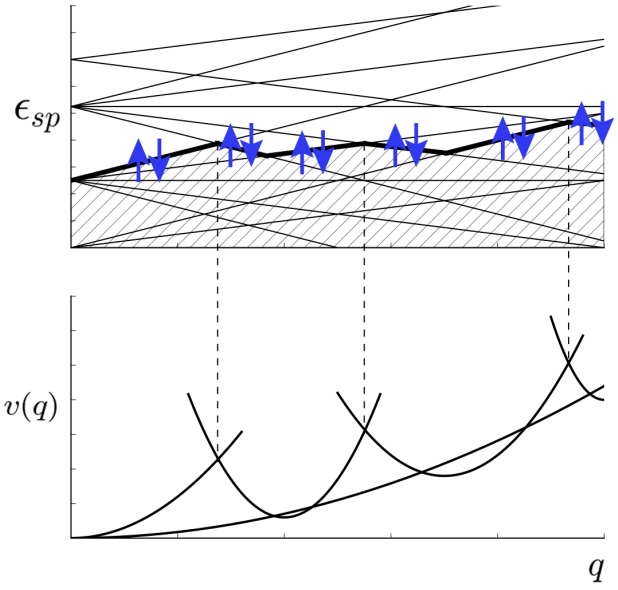

Figure 22: Top: Schematic evolution of single-particle orbitals as a function of deformation. The thick line represents the last occupied state and the up and down arrows the Cooper pairs of nucleons on that level. Bottom: corresponding evolution of the total nuclear energy. Each crossing of the s.p. level results in the transition to a new intrinsic configuration and change of the potential energy. Figures reproduced with permission from [355] courtesy of Shi; copyright 2019 by The American Physical Society.
⟨fig:crossings⟩

The TDHF and TDHFB formalisms are often called semi-classical, in the sense that they do not allow collective quantum tunneling: if a TDHF(B) evolution was initialized in a configuration $\rho(t=0)$ ($\mathcal{R}(t=0)$) inside a potential well determined from constrained HF(B) calculations, the system would remain inside that well [59]. As a practical consequence, the initial state of such calculation for fission always lies after the saddle point with a rather large deformation. Various extensions of the TDDFT methods to imaginary time have been proposed to handle quantum tunneling but have rarely been applied in practical calculations [230, 231, 376, 232, 234, 235]; see also Section 3.1.

In spite of its advantages, current implementations of TDDFT are also not well adapted to describing large fluctuations of observables, i.e. the quantity $\langle \Delta \hat{O}^2(t) \rangle = \langle \hat{O}^2(t) \rangle - \langle \hat{O}(t) \rangle^2$ [363, 377, 365]. This limitation stems from the restriction of the many-body wave function to a Slater or Bogoliubov state that does not encode enough correlations. As a result TDDFT predictions capture well the features of the *average* fragmentation but systematically underestimate the associated quantum fluctuations. For this reason, they are not the most efficient tools to generate, e.g., fission fragment distributions. There have been several attempts to go beyond "simple" TDHF(B). In the stochastic mean field theory, random fluctuations of the density matrix are used to generate an ensemble of trajectories (in the space of density matrices) that are similar to TDHF [378, 379, 380]. This trick allows extracting reasonable estimates of kinetic energy distributions but the quantum coherence of the system is lost. Other on-going investigations along this line simply introduce various phenomenological terms simulating dissipation and fluctuations in the TDHFB equation [381]. The Time-dependent RPA as well as the Balian-Veneroni variational principle are other approaches that could be used, in principle, to get additional fluctuation while retaining quantum coherence [365, 382], but it has only been applied in heavy-ion collisions so far [196, 383]. Another possibility consists in mixing TDDFT trajectories in the quantum-mechanical sense: early attempts were based on TDHF trajectories [384] while more recent ones rely on full TDHFB solutions (albeit in a simplified system) [385].

As discussed in the previous section, the strongly dissipative nature of fission is another result that had been invoked as a reasonable hypothesis by many authors and was observed in the context of TDHFB simulations [360, 56, 355]. However, whether this strong dissipation would remain when exploring a larger variational space than in current implementations of TDDFT, e.g., involving a quantum mixing of time-dependent mean-field states with different deformations at any given time, is yet to be determined. Finally, note that dissipation is also largely caused by pairing correlations: the same mechanism that allows the system to go across single-particle crossings explains both that the system can deform sufficiently up to scission *and* that the collective energy is dissipated into changes of intrinsic configurations [386].

4.4. Time-Dependent Generator Coordinate Method

bsec:TDGCM_GOA⟩

Because of the many successes of collective approaches, from the seminal paper of Bohr and Wheeler to the predictions of fission isomers, spontaneous fission half-lives or fission fragment distributions, there is a rather large consensus that fission can be well described by invoking a few collective variables such as shape deformations. This idea motivates the search for approaches reducing the complete quantum many-body dynamics to an evolution in a small-dimensional collective space. The ATDHF theory mentioned in Section 3.1 in the context of spontaneous fission [387, 388, 389, 390], and its ATDHFB extension with pairing [391], are the poster child of this philosophy. They reduce the complexity of TDDFT, which involves all the one-body degrees of freedom, to a classical collective dynamics on a manifold parameterized by a few collective variables [59]. Another approach leading to a quantum collective dynamics is the time-dependent generator coordinate method (TDGCM) and especially its Gaussian overlap approximation (GOA). Note that re-quantizing the ATDHFB theory leads in fact to an equation of motion similar to the TDGCM+GOA. The theoretical framework of the TDGCM is presented in great details in [324]. In this section,

we will thus discuss only the case of the TDGCM under the Gaussian overlap approximation which is, as of today, the only quantum microscopic approach that has been tested in predictions of actual primary fragments distributions.

The first step of the TDGCM approach consists in building an ensemble S of generator states (sometimes referred to as a collective path) parameterized by a few collective variables $S = \{|\Phi(\boldsymbol{q})\rangle \, | \boldsymbol{q} \in \mathbb{R}^N\}$. In the context of fission the generator states are most often time-even Bogoliubov states obtained by solving the constrained HFB equations as discussed in Section 2.2. The collective variables are typically related to the first multipole moments of the one-body density in order to encode the physics of deformation. With this family of generator states, the TDGCM proceeds with a variational principle applied to the Hill-Wheeler ansatz for the wave function

$$|\psi(t)\rangle = \int_{\boldsymbol{q}} f(\boldsymbol{q},t)|\phi(\boldsymbol{q})\rangle d\boldsymbol{q}. \tag{30}$$ eq:tdgcm_ansat

The time-dependent mixing function $f(\boldsymbol{q},t)$ is the direct variational unknown but it is often more convenient to deal with a transformed function $g(\boldsymbol{q},t)$ that could be interpreted as a wave packet in the collective space. All operators associated with physical observables can also be mapped onto operators acting on the collective space (a subspace of functions of the $\boldsymbol{q}$ variable) [177]. Under the Gaussian overlap approximation in its simplest form, the equation of evolution for the collective wave function reduces to

$$i\hbar\frac{\partial}{\partial t}g(\boldsymbol{q},t) = \left[-\frac{\hbar^2}{2}\sum_{\alpha\beta}\frac{\partial}{\partial q_\alpha}B_{\alpha\beta}(\boldsymbol{q})\frac{\partial}{\partial q_\beta} + V(\boldsymbol{q})\right] g(\boldsymbol{q},t), \tag{31}$$ eq:evolution0

where $V(\boldsymbol{q})$ is the potential energy and $\mathsf{B}(\boldsymbol{q}) \equiv B_{\alpha\beta}$ is the collective inertia tensor. The potential energy and collective inertia have the same meaning as in Section 4.2 and Section 3.1. An important point is that these quantities derive from the variational principle and are, respectively, the zeroth- and second-order derivatives of the reduced Hamiltonian kernels between the generator states. After the determination of these quantities, (31) needs to be numerically integrated in time starting from a given initial state. Initial states used in the literature are typically a collective wave packet $g(\boldsymbol{q}, t = 0)$ mostly localized at low deformations inside the first potential well. The impact of various prescriptions for the initial state on the predictions of the fragments properties is discussed in [392, 393, 394].

The adaptation of the TDGCM+GOA formalism to fission dynamics was performed in the 1980's [395, 151]. These initial developments led to the first prediction of fission fragment mass distributions in a completely microscopic theory [392]. Advances in computing capabilities and new algorithmic developments [396, 397] renewed interest in this approach in the 2010's. Since then, the theory has been applied largely to compute the charge, mass and isotopic primary mass distributions of fission fragments [398, 393, 394, 399, 400, 401, 402, 403]. Figure 23 shows an example of such calculations for the primary mass distribution $Y(A)$ in ^{236}U and ^{240}Pu extracted from the solution to the TDGCM+GOA evolution equation.

Obviously, results of TDGCM+GOA calculations will depend on the choice and number of collective variables, the choice of an energy density functional and, in the context of fission, the choice of an initial state and definition of scission configurations. We already mentioned the recent introduction of pairing collective variables [216, 220, 217] for spontaneous fission; very few TDGCM calculations have been performed in such extended spaces [413]. Let us highlight an interesting attempt to use the collective variables $D = |z^{(1)}_{\mathrm{CM}} - z^{(2)}_{\mathrm{CM}}|$ and $\xi = |A_1 - A_2|/A$, with $z^{(i)}_{\mathrm{CM}}$ the

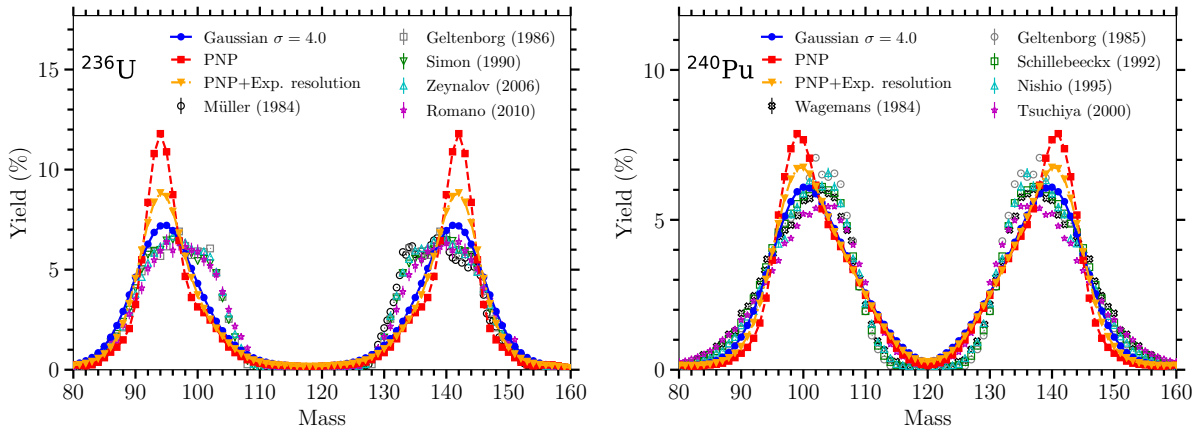

Figure 23: Left: Fission fragment mass distribution of ^{236}U for thermal neutrons obtained by solving the TDGCM+GOA equation with the SkM* parameterization of the Skyrme EDF, compared with experimental data taken from [404, 405, 406, 407, 408, 409, 410, 411, 412]. The raw TDGCM+GOA results are convoluted following three different methods that yields the blue circles, the red squares and the orange triangles. Right: Same quantity for ^{240}Pu. Figures reproduced with permission from [403] courtesy of Verriere; copyright 2021 by The American Physical Society.

⟨fig:YA⟩

coordinate of the center of mass of fragment i and A_i its total number of particles [398, 37]. Such coordinates, which were inspired by classical shape parameterizations, are much better adapted to describing fission fragments than the standard multipole moments and cover most of the set of all possible fragmentations. The role and importance of the collective inertia tensor also remains an open problem, and it is not clear if it has as large an impact for induced fission as it has for spontaneous fission. Similarly, the role of time-odd collective momenta, which have been neglected so far, is worth investigating since they provide the proper asymptotic values of the collective inertia (at least in the case of translations) [204, 177]. A preliminary study of these terms in the static case of particle number projection suggests a large effect [414]. A first attempt to solve the exact TDGCM without the GOA was also reported in [415].

Finally, a major limitation of the current implementations of the TDGCM is to rely only on constrained HFB states with the lowest energy for a given constraint. This causes discontinuities in the manifold of generator states that break down the GOA [416, 417]. In addition, TDDFT calculations have shown that the most probable path toward fragmentation involves HFB states with significant intrinsic excitation energy. The very fact that fission fragments emit light particles (cf. Section 5) proves that they are produced in an excited state. With the standard family of generator states, the ansatz (30) can not model such effects, which prevents the TDGCM from describing properly the dynamics in the neighborhood of scission. In a pragmatic approach, the description of fission dynamics with the TDGCM should therefore always be stopped with di-nuclear configurations before scission, where the two prefragments still significantly interact by nuclear forces. A possible way to overcome this issue consists in expanding the collective space to include intrinsic excitations, e.g., sets of two-quasiparticle states built on top of constrained HFB vacuua [418]. Such an extension would allow incorporating both some amount of collective dissipation in the theory and the possibility to describe excited nascent fragments. Another possibility consists in solving (31) on a manifold of finite-temperature HFB states [400], even if the TDGCM+GOA framework has not yet been properly defined at finite

temperature. Let us also mention an alternative approach that consists in deriving a quantum theory of transport that combines a GCM description of collective dynamics with quantum statistics to account for thermal excitations and dissipation [419].

4.5. *Comments on Adiabaticity and Dissipation*

sec:adiabatic⟩?

The TDGCM, ATDHFB and adiabatic self-consistent collective (ASCC) methods are often referred to as adiabatic theories of large-amplitude collective motion. However, while this adjective has a clear definition in classical thermodynamics, it is often employed with a different (or several different) meaning(s) in fission theory and the theory of large-amplitude collective motion in general. In the literature, the concept of adiabaticity has been used as a proxy for three very different hypotheses, which are sometimes combined: (i) the collective motion, i.e., the change of shape leading to fission, is very slow [294, 386], (ii) the coupling between the collective degrees of freedom and single-particle, or intrinsic degrees of freedom is so small that it can be neglected [420, 204, 421] and (iii) the intrinsic DoFs stay in the lowest-energy configuration while the collective variables evolve [418, 360]. The differences between these definitions together with rather arbitrary definitions of collective and intrinsic excitations may lead to confusions. We discuss below some common pitfalls related to this topic.

As a first example, TDDFT calculations clearly suggest that the collective motion is strongly dissipative, i.e. the shape of the system evolves slowly and toward configurations which minimize the collective potential energy while the system populates single-particle states with high energies [373, 56, 355]. Overall, TDDFT predicts time scales in the range of $10^{-20} - 10^{-19}$ s to go from the saddle point to scission. On the one hand, this very slow collective motion justifies the reduction of TDDFT dynamics to its adiabatic counterparts, specifically, the hypothesis of small collective momenta that underpin, e.g., the ATDHF(B) theory [387]. On the other hand, TDDFT dynamics is often qualified of diabatic in the sense of point (iii) above, because excited single- or quasi-particles states are populated. One should thus be very careful when employing the adjective of adiabaticity to refer to slow collective motion.

The definition (ii) of adiabaticity is often meant to refer to the dissipation of energy from the collective DoFs to the intrinsic ones. Such dissipation is known to be a crucial ingredient in the Langevin dynamics as mentioned in Section 4.2. It appears in the form of the friction and random force terms in the collective equation of motion. The TDDFT picture does not give direct insight into such dissipation since it does not rely on an explicit splitting of the DoFs between collective and intrinsic. It is possible to estimate *a posteriori* the kinetic energy associated with any collective variable represented by a local one-body operator [360]. Such an approach suggested a strong dissipation of the quadrupole moment kinetic energy during the fission dynamics. With this in mind, it might seem puzzling that the ATDHF(B) approach based only on the assumption of slow collective motion (which seems to be valid) yields a collective equation of motion with no friction or dissipative terms [59]. In addition, the TDGCM produces primary fragments distributions similar to the one obtained by Langevin approaches while also introducing no explicit friction term. This suggest that primary fragments mass/charge distributions are simply not very sensitive to dissipation. In contrast, predictions of the excitation energy of the primary fragments, which are not well described by TDGCM, are a much better probe into the dissipation mechanism.

In the case of ATDHF(B), there is another deeper reason for the absence of a collective dissipation mechanism. Contrary to the current implementations of TDGCM, which rely on a set of constrained HFB generator states, the collective path in the original formulation of the ATDHF(B) approach is determined out of the time-even component of the states along a TDHFB trajectory. These states can already contain significant single- or quasi-particle excitations and only the small energy component related to the residual time-odd part needs to be taken into account by the collective dynamics. Following this idea, [420] builds the collective path from a variational principle that decouples *by design* the collective dynamics from other DoFs. This philosophy was formalized in the development of the ASCC model, which generalizes ATDHF theory while solving some of its inconsistencies [212, 422, 202, 144, 68]. In other words, the collective phase space constructed formally in these approaches is in fact completely different from the one used either in current TDGCM implementations or in Langevin approaches. Therefore, it is very possible that some theories require an explicit treatment of collective dissipation while others do not. The presence and strength of dissipative terms in the collective equation of motion strongly depends on the arbitrary choice of the collective phase space. One should keep this in mind while discussing adiabaticity in the sense of point (ii) above or comparing the dissipative features of various theories.

4.6. Ternary Fission

Ternary fission is the rare process where the fission of a heavy element is accompanied by the emission of an α particle or, much less frequently, a light nucleus ranging from Lithium ($Z = 3$) to Oxygen ($Z = 8$) isotopes [423, 424]. More precisely, it is the (quasi)-simultaneous divide of the fissioning nucleus in three fragments – one of them much lighter than the others. This phenomenon is usually quantified by the α-emission probability P_α or, equivalently, the relative number N_α of emitted α over the entire number of fission events N_f [425]. Ternary fission does not lend itself easily to a description in terms of geometric collective variables as discussed in Section 2 unless one enforces some amount of clustering, e.g. via a three-center basis [426] or an explicit 3-body model with phenomenological α-N interaction potentials [427]. Neither can such a process be easily simulated by the simple ansatz of TDDFT, where the nuclear wave function is a "standard" product state of particles or quasiparticles. In fact, the proper quantum-mechanical treatment of ternary fission should probably include a mechanism to rigorously simulate nuclear clustering. For these reasons, all models of ternary fission tend to be rather phenomenological. Probably the most advanced one relies on estimating P_α by solving the time-dependent Schrödinger equation for the α particle moving in a time-dependent mean-field potential, which is obtained by simply parametrizing with t specific trajectories across the potential energy surface [428, 429]. Alternative methods involve the random-rupture neck model, where it is assumed that the neck between the prefragments ruptures at two different locations nearly simultaneously, the part of the neck between these two locations forming the light particle [430]. The rupture-neck model was also combined with statistical theory (see Section 4.1) to account more realistically for the available excitation energy at scission [431].

5. Emission of Light Particles

c:deexcitation⟩

After the scission point, nuclear forces between the two fragments quickly drop to zero while Coulomb repulsion drives the acceleration and kinematics of the fission fragments. This is the acceleration phase of the fragments. We can estimate an order of magnitude for the time scale of the acceleration from the classical dynamics of two point-like particles. Let us consider an initial situation where the surfaces of the two fragments are separated by a distance of a few fermis and neglect the relative velocity between the fragments at this stage. Integrating the classical equation of motion results in a fast acceleration of the two fragments that reach 90% of their final speed (2-5% of the speed of light) within 5 zs. Within this time range, the fragments typically cover a distance of several tens of fermis.

The large deformation of the prefragments at scission, the effect of the Coulomb repulsion on the inhomogeneous charge densities in the fragments, as well as the internal excitation created during the descent from the saddle point to scission produce two excited fragments far from their ground-state equilibrium. On average, about 30 MeV of excitation energy is shared between the two fragments in the fission of an actinide while several theoretical and experimental arguments indicate that the typical spin of the fragments lies in the range of 5-12 $\hbar$ units (cf. Section 6). The primary fragments lose their energy mostly by emitting neutrons and γ rays. The post-neutron pair of fragments resulting from this neutron emission phase are called secondary fragments. Further β decays and possible delayed neutron/γ emission may follow this process leading to a final pair of nuclei, the fission products; see Fig. 1.

The characteristics of the emitted fission neutrons and γ rays, such as their multiplicity and energy spectrum, are key nuclear data for energy applications and give stringent constraints on our understanding of the primary fragments formation. State-of-the-art theoretical approaches predicting these observables generally rely on a statistical deexcitation model to simulate cascades of particle emissions from the excited fragments. In the specific case of fission, such deexcitation simulations have to be repeated for every combination of primary fragments pairs and set of relevant initial properties that may impact the evaporation process. These generally include the kinetic energy, excitation energy, spin and parity of the primary fragments. The final observables are then obtained by averaging fission events both over the large set of primary fragments configurations as well as over the set of deexcitation cascades for each of these configurations. Each event is weighted by its associated probability of appearance. This averaging can be performed in a deterministic way [432] as long as the phase space considered for fission events is small enough. For more detailed descriptions of deexcitation cascades including for instance the spin of the emitted particles the phase space of fission events becomes so large that fragments deexcitation models often turn to a Monte-Carlo estimation [433] of observables. In this case, the code samples a large but limited number of fission events according to their probability distribution and the observables are deduced as averages over these events.

The success of such approaches relies on high-accuracy and high-precision estimates of the primary fission fragment distributions, especially for the total kinetic energy, which directly determines the total energy available for neutron/γ emission. As a consequence, it is customary to rely mostly on experimental data or empirical models for the primary fragments distributions. In this section we will give an overview of such empirical treatments. More recent efforts geared toward replacing progressively these inputs by genuine predictions from microscopic theories will be discussed in Section 6.

Code	PbP [432]	GEF [434]	FREYA [435]	CGMF [290]	FIFRELIN [57]
Pre-fission emission	–	n_{pe},n_{stat},γ	n_{pe},n	n,γ	–
Wide range of fissioning systems	no	yes	no	no	no
Neutron-γ competition	no	yes	partial	full	full
Gamma deexcitation	no	yes	yes	yes	yes
Deexcitation model	Weisskopf	Weisskopf	Weisskopf	Hauser-Feshbach	Hauser-Feshbach
Statistical fluctuation	no	no	no	no	yes
Open-source	no	yes	yes	yes	no

Table 1: Summary of some features of fission fragments deexcitation models. In the pre-fission emission row, n_{pe} denotes pre-equilibrium neutrons and n_{stat} corresponds to statistical neutrons. 'Statistical fluctuation' denotes taking into account fluctuations of nuclear structure properties on top of average quantities such as the level density and the averaged partial widths.

itation_models⟩

The statistical description of nuclear deexcitation cascades is by itself an old problem quite independent of fission studies. It started with the seminal paper of Weisskopf in 1937, which was concerned with the spectrum of neutrons emitted from highly excited nuclei [281]. Grover and collaborators pioneered the use of the Hauser-Feshbach model of deexcitation for the study of neutron, γ and α evaporation [436, 437, 438] and published the first study quantifying the impact of the spin of the fission fragments on such decays [439]. Many of the developments of statistical reaction theory in the 1970's and 1980's aiming at going beyond Hauser-Feshbach theory [288, 289], which were briefly mentioned in Section 3.2.2, were not really tested in practical simulation of fission fragment decay. Interest for this subject surged in the 2000's, especially because of the growing issue of γ heating in nuclear reactors [440, 441, 442] as well as the development of new technologies such as neutron/γ interrogation or advanced Monte-Carlo simulations of detection devices.

Today, several codes, implementing different models, are dedicated to the description of fission fragment deexcitation. In this section we will only review the most commonly-used and complete ones: FREYA [435], GEF [434], CGMF [290], FIFRELIN [57] and the Point-by Point-(PbP) [432] model. We summarize in Table 1 the main features of these codes. The more recent code HF^3D [443, 444] will not be discussed since it implements a similar physics as CGMF with a different numerical resolution (deterministic for HF^3D versus Monte Carlo for CGMF). Other codes implement nuclear deexcitation cascades for specific applications, for example GEMINI++ for the deexcitation of fragments produced in heavy-ion reactions [445]. Conversely, general-purpose codes such as TALYS [446] or EMPIRE [447] have a much broader scope of applications and aim at describing any type of nuclear reactions. For the sake of completeness, let us also mention the work of Lestone [448] focused on the very precise reproduction of the prompt fission neutron multiplicities, spectrum and angular correlations.

5.1. Distribution of Primary Fragments Properties

The properties of the primary fission fragments could in principle be obtained as the result of a statistical or dynamical approach to the large-amplitude collective motion as outlined in Section 4. However, one should keep in mind that

predictions of prompt particle emission are very sensitive to the characteristics of the primary fragments. For instance, microscopic theories can predict the kinetic energy of the fragments at best within a few percent precision [355]. In the fission of an actinide, this would typically lead to an uncertainty of a few MeV on the total excitation available for deexcitation, which would translate into a $0.5 - 1$ uncertainty on the average prompt neutron multiplicity. For comparison, measurements of the prompt neutron multiplicity can typically reach precision below one percent ($\simeq 0.015$ neutrons for ^{252}Cf spontaneous fission in [449]).

Adopting a pragmatic strategy, most fragments deexcitation models thus start by estimating the primary fragments distributions either by directly using some available experimental data or by relying on empirical models previously calibrated on a set of experimental measurements. These fragment distributions are then used as an input to the statistical deexcitation model. Note that such an approach discards any quantum correlations between the various primary fragments configurations. Let us highlight the different ingredients and models used to determine the empirical distribution of the primary fragments configurations.

Proton and neutron numbers. The principal characteristics of the primary fragments configurations are the number of protons and neutrons in each fragment. In the standard approach the probability distribution that fission produces a fragment with a number of mass A_f and a number of charge Z_f given the excitation energy E of the compound system is factorized into

$$P(A_\mathrm{f}, Z_\mathrm{f}|E) = Y(A_\mathrm{f}|E)P(Z_\mathrm{f}|A_\mathrm{f}). \tag{32}$$ {?}

The factor $Y(A_\mathrm{f}|E)$ stands for the primary mass distribution whereas $P(Z_\mathrm{f}|A_\mathrm{f})$ accounts for the charge probability distribution given the mass number A_f. The complementary fragment is always determined through mass and charge conservation (i.e. ternary fission is neglected)

$$A_\mathrm{f2} = A_\mathrm{CN} - A_\mathrm{f1}, \qquad Z_\mathrm{f2} = Z_\mathrm{CN} - Z_\mathrm{f1}. \tag{33}$$ {?}

Fragments deexcitation models assume a normal distribution for the charge with a mass-dependent mean $\bar{Z}_\mathrm{f}(A_\mathrm{f})$ and standard deviation $\sigma_Z(A_\mathrm{f})$,

$$P(Z_\mathrm{f}|A_\mathrm{f}) \propto \exp\left[-\frac{1}{2}\left(\frac{Z_\mathrm{f} - \bar{Z}_\mathrm{f}(A_\mathrm{f})}{\sigma_Z(A_\mathrm{f})}\right)^2\right]. \tag{34}$$ {?}

The mean of this distribution is either directly determined from the Unchanged Charge Distribution (UCD) approximation (as in FREYA) or includes an additional polarization charge effect. In the later case, the polarization of charge is parameterized as a function of A_f (PbP model) or estimated from the Wahl's systematics [450] (FIRELIN, CGMF).

As for the mass distributions, a possible strategy relies on using experimental data, either in tabulated form, or described in terms of a few fission modes [184]. The codes FIFRELIN and PbP model implement such an approach, which is limited to the few fissioning systems and energies for which experimental data is available. To overcome this issue, several deexcitation models favor a description of the primary mass yields as a sum of a three or five Gaussians. For a given fissioning system, the mean (average mass), the width, and the weight of each Gaussian (also known as fission mode) are fitted to reproduce a set of experimental data spanning a range of excitation energies. For example, the code CGMF implements a parameterization of the mass yields with 3 Gaussians whose means and widths linearly

depend on the excitation energy [444, 290]. A similar technique is adopted in FREYA based on five Gaussians with energy-independent means and a quadratic dependency of the widths [451]. Such an approach enables systematic studies of prompt particles emission as a function of the energy in the input channel. Because of the dependency on experimental data, this approach only enables calculations on a few well-known fissioning systems.

Going one step further, the philosophy of the GEF code is to provide an empirical yet systematic estimation of the mass yields for a wide range of energies and fissioning systems. In this model, the fissioning system is described by an elongation degree of freedom coupled to several transverse collective DoFs such as the mass of the fragments, and to a thermal bath describing the remaining degrees of freedom. The distribution of proton and neutron number of the fragments is determined from a two-step statistical process guided by the physics of the collective dynamics,

$$P(A_\mathrm{f}, Z_\mathrm{f}) = P(\mathrm{mode})P(A_\mathrm{f}, Z_\mathrm{f}|\mathrm{mode}). \tag{35}$$ {?}

In the first step, a statistical population of the available states in the neighborhood of the outer saddle point gives the probability for the system to choose a particular fission mode. The probability associated with a fission mode $P(\mathrm{mode})$ is proportional to

$$P(\mathrm{mode}) \propto \exp\left(-\frac{E^0_\mathrm{mode}}{kT}\right), \tag{36}$$ {?}

where E^0_mode is the minimum of the potential energy of the mode at an elongation corresponding to the outer barrier, relatively to the energy of the lowest mode, and T is the temperature of the system. In practice, five to seven modes are considered. In the second step, the distribution of particle numbers in the fragments $P(A_\mathrm{f}, Z_\mathrm{f}|\mathrm{mode})$ is determined from the properties of the system close to scission. The potential energy surfaces in the transverse directions associated with either the charge or mass number are described as harmonic potentials functions of Z and A with a minimum value at Z_mode and A_mode. A second statistical population of states in the neighborhood of scission configuration then leads to the following distribution in each mode:

$$P(A_\mathrm{f}, Z_\mathrm{f}|\mathrm{mode}) = P(A_\mathrm{f}|\mathrm{mode})P(Z_\mathrm{f}|A_\mathrm{f}, \mathrm{mode}), \tag{37}$$ {?}

with

$$P(A_\mathrm{f}|\mathrm{mode}) \propto \exp\left(-\frac{(A_\mathrm{f} - A_\mathrm{mode})^2}{2\sigma^2_{A,\mathrm{mode}}}\right), \quad P(Z_\mathrm{f}|A_\mathrm{f}, \mathrm{mode}) \propto \exp\left(-\frac{(Z_\mathrm{f} - Z_\mathrm{mode})^2}{2\sigma^2_{Z,\mathrm{mode}}}\right). \tag{38}$$ {?}

The widths $\sigma_{A,\mathrm{mode}}$ and $\sigma_{Z,\mathrm{mode}}$ depend on the energy balance estimated for each mode. Note that a special treatment involving a non-harmonic potential is applied to the Standard 2 mode (S_2). The GEF model finally includes the odd-even staggering of the fission yields as an additive correction based on an equal-filling assumption of the intrinsic states. Overall, the determination of the primary fission yields relies on a set of free parameters that are calibrated to a large body of experimental data, which includes high-resolution data from inverse kinematic experiments [452]. This approach is then capable of estimating systematically and with good accuracy the primary fragments yields as a function of the mass, charge and energy of the fissioning nucleus. This feature is quite unique, and other fragment deexcitation models sometimes directly take the yields predictions from GEF as an input to their own deexcitation engine [453, 454, 455].

Energy sharing. The excitation energy available in each primary fragment before particle evaporation is a crucial ingredient, since it is the primary driver of the prompt neutron emission. To estimate this quantity for any given mass and charge split, most of the deexcitation codes rely on an energy balance of the system before the reaction and after the complete acceleration phase of the fragments. For neutron-induced fission, the energy balance reads [442]

$$\mathrm{TXE} + \mathrm{TKE} + M(Z_\mathrm{H}, N_\mathrm{H}) + M(Z_\mathrm{L}, N_\mathrm{L}) = M(Z, N) + S_n(Z, N) + E_n, \tag{39}$$

eq:energy_bala

where $M(Z, N)$ is the mass of the nucleus (Z, N), S_n the neutron separation energy in the nucleus (Z, N), E_n the energy of the incident neutron in the center of mass frame, TXE the total excitation energy available to both fragments, and TKE the total kinetic energy of the fragments. In the case of spontaneous fission, this formula can be applied with $S_n = E_n = 0$; for photofission, $S_n = 0$ and $E_n \equiv E_\gamma$. The evaluation of masses and neutron separation energy is performed on a regular basis (see [456, 457] for the latest one) and data are available in nuclear structure databases such as ENSDF [29], leaving only the total kinetic energy and the total excitation energy to determine. Because of the quantum fluctuations in fission, we can treat TKE as a random variable with a large variance. In fragments deexcitation codes, its probability distribution is typically assumed Gaussian [290] with a mean and variance that depend on the mass split

$$P(\mathrm{TKE}|A_\mathrm{f}, Z_\mathrm{f}, E) \propto \exp\left[-\frac{1}{2}\left(\frac{\mathrm{TKE} - \overline{\mathrm{TKE}}(A_\mathrm{f})}{\sigma(A_\mathrm{f})}\right)^2\right]. \tag{40}$$

eq:tke_distribu

These moments of the probability distribution are in general extracted from experimental measurements of the fragments kinetic energies (e.g. see [458]) and may also include a dependency on the energy of the entrance channel [290]. Combining equations (40) and (39) yield a distribution of probability for the total excitation energy TXE available for the emission of particles.

Note that such a scheme neglects the possible emission of particles (especially neutrons) before the complete acceleration of the fragments. Although this hypothesis is strongly supported by the angular distribution of the prompt neutrons [404], which is peaked at forward angles, it remains an open question whether, and to which extent, some of the neutrons are emitted before the complete acceleration. Numerous papers from the 2010's attempt the challenging prediction of scission neutrons and/or pre-acceleration neutrons based on a time-dependent average nuclear potential approach [459, 460, 461]. Other studies were performed based on static potentials [462] and even on a full TDHFB calculation [56]. As of today, no clear consensus exists between the results of these theoretical approaches, and experimentally verifying their predictions remains difficult. In practice, most deexcitation codes neglect this kind of neutron emission.

After the determination of the total excitation energy available, one still needs to split this energy between the two fragments. This energy sharing results from the complex competition between various energy reservoirs (intrinsic energy, deformation energy, etc) that interact with each other during the fission dynamics. The repartition of the energy strongly depends on the mass of the fragments and it is expected to be highly correlated with the prompt neutron multiplicity $\bar{\nu}(A)$. Fragments deexcitation codes therefore rely on empirical laws for the total excitation energy sharing, which are guided by, or directly fitted on, this neutron multiplicity. The code CGMF assumes for instance that the excitation energy is of thermal nature and build an empirical law for the temperature of the fragments

as a function of its mass number. The code FREYA follows a similar approach with the introduction of a parameter that governs the ratio of temperatures of the two fragments. In FIFRELIN, the excitation energy in each fragment is recast into the sum of a rotational and a thermal contribution, with again a mass-dependent temperature ratio. The point by point model (PbP) describes the excitation energy in terms of a thermal excitation and a deformation component that depends on the mass. Finally, the GEF model shares the major part of TXE according to a maximum entropy principle at scission and the remaining collective kinetic energy is split evenly between the fragments. Despite the apparent diversity of assumptions in all the models, we note that the shape relaxation and the mass split dependency are the key ingredients that enable all these models to reproduce a sawtooth shape for the neutron multiplicity $\bar{\nu}(A)$.

Spin-Parity Distribution. As will be shown in Section 5.2, the spin distribution of the fission fragments plays a very important role in setting the photon multiplicities, i.e., the average number of photons emitted during the deexcitation. The statistical theory assumes that the probability for a nucleus to have spin J is approximately given by [463]

$$p(J) \propto (2J+1)\exp\left[-\frac{1}{2}\frac{(J+\frac{1}{2})^2}{\sigma^2}\right], \tag{41}$$ eq:spin_distri

where σ is called the spin-cutoff parameter. Note that the spin-cutoff parameter is proportional to the expectation value $\langle \hat{J}^2 \rangle$ of the total angular momentum in the system – the mean of the actual distribution $p(J)$ [464, 465]. In the Fermi gas model, it is proportional to the moment of inertia of the system as well as to its temperature (or excitation energy) [466]. Given this background, we can now summarize the different features of each deexcitation code:

- CGMF – The spin of each fragment is sampled from the distribution (41). The spin-cutoff parameter is explicitly parametrized by the product of the nuclear moment of inertia $\mathcal{I}$ and temperature T. The Z- and A-dependence of $\mathcal{I}$ is taken into account but not the variations as a function of deformation, angular momentum or temperature [290]. There is no constraint on the relative angular momentum between the fragments.

- FIFRELIN – The treatment of the spin is very similar to CGMF, but with an additional constraint used to simulate the damping of shell effects with increasing temperature [467, 468].

- FREYA – This code uses a semi-classical treatment of angular momentum [469]. It assumes that the system can be treated as a dinuclear (binary) system of a heavy and a light fragment, each characterized by their moments of inertia $\mathcal{I}_H$ and $\mathcal{I}_L$ and spins $\boldsymbol{J}_H$ and $\boldsymbol{J}_L$, as well as a relative angular momentum $\boldsymbol{L}$. Angular momentum is thus explicitly conserved in this treatment. The total rotational energy of the dinuclear system is then expressed in terms of specific rotational modes, which are sampled separately based on a statistical formula [470]. The dependency on nuclear structure inputs is encoded in the nuclear moments of inertia which, in most applications of FREYA, was approximated by its A-dependent rigid-body value. This approximation was improved recently following guidance from microscopic calculations [469].

- PbP – The spin of the fragments is not taken into account.

- GEF – As for CGMF and FIFRELIN, the spin of the fragments is sampled from (41), but this is only done for the post-statistical emission spin. The statistical neutron and γ emission is spin-independent.

Without any strong physical arguments as for the parity of the primary fragments, all these models assume equiprobable parities.

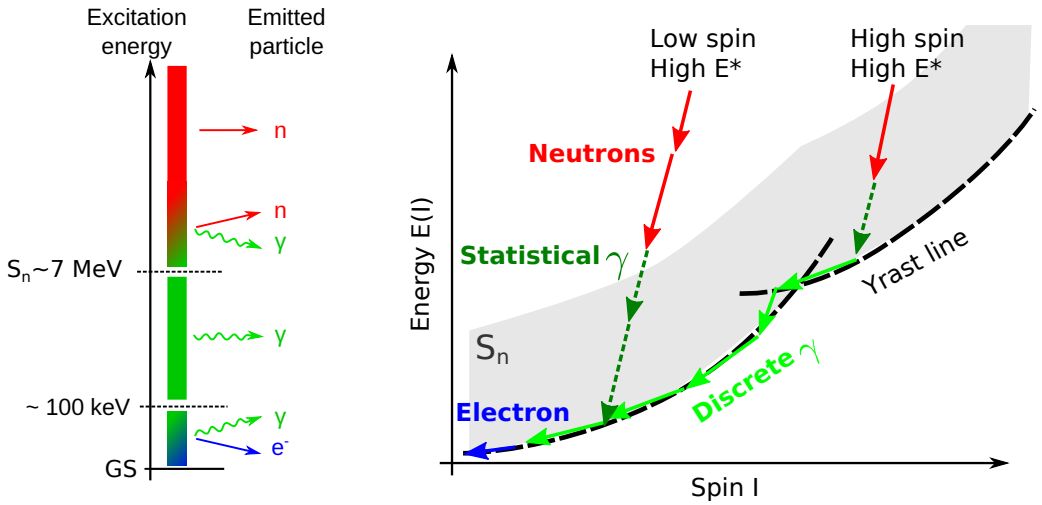

Figure 24: Left: Schematic representation of particle emission as a function of the excitation energy. Right: Yrast plot showing decay mechanisms in the $E(I)$ plane. Neutron emission (in red) dominates at high excitation energy. Starting just above the neutron separation energy S_n of the residual nucleus, statistical γ emission (dotted dark green) takes over until the Yrast line is reached, at which point discrete γ transitions (green) occur until final deexcitation or the emission of a conversion electron (blue).

ntDeexcitation⟩

5.2. *Prompt Particle Emission*

⟨subsec:prompt⟩

Starting from a highly exited state, fission fragments first deexcite through successive emission of particles. As pictured in the left panel of Fig. 24, the dominant type of emitted particle depends on the excitation energy and spin of the fragment. For fission fragments, the α emission channel is usually closed and proton emission can be neglected. At energies above 10 MeV, the neutron emission channel is open and state-of-the-art theories agree on the fact that it is largely favored. Just above the neutron separation energy, the nucleus enters an area of competition between neutron and γ emission. As the energy of the fragment decreases, the γ emission channel becomes dominant down to energies of the order of 100 keV. At first, this γ emission is mostly statistical in nature and heavily fragmented i.e., one cannot recognize individual rotational bands. Statistical models predict that these initial high-energy γ rays are mostly of $E1$ multipolarity [471]. Indeed, the γ-strength function associated with dipole radiation is several orders of magnitude higher than its counterparts for other multipolarities. Measurements of the angular distribution of the prompt γ rays indicate that typically one third of the total γ multiplicity would be of $E1$ nature [472]. When the nucleus has reached the lowest possible energy at a given spin I, what is known as the Yrast line [102], discrete γ transitions take place all the way down to the ground state. This kind of emission is mostly of $E2$ nature [249] and leads to various low-energy peaks in the prompt γ spectrum [473]. At energies of the order of $\sim$ 100 keV, the internal conversion phenomenon becomes important: the electromagnetic quanta emitted by the nucleus have a non negligible probability to interact with the electrons of the atom, leading to the emission of an internal electron accompanied by X-rays.

The prompt emission of particles takes place over a broad range of time scales. Arguments related to the statistical evaporation of the neutrons lead to typical emission times ranging from 10^{-18} to 10^{-13} s [474]. This upper bound is actually the official definition of prompt neutrons for the United State Department of Energy [475]. The prompt γ emission mostly takes place within a few nanoseconds. During this cascade, isomeric states of the fission fragments can be populated leading to γ transition at post-scission times of up to several microseconds. The relative population of these isomeric states, which is quantified by the branching ratios, has a strong impact on various fission properties [464, 476, 477, 478].

State-of-the-art theoretical approaches aiming at predicting the deexcitation process of the compound nucleus and/or the fission fragments are based on a statistical deexcitation approach. In such models, the dynamics of the deexcitation process is not explicitly described. Given an initial excited state $|i\rangle$ of the nucleus, the statistical model predicts the probability for the emission of a series of particles leading to a final state $|f\rangle$ for the residual nucleus. In this statistical picture, a deexcitation cascade is seen as a multi-step process in which the system jumps from one intermediate state to another while emitting each time one particle. A cascade of deexcitation is therefore defined by (i) a series of transitions $|i_{k-1}\rangle \rightarrow |i_k\rangle$ between nuclear states or resonances and (ii) the particles p_k emitted at each transition along with their physical properties (kinetic energy, spin/multipolarity, etc). Owing to the quantum nature of the deexcitation dynamics, any possible deexcitation cascade or channel, generically denoted by the letter c below, may happen with a given probability. In standard approaches this probability is factorized as a product of individual transition probabilities

$$P(c) = P(i = i_0 \rightarrow i_1, p_1) \times \cdots \times P(i_{k-1} \rightarrow i_k, p_k) \times \cdots \times P(i_{n-1} \rightarrow i_n = f, p_n). \quad (42)\ \{?\}$$

The probability $P(i_{k-1} \rightarrow i_k, p_k)$ represents the transition probability from the nuclear state $|i_{k-1}\rangle$ to the nuclear state $|i_k\rangle$ with the emission of a particle p_k. Such a factorization translates the Bohr hypothesis, which is assumed to be valid at each step of the cascade. In particular, it neglects possible quantum interferences between the cascades. After determining the probabilities associated with all possible deexcitation cascades, one can compute any observable of interest as a statistical average over all these events. For example, the average γ multiplicity of the process is determined as

$$M_\gamma = \sum_{c \in \mathcal{C}} P(c) M_\gamma(c), \quad (43)\ \{?\}$$

where $P(c)$ is the probability of occurrence of the cascade c and $M_\gamma(c)$ the number of γ rays emitted during this cascade. A key aspect of the method is the proper determination of the set of all possible cascades, which is related both to the structure of the nuclei involved and to the probabilities $P(i_{k-1} \rightarrow i_k, p_k)$ driven by the strength of the particle emissions.

At low excitation energies (below a few MeV), the structure of most of the fission fragments is partially known from γ spectroscopy. The ENSDF database records the first discrete energy levels, their spin and parity, electronic conversion coefficient and possibly the transition rates to other discrete levels. Deexcitation models such as FIFRELIN, CGMF or FREYA include this experimental structure information in their deexcitation engine through tabulated databases such as the RIPL library [466]. At higher excitation energies experimental data are not available and, ulti-

mately, neighboring neutron resonances overlap. To tackle this energy range, deexcitation models rely on a statistical description of nuclear structure [479, 480, 481] identical to the ideas developed for the compound nucleus in the context of neutron-induced reactions; see Section 3. The level scheme is described by the level density, which encodes the average number of states/resonances in the neighborhood of a given excitation energy. Fluctuations of the the level spacing as determined from, e.g, the Gaussian orthogonal ensemble (GOE) may further refine the level density information. Such a statistical description also applies to the transition probabilities from one level to the other. The transmission coefficient $T_a(\epsilon)$ encodes the average probability to emit a particle characterized by the output channel a and the energy ϵ. On top of this mean value, one can take into account the so-called Porter-Thomas fluctuations [482] or Ericson fluctuations [483] at higher energies. These concepts form the backbone of all fragment deexcitation models. The details of their implementation vary significantly between models, with two major trends: models based on a Weisskopf-Ewing deexcitation spectrum and models based on the Hauser-Feshbach framework.

Weisskopf-Ewing evaporation. The Weisskopf-Ewing approach gives the energy spectrum of particle evaporation from an excited nuclear state. It originates from the seminal paper of Weisskopf focused on neutron emission far above the neutron separation energy [281]. The Weiskopf evaporation spectrum $\chi(\epsilon)$ in the center-of-mass frame reads

$$\chi(\epsilon) \propto \sigma_{\mathrm{CN}}(\epsilon)\, \epsilon \exp\left(-\frac{\epsilon}{T}\right), \tag{44}$$

eq:weisskopf_sp

where ϵ is the kinetic energy of the emitted particle (e.g. neutrons), $\sigma_{\mathrm{CN}}(\epsilon)$ is the inverse cross section for the formation of the excited compound nucleus by absorption of this same particle, and T is the temperature of the residual nucleus after neutron emission. Such a spectrum results from the summation over all possible transitions for the particle energy ϵ [193]. This implies that the detailed structure of the nuclei involved in the deexcitation cascade does not need to be computed within this approach. Also, the spin/multipolarity of the particle and the spin-parity of the residual state are not explicitly taken into account.

The deexcitation engine of the codes FREYA, PbP and GEF relies on the Weiskopf-Ewing evaporation spectrum. For neutron emission, the probability $P(i_{k-1} \to i_k, p_k)$ of a transition is proportional to (44). The PbP model relies on an optical model calculation for the inverse cross section $\sigma_{\mathrm{CN}}(\epsilon)$ whereas FREYA assumes it is constant and GEF takes its energy dependency as $1/\sqrt{\epsilon}$. The Weisskopf-Ewing approach does not provide the relative probability of neutron emission versus γ emission. These deexcitation models therefore assume that successive neutron emissions take place first, followed by the emission of γ rays; see Fig. 24. The excitation energy at which the nucleus switches to γ emission is set to S_n in the case of the PbP model. To better account for the neutron/γ competition, FREYA implements an empirical shift of this energy threshold toward higher energies. Another option explored by GEF consists in using an empirical formula for the neutron versus γ relative probability that only depends on the excitation energy of the fragment. Once the neutron evaporation is completed, γ emission can be treated in a similar manner. For instance, FREYA uses the following Weiskopf-Ewing spectrum for γ emission

$$\chi_\gamma(\epsilon) \propto \epsilon^2 \exp\left(-\frac{\epsilon}{T}\right). \tag{45}$$ {?}

Contrary to a complete Hauser-Feschbach approach, such Weisskopf-Ewing evaporation is expected to fail when the level density of the residual nucleus starts to be discrete. The study in [484] compares the predictions obtained from FREYA and the Hauser-Feshbach code CGMF to experimental measurements of ^{252}Cf spontaneous fission. It found quantitative differences between model predictions but an overall agreement of both models to experimental data.

Hauser-Feshbach Formalism. As briefly descried in Section 3.2.2, the Hauser-Feshbach approach associates with each open channel (neutrons, γ, fission, etc.) a partial width Γ that is inversely proportional to the characteristic time of the corresponding transition. The probability of a transition is directly proportional to its associated partial width

$$P(i_{k-1} \rightarrow i_k, p_k) = \frac{\Gamma(i_{k-1} \rightarrow i_k, p_k)}{\sum_{i'p'} \Gamma(i_{k-1} \rightarrow i', p')}. \quad (46)$$ eq:hauser_proba

Contrary to the Weisskopf-Ewing approach, the partial widths depend here on all characteristics of the emission channel, including the spin of the emitted particle as well as the spin-parity of the residual nucleus. In addition, this approach naturally accounts for the competition between different kinds of emissions. Computing the probability distribution of any single emission requires the knowledge of the structure (discrete levels or statistical level scheme) of all possible residual nuclei. Therefore, the implementation of one decay step amounts to (i) listing all possible emission channels starting from the initial state, (ii) determining the structure of all potential residual nuclei, (iii) computing the partial widths of all possible transitions, (iv) computing the sum of these partial widths to normalize the distribution of probability. In the context of fission, the codes CGMF an FIFRELIN implement such a Hauser-Feschbach scheme.

At low excitation energy, the partial widths may be known from γ spectroscopy and directly incorporated into (46). For higher excitation energies, one relies again on a statistical description of these quantities. For neutron emission, the average partial width can be determined from an optical model calculation,

$$\langle \Gamma_n(i \rightarrow f, l, j) \rangle = \frac{T_{l,j}(\epsilon)}{2\pi\rho(E_i, J_i, \pi_i)}. \quad (47)$$ {?}

The transmission coefficient $T_{l,j}(\epsilon)$ corresponds to a neutron emission with an orbital moment l, a total spin j and a kinetic energy ϵ. In the denominator, $\rho(E_i, J_i, \pi_i)$ stands for the spin-parity-dependent level density of the mother nucleus. The average γ partial width associated with the emission of a γ ray of multipolarity XL ($X = E, M$) and energy ϵ is given by

$$\langle \Gamma_\gamma(i \rightarrow f, XL) \rangle = \frac{\epsilon^{2L+1} f_{XL}(\epsilon)}{\rho(E_i, J_i, \pi_i)}. \quad (48)$$?eq:DefFonction

The γ-strength function f_{XL} contains the information related to the inverse cross section reaction. Although it can be inferred from the results of QRPA calculations [485, 486, 487], it is most often parameterized as a Lorentzian shape corrected for various physical effects (Pigmy resonance, low energy shift). Such a parameterization is rooted in the Brink-Axel hypothesis that establishes a simple link between the γ-strength function, which depends only on the energy and multipolarity, and the photoabsorption cross section from any excited state [488]. More elaborate models such as the Enhanced Generalized Lorentzian (EGLO) overcome this assumption by including a temperature dependency in the gamma strength function [466].

These partial widths correspond to probabilities of transition averaged over the detailed nuclear structure near the initial and final states i_{k-1} and i_k. Significant variations from these averages can occur due to Porter-Thomas fluc-

tuations [482] (fluctuation in the strength of the decay) or Ericson fluctuations at higher energies [483]. Different methods are possible to take into account these fluctuations [489]. Although their impact on the deexcitation observables is weak in general, it can become significant when the number of open neutron channels comes close to unity.

5.3. *Pre-fission Particle Emission*

ec:prefission⟩?

If the entrance channel of the reaction supplies sufficient energy to the system, the emission of particles before fission happens is likely. For example, in the neutron-induced fission of actinides with fast neutrons, the emission of neutrons before fission leads to the well-known phenomenon of second- and third-chance fission: not only does the original compound nucleus with Z and N neutrons undergoes fission, but so does the isotope with $N-1$ neutrons (second-chance), $N-2$ neutrons (third-chance), etc. Since such processes carry away part of the energy and spin of the initial system, it is essential to take them into account to obtain realistic estimates of the prompt emission characteristics. The fission models discussed here may take into account this phenomenon with different degrees of refinement.

As already mentioned in Section 3, fission competes with other light particles channels. The ratio of a channel width Γ_c to the total width – the sum of widths over all channels – gives the relative probability of the channel c. For instance the fission probability reads

$$P_f = \frac{\Gamma_f}{\Gamma_f + \Gamma_n + \Gamma_\gamma}. \tag{49}$$ {?}

Codes like FIFRELIN or PbP do not implement this competition mechanism and assume a probability one for fission. This restricts their usage at energies below the threshold of emission before fission. Other codes like GEF and FREYA account for pre-fission emission of neutrons and/or γ rays. To do so they parameterize the total width of pre-fission emissions channels with analytical formulas. For example, GEF evaluates the neutron and γ channels from the compound nucleus mass, temperature of the intrinsic DoFs at different steps of the fission process as well as the fission barrier [434]. In FREYA, only neutron emission is considered *before* the fission process (no γ). Both statistical and pre-equilibrium neutrons emission are possible. The ratio Γ_n/Γ_f is determined based on the level density of the residual nucleus. For the case of fission, the density considered is at the top of the fission barrier; see Eq. (2) of [435] and [490] for more detailed information. Finally, the code HF^{3}D, a deterministic equivalent of CGMF, computes the fission widths coming from the Hill-Wheeler formula (20) like in TALYS [446] and EMPIRE [447]. In these calculations, the fission width competes with possible neutron- and γ-emission widths depending on the energies and possibly multipolarities of the emission: this is a fully fledged Hauser-Feschbach calculation. Additional details are given in [444].

5.4. *Applications of Fragments Deexcitations Models*

Deexcitation codes developed specifically to describe the decay of fission fragments are obviously important tools to evaluate the prompt fission spectrum or provide constraints on the theoretical models aiming to describe the physics of scission. In recent years, their range of application has also grown to encompass more specific applications in nuclear technologies or transport codes. In this section, we summarize some of these developments.

5.4.1. *Benchmarks of Prompt Observables*

The fission fragments (FF) deexcitation models have been extensively compared to the available experimental data on prompt neutron and γ rays during the last decade. Most of the relevant literature is focused on the spontaneous fission of ^{252}Cf, because of the quality of the experimental data, and on the thermal neutron-induced fission of ^{235}U and ^{239}Pu because of their importance in nuclear technology. Global benchmarks of the models with experimental data can be found in [57] for FIFRELIN, [490] for FREYA, [432] for PbP, [434] for GEF and [491, 492] for CGMF. A few benchmark comparisons between some of these models have also been published [493].

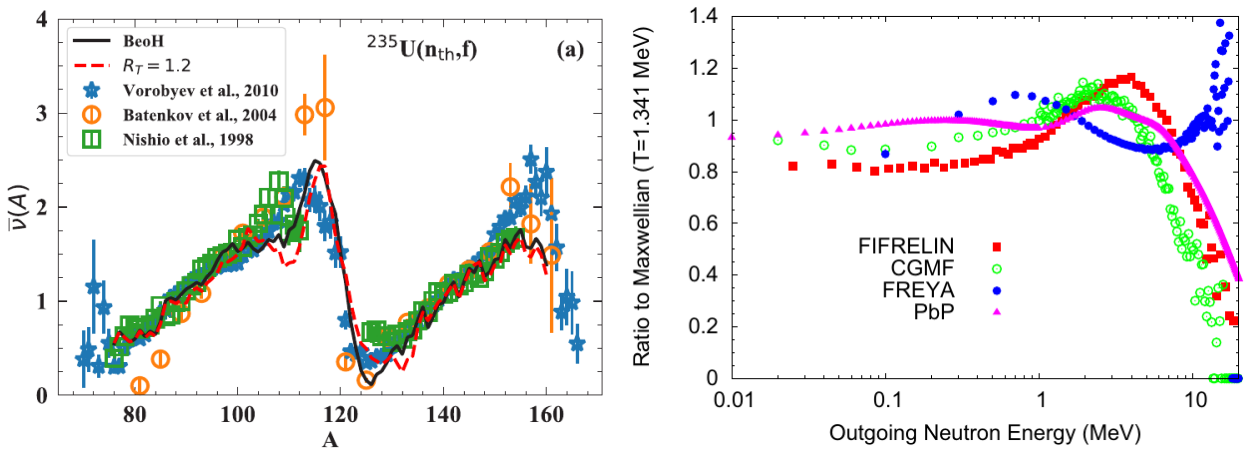

Figure 25: Left: Average prompt neutron multiplicity of ^{235}U(n$_{th}$,f) as a function of the primary fission fragment mass. Results predicted by the BeoH code compared to experimental data. Figure reproduced with permission from [444] courtesy of A. Lovell; copyright 2021 by The American Physical Society. Right: Prompt neutron spectrum from the thermal induced fission on ^{235}U. The spectrum is represented as its ratio to a Maxwellian with temperature $T = 1.341$ MeV. The predictions obtained with the FF deexcitation models FIFRELIN, CGMF, FREYA and PbP are compared using the same primary FF mass and charge yields. Figure reproduced with permission from [494] courtesy of R. Capote; copyright 2016 by Elsevier.
_prc_2021_fig6⟩

One of the key observables in FF deexcitation is the average neutron multiplicity as a function of the mass/charge of the primary fragment. The number of emitted neutrons is indeed closely related to the available excitation energy in the primary FFs and presents a so-called sawtooth shape as shown in the left panel of Fig. 25. This sawtooth behavior is mostly understood as coming from the shape relaxation of the fragments from their configuration close to scission to their ground-state deformation. Typically, heavy fragments close to ^{132}Sn are assumed to be produced only with a low deformation at scission, which translates into a low excitation energy after shape relaxation. This reasoning explains the dip in the observed neutron multiplicity $\bar{\nu}(A)$ near $A = 132$. Reproducing the sawtooth shape in the neutron multiplicity is the primary driver for current implementations of excitation energy sharing between the fragments enumerated in Section 6.4. All deexcitation models discussed in this section reproduce qualitatively this sawtooth behavior. A widespread discrepancy compared to experiment was the prediction of a minimum in the neutron multiplicity at $A = 132$ instead of the the measured A=130 in the fission of actinides. This deviation was recently attributed to the assumption of shell closure at A=132 which is actually shifted by a few mass units if one also

considers octupole deformations in the fragments [116].

Along with the neutron multiplicity, the prompt neutron spectrum is of particular interest for nuclear technology applications. On this specific topic, [494] reviews in details predictions obtained from the available deexcitation models with regard to measurements and needs for evaluated data. Despite the efforts of the community, deexcitation models do not yet predict the prompt fission neutron spectrum (PFNS) with the accuracy required for such applications. This is illustrated in the right panel of Fig. 25, which shows the large discrepancy between the PFNS predicted by four state-of-the-art deexcitation models. Recent studies suggested that modifications both of the width of the FF distribution and of the spin assignment of a few low-lying states in the FF structure could improve significantly the PFNS predictions [443].

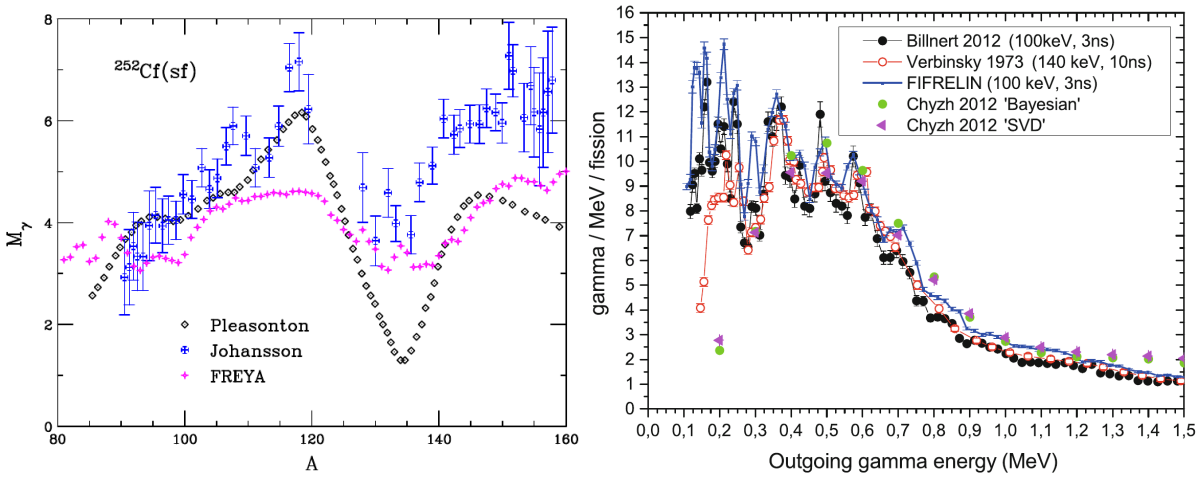

Figure 26: Left: Prompt γ multiplicity of ^{252}Cf(sf) predicted by FREYA and compared with two experimental results. Figure reproduced with permission from [490] courtesy of R. Vogt; copyright 2017 by the American Physical Society. Right: Comparison of the prompt γ spectrum of ^{252}Cf predicted by with FIFRELIN to experimental data. Figure reproduced with permission from [57] courtesy of O. Litaize; copyright 2015 by Springer.

prc_2017_fig21⟩

Figure 26 is representative of typical predictions for the prompt γ multiplicity and spectrum. In general, the total prompt γ ray multiplicity is less known than the neutron multiplicity and differences in theoretical predictions are more pronounced. The total γ multiplicity as a function of the primary fragment mass is particularly sensitive to the initial distribution of spins of the fragments [491, 495]. This makes deexcitation models a good tool to constrain our knowledge of the primary fragments spins from γ multiplicity measurements as discussed in Section 6.3. The right hand side of Fig. 26 compares the low-energy part of the prompt γ spectrum of ^{252}Cf spectrum obtained from FIFRELIN with three sets of experimental data. The overall magnitude of the spectrum reproduces the experimental spectrum within ± 1 γ per fission. It is also very noticeable that the deexcitation codes based on the Hauser-Feshbach method reproduce very well the low-energy structures in the spectrum. This is directly related to the fact that the low-energy structure of all possible FFs is taken into account as an input of these codes, usually by reading it from existing data libraries [466].

5.4.2. *Probes into the Scission Mechanism*

Beyond their ability to predict the prompt particles multiplicities and spectra, most of the deexcitation models provide information on other observables such as the multipolarity of the γ transitions as well as their correlations. Comparing these results with a large body of experimental data puts stringent constraints on the empirical modeling of primary fragment properties and enables to infer information on the physics of scission itself. A recent example is the study of the ^{237}Np(n,f) reaction as a function of incident neutron energy [495]. This paper shows that different models with incompatible energy sharing mechanism and primary fragment spin distributions reproduce equally well the experimental neutron multiplicity $\bar{\nu}(A)$ (cf. Fig. 27) but differ significantly on their predictions on the neutron-γ correlation $M_\gamma(\bar{\nu})$.

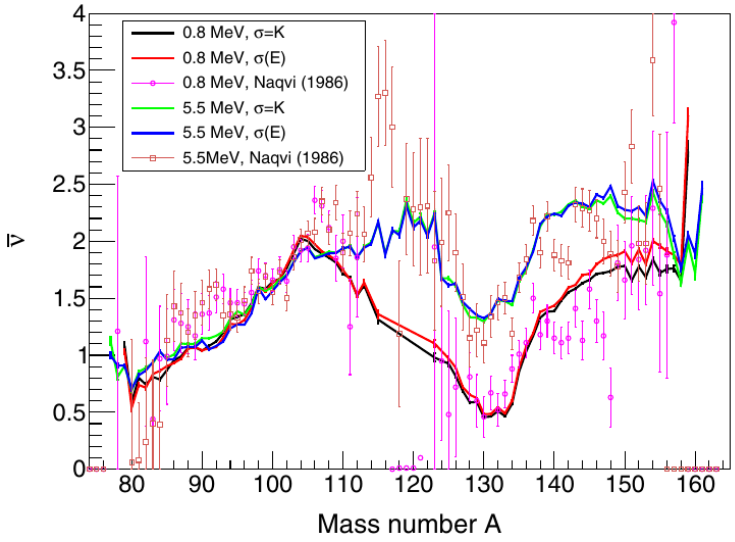

Figure 27: Neutron multiplicity as a function of the primary fragment mass for two excitation energies of the fission system ^{238}Np. Increasing the excitation energy of the system mostly increases the neutron multiplicity of the heavy fragment. This behavior is correctly reproduced when assuming an energy- and mass-dependent temperature ratio between the two fragments. Figure reproduced with permission from [495] courtesy of O. Litaize; copyright 2019 by the American Physical Society.

_prc_2019_fig5⟩

Many studies have also attempted to unfold the primary fragments spin distribution by matching particle emission predictions to known measurements. Work along this line have focused on the γ multiplicity [492, 491, 496, 470] as well as on the isomeric ratios in the fragments [476, 497, 496]. We discuss in more details theoretical efforts to predict from microscopic theory the primary fragments spins in Section 6.3.

5.4.3. *Evaluated Data for Nuclear Technology*

One possible application for deexcitation codes consists in contributing to the evaluation of nuclear data. The fact that a model predicts the neutron and γ-rays spectra and multiplicities in a consistent way is a unique opportunity to augment the nuclear databases with correlated evaluations as well as their associated uncertainties. The joint effort in [494] is a first step in this direction, focusing on the evaluation of the PFNS based on various models including the PbP model and FREYA. Covariance matrices of the uncertainty of the PFNS at various outgoing neutron energies

were computed within FREYA.

Whereas alternative models exist to evaluate the prompt neutron spectrum, deexcitation models are basically the only existing tools capable of predicting prompt γ observables. In the 2000's, the needs for better nuclear data associated with the prompt γ production were officially formulated in the Nuclear Data High Priority Request List of the Nuclear Energy Agency of the OECD [441]. This surge of interest was mainly due to the topic of γ-ray heating in the structural materials of GEN-IV reactors, especially in large reflectors [498]. For this reason, prompt γ multiplicity distributions predicted with the CGMF code have been incorporated in the ENDF/B-VIII.0 [499]. In this work the deexcitation code also supported the evaluation process of the prompt γ spectrum. Similarly, in the JEFF-3.3 libraries, the code FIFRELIN was used to complete the experimental prompt fission γ spectrum data below and above experimental energy thresholds [27]. These efforts illustrate a recent trend of including deexcitation codes into the evaluation process. Further extensions of the scope of such codes suggested in [497] would be the evaluation of the independent yields and of the branching ratios toward metastable states in the deexcitation cascade.

5.4.4. Fission Event Generators in Neutron Transport Codes

In general-purpose neutron transport codes such as MCNP or TRIPOLI, fission events and their associated emission of prompt particles are taken into account in an average way. The number of prompt neutrons generated is typically sampled between the two integers closest to the average neutron multiplicity instead of a complete distribution ranging from 0 up to 10 neutrons. The correlations in energy or emission angles between the emitted particles are neglected. This simple modeling of the prompt particles emission turns out to be sufficient for criticality problems in large systems. On the other hand, neutron transport codes are nowadays targeting new applications requiring more precise inputs related to fission. This includes simulation of detectors for experimental nuclear physics and neutron interrogation technologies [500, 501]. Such applications often involve smaller geometries for which the anisotropy of transported particles becomes important. The development of these applications together with the capability of FF deexcitations codes to predict angular correlations (see for instance [502]) is an incentive to use these models as fission events generators in neutron transport codes.

As of today, the codes FREYA and CGMF can be used as fission event generators in the MCNP6.2 [503] code and were also interfaced with the MCNPX-PoliMi transport code [493]. On the other hand, the codes FREYA and FIFRELIN can also be used within the TRIPOLI-4 transport code [504, 505]. Only a few applications have been published so far. These include the simulation of a prompt neutron-neutron angular correlation detection apparatus [505], which would not have been possible without a fission event generator, and the study of the neutron/photon multiplicities correlations measurement [484].

5.4.5. Experimental Data Analysis

nterpretation)?

Fission fragments deexcitation models often provide important insights into the interpretation of experiments thanks to their ability to estimate the sensitivity of various observables to an isolated physical effect. For example the effect of the Doppler shift of the prompt γ-ray emission due to the velocity of the FFs on the low energy γ spectrum can be explicitly calculated [471]. Taking into account this effect reproduces quantitativaly the experimental

prompt γ-ray spectrum of ^{252}Cf measured in [506].

Fission events generators are capable of estimating the impact of experimental parameters such as the coincidence time window or the detection energy threshold on the measured γ multiplicity. These two parameters turn out to be critical for the precise determination of the γ multiplicity. Typically, the late-time γ emission from a few nanoseconds to a few microseconds after scission represents a significant part of 3% to 7% of the total number γ rays [478, 507].

Finally, some specific features of the overall prompt particles spectra may sometimes be assigned to a specific FF by a deexcitation code analysis. Interpreting an experiment measuring the high-energy γ spectrum between 0.8 and 20 MeV of ^{235}U(n,f) with the code CoH, [508] showed that the high-energy γ (> 10 MeV) mostly come from a few FFs. They were also able to assign a bump in the spectrum near 4 MeV to emission from the heavy fragments near the shell closure $Z = 50$, $N = 82$.

Beyond these applications in the specific context of fission, fragments deexcitation codes contain general deexcitation models and have therefore been used in other fields such as the physics of neutrino detection [509, 510].

5.5. Delayed Emission

ubsec:delayed⟩?

After the prompt emission, β decay in the fission fragments can still populate daughter nuclei with a significant amount of energy. Reaching the ground state of the fission products requires the emission of delayed neutrons and/or γ rays. A typical fission of actinide will emit approximately one delayed neutron every 100 fissions [450]. Most of the deexcitation codes reviewed in this section do not simulate this delayed emission yet. There have been a few studies performed with the HF^{3}D code to simulate the delayed neutron emission [497, 511]. They especially focus on the prediction of the cumulative fission yields as well as of isomeric ratios.

6. Toward a Consistent Description of Fission

tial_fragments⟩

The deexcitation of fission fragments is largely dictated by the properties of the primary fragments after their complete acceleration. We have shown in Section 5 that state-of-the-art fragment deexcitation models rely on empirical estimates of these properties, which are calibrated on experimental measurements. Yet, both technological and astrophysical applications require robust predictions of the light-particle emission resulting from the fission of many short-lived isotopes over a broad range of energies. In many cases, experimental data for such systems either are very incomplete or simply do not exist. This provides a strong incentive to use theoretical models of the formation of primary fragments to provide inputs to fragments deexcitation codes. The past decade has witnessed tremendous progress in this direction especially in the context of the EDF framework. In this section, we report on such recent achievements, which bring us closer to a consistent description of both the formation and deexcitation of fission fragments.

The EDF framework, whether explicitly time-dependent or not, provides potentially powerful tools to characterize the primary fission fragments starting from (effective) nuclear forces among nucleons. The most important problem is to identify nearly-isolated fragments with good quantum numbers and well-defined excitation energy. Until very recently, most work focused on estimating the properties of the fragments close to scission were based on average properties only (i.e. expectation value of one-body operators). For instance the expectation value of any one-body,

spatially local operator $\hat{O}$ such as, e.g., particle number, angular momentum, multipole moments, etc., in the left fragment can be computed simply from

$$\langle \hat{O} \rangle_{\mathrm{L}} = \int_{-\infty}^{\infty} dx \int_{-\infty}^{\infty} dy \int_{-\infty}^{z_{\mathrm{N}}} dz\, \hat{O}(\boldsymbol{r}) \rho(\boldsymbol{r}), \tag{50}$$

eq:obs_classica

where z_{N} refers to the position of the neck between the two prefragments along the axis of elongation. Several pioneering studies of neutron-induced fission relied precisely on such average estimates in the neighborhood of scission [512, 392, 183, 513, 182, 167, 514]. The principal deficiency of this procedure is that some results are not realistic. For example, the particle numbers in the fragments typically take non-integer values. In addition, static calculations do not deal with isolated fragments but with entangled prefragments [182]. Although special procedures can be designed to mitigate and somewhat quantify this effect, they do not completely solve the problem [182, 167]. In this respect, TDDFT provides much cleaner estimates since one can wait until the fragments have fully separated and only interact with one another through the Coulomb repulsion [368]. In the following, we are reviewing recent improvements on the determination of these primary fragments properties crucial for the simulation of light particles emission.

6.1. Number of Particles

sec:particles⟩?

The number of particles in the fragments is the most basic property one would expect a fission model to provide. Yet, the naive application of (50) almost always gives fragments with non-integer numbers of particles – a problem made worse in static theories where results depend on the definition of scission; see Section 2.3. The solution is to extend well-known particle number projection (PNP) techniques to the case of a fission fragment following an idea originally proposed by Simenel for heavy-ion collisions [515]. In this case, the "only" difference with standard projection is the definition of the particle number operator, which now reads, e.g., for the left fragment,

$$\hat{N}_L = \sum_{\sigma} \int_{-\infty}^{\infty} dx \int_{-\infty}^{\infty} dy \int_{-\infty}^{z_{\mathrm{N}}} dz\, c^{\dagger}(\boldsymbol{r},\sigma) c(\boldsymbol{r},\sigma), \tag{51}$$

{?}

where $(c^{\dagger}(\boldsymbol{r},\sigma), c(\boldsymbol{r},\sigma))$ are the usual particle creation and annihilation operators. The first application of this technique to fission was reported in [373]. It was later extended and formalized in [516] and applied to estimate particle numbers for a large set of static scission configurations of ^{240}Pu and ^{236}U [517, 403].

The left panel of Fig. 28 illustrates that every single scission configuration, which is characterized by an average number of particles as estimated from (50), contains in fact a superposition of states with different, integer-valued particle numbers. For the smaller values of the neck radius, the method predicts the appearance of an odd-even staggering in the charge distribution. This technique can be applied to both proton and neutron numbers in every scission configuration. When combined with the time evolution of the collective packet in the TDGCM to populate these scission configurations (see Section 4.4), this method enabled the first prediction of two-dimensional $Y(A,Z)$ isotopic primary fragments distributions within the EDF framework [403].

Another method to obtain integer-valued particle numbers in the fragments has been explored in the context of the microscopic-macroscopic models. The idea is to rely on collective variables that specifically represent the average number of particles in each fragment on a discrete mesh [519]. In addition to giving integer numbers, this technique

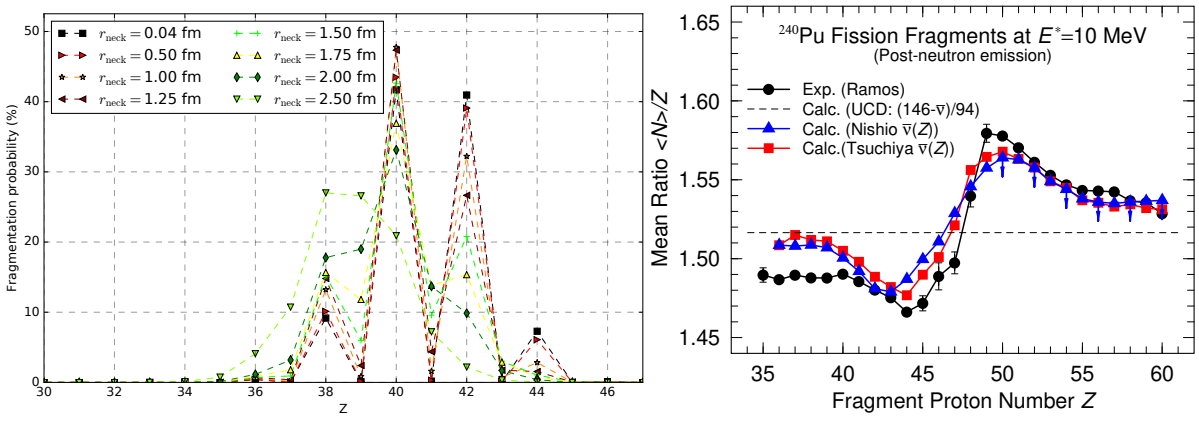

Figure 28: Left: Charge fragmentation probabilities for the light fragment for a scission configuration in ^{240}Pu. Each curve corresponds to a different size of the neck between the prefragments. Figure courtesy of Verriere. Right: Calculated post-neutron fission-fragment average neutron-to-proton ratio $\langle N \rangle / Z$ versus fragment charge compared with experimental data and the unchanged charge distribution (dashed line). Curves with blue and black symbols rely on different estimates of the average number of emitted neutrons. Figure reproduced with permission from [518] courtesy of Schmitt; copyright 2021 by Elsevier.

ents_particles⟩

was used to probe different neutron/proton ratios in the fragments and therefore computing isotopic yields [518, 519]. The right panel of Fig. 28 shows an application of this technique to compute the ratio of the mean number of neutrons per element in the fragments, as a function of the fragment charge number. Results clearly indicate that the popular Unchanged Charge Distribution (UCD) [520], which assumes that this ratio does not depend on the fragment charge number and is the same as in the fissioning nucleus, is not valid. This result, well known from experiments, was also reproduced by microscopic calculations with PNP [403].

6.2. *Deformations of the Fragments*

c:frag_deform⟩?

The deformation of fission fragments is another important property, which has a direct impact on the number of emitted neutrons [521] and on the spin distribution of the fragments; see also next section. One of the major advantages of EDF over macroscopic-microscopic approaches is that these deformations are *predicted* at scission, simply owing to the variational nature of the (TD)HFB equation and the fact that deformations are outputs of the calculations [183, 513]. By contrast, models based on parametrizing the nuclear shape treat deformations as inputs: to obtain deformed fission fragments, one has to explicitly set these deformations.

Figure 29 is a spectacular confirmation of this property. Systematic TDDFT simulations of the fission of actinide nuclei showed that the heavy fragment has a sometimes substantial octupole deformation [116]. This explains why the charge of the most likely heavy fragment in actinide fission is not centered around $Z = 50$, as would naively be expected from considerations of spherical shell effects in the fragments, but rather around $Z = 52 - 54$, depending on the fissioning system. This small shift is caused by the well-known octupole shell closure at $Z = 56$ [522].

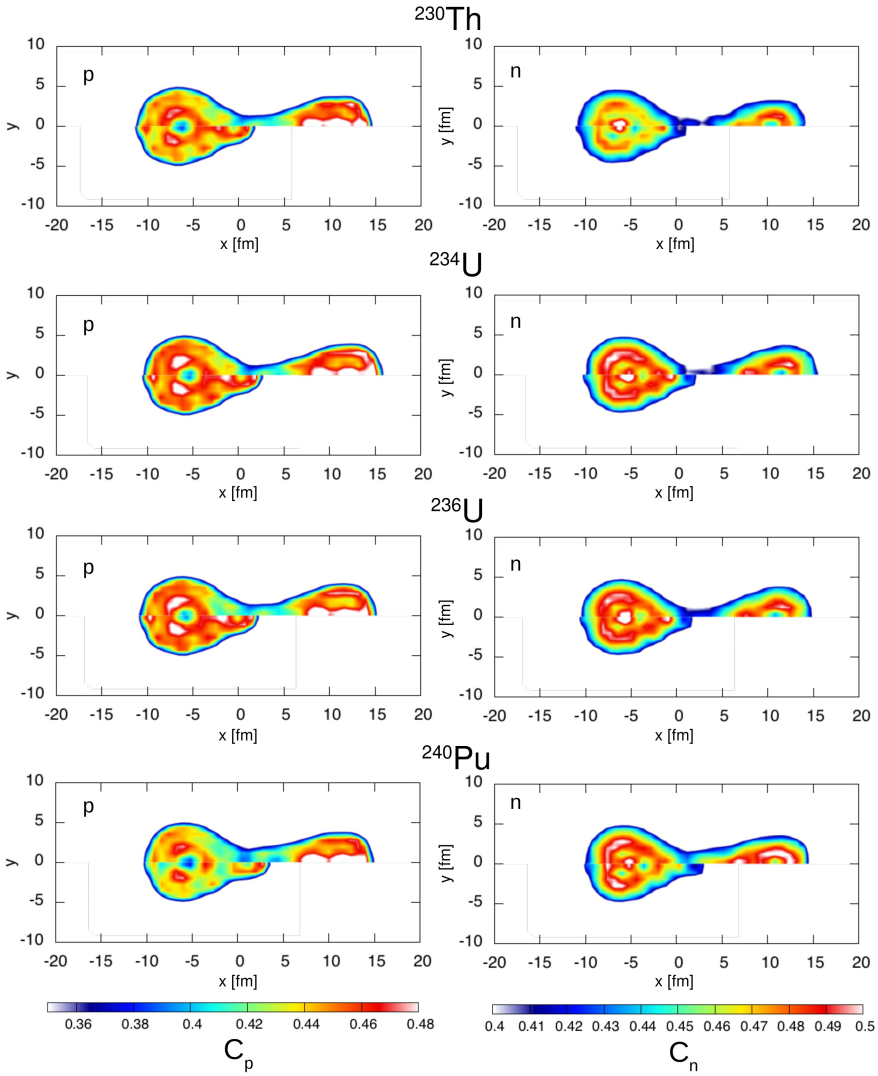

Figure 29: Identification of the heavy pre-fragment in asymmetric fission of actinides. Localization functions of the fissioning nucleus at scission (upper half of the contour plot in each frame) and localization function of the octupole deformed ^{144}Ba (lower-half of the contour plots). Figures reproduced with permission from [116] courtesy of Scamps; copyright 2018 by Nature.

⟨s_deformations⟩

6.3. Spin Distributions

⟨subsec:spin⟩

In addition to particle number, projection techniques have also been recently proposed to estimate the spin of fission fragments using angular momentum projection (AMP), following again an idea borrowed from theoretical models of heavy ion collisions [445]. The extension of AMP to fission fragments is very similar to particle number and involves redefining the angular momentum operator so that it acts only in the subspace containing a single fragment. the method was tested both in static HFB calculations for nearly all mass fragmentations of ^{240}Pu [523] and in TDDFT for the most likely fission [367]. Note that in this context the projection is always performed after the variational determination of the (TD)HFB many-body state. Results of static calculations suggest that the average spin of the light fragment is higher than the one of the heavy fragment and that shell effects at scission are very important to set

the initial amount of angular momentum in the fragment. This is shown in Fig. 30. The left panel shows that the spin distribution of a few primary fragments near ^{132}Sn extends up to relatively high value of J, which is indicative of deformed configurations. In their ground state, these same nuclei are spherical (as shown in the inset of the left panel), which would give a spin distribution centered on 0. The right panel shows the average spin of the fragments before and after the emission of neutrons and statistical photons. Surprisingly, static calculations (constrained HFB) and full TDHFB simulations give very similar results for the spin distribution of the most probable fragment pair – even if the fragments are much more excited in TDHFB than they are in static HFB calculations. Time-dependent calculations also suggest that the intrinsic spins of the two FFs are correlated and perpendicular to each other [524].

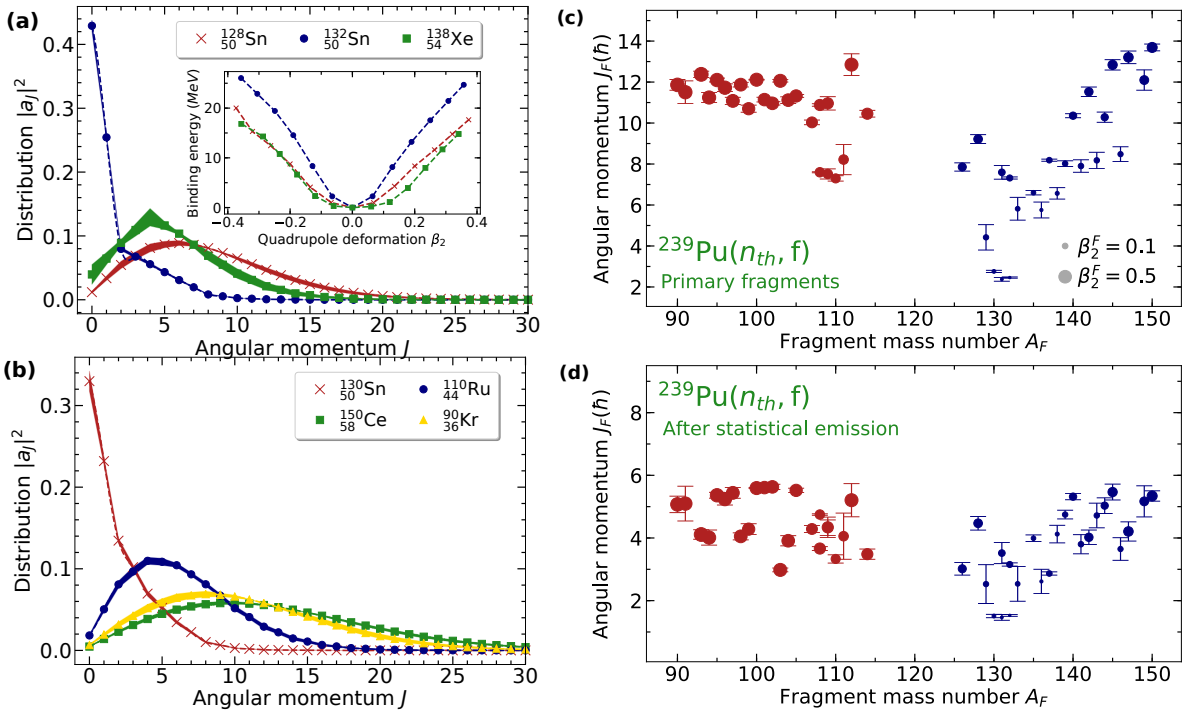

Figure 30: Panel (a): Spin distributions of a few primary fission fragments near the doubly-closed shell ^{132}Sn at scission. The inset shows that all three isotopes are spherical in their ground state, which would give a spin distribution centered on 0. Panel (b): Spin distributions of fragment pairs at scission.Panel (c): Average angular momentum of the fission fragments of ^{240}Pu before statistical emission. Panel (d): Same as panel (a), only after statistical emission. Figures reproduced with permission from [523] courtesy of Marevic; copyright 2021 by The American Physical Society.

ragments_spins⟩

These theoretical results partly confirm recent measurements of the spin distribution after the emission of statistical neutrons and γ in three actinide nuclei [525]. Specifically, the overall dependency of the spin on the fragment mass is very similar, and both theory and measurements suggest that the spin of the light fragment in the most probable fragmentation is larger than the one of the heavy fragment. Such conclusions were also obtained independently from studies of the fission spectrum with the code FIFRELIN [495], where a light fragment spin higher than the heavy one naturally emerges from the fit of the spin-cutoff parameter to the light and heavy neutron multiplicities; see Section 5.2 for more details. Although several parameterizations of this code may lead to similar results, it shows at least that

$\langle J_L \rangle > \langle J_H \rangle$ is not incompatible with a qualitative reproduction of both prompt-neutron and prompt-γ observables. Contrary to the argument put forward in [525], the most advanced theoretical studies of the deexcitation of these fragments did not show evidence that statistical photon emission leads to a constant shift of the average angular momentum [526, 496]. All three different theoretical approaches explain this result by the fact that the spin of the fragments is largely dependent on their deformation at scission [526, 523, 367].

6.4. Excitation Energy

bsec:initial_e⟩

The determination of the excitation energy of fission fragments is more difficult. Two approaches are possible: (i) estimate the total kinetic energy TKE (or rely on existing measurements), which sets the value of TXE, and model how this total excitation energy is shared among the fragments, i.e., with a statistical model; (ii) try to directly estimate the individual excitation energy of each fragment $E^*_{\rm H}$ and $E^*_{\rm L}$. In this case, the total excitation energy is simply $\mathrm{TXE} = E^*_{\rm H} + E^*_{\rm L}$ and can be used to reconstruct the value of the TKE.

Adiabatic models based on static PES give by definition cold fragments where the excitation energy comes entirely from deformation effects and the fact that a fragment (Z, N) may have a different deformation from its ground-state value. An estimate of the value of the excitation energy can still be set "by hand" based on the total energy balance of the reaction at scission similar to (39). In this case, the first step consists in determining the total kinetic energy of the static configurations in the neighborhood of scission. Since most of the kinetic energy carried away by the fragments derives from the Coulomb repulsion between them, the most simple estimate of TKE is given by

$$\mathrm{TKE} \approx \frac{e^2}{4\pi\epsilon_0}\frac{Z_{\rm H}Z_{\rm L}}{R}, \tag{52}$$ {?}

with R the distance between the two fragments, which can be estimated from the position of the two centers of mass [527]. Refinements of this formula involve adding the pre-scission kinetic energy of the fragments, which can be estimated as the collective energy term $\frac{1}{2}\sum_{\alpha\beta} B_{\alpha\beta}\dot{q}_\alpha\dot{q}_\beta$ in the context of the Langevin equation (26); see, e.g., [528, 340, 343]. The remaining total excitation energy of the system then needs to be shared between the fragments. This mechanism of energy sharing, also called energy sorting, is often described based on a statistical argument [529]: in the Fermi gas model, the excitation energy of the fragment E^* is related to its temperature through $E^* = aT^2$, where a is the level-density parameter [58]. If we assume statistical equilibrium between the two fragments at scission, then the temperatures satisfy $T_{\rm H} = T_{\rm L}$, and one can easily estimate $E^*_{\rm H}$ and $E^*_{\rm L}$. Simulations of the fission spectrum prompted a discussion of the validity of the equality between the two temperatures and the need to phenomenologically parametrize the ratio $R_T = T_{\rm H}/T_{\rm L}$ [530, 467, 531, 532, 533]. Since 2020, yet another energy sharing mechanism was proposed, based on more realistic calculations of level densities in the fragments [534, 535].

The second approach to estimating directly the excitation energy of each fragment is the direct result of progress in microscopic fission theory, especially real-time TDDFT simulations of fission events. In such cases, the total energy of the system is conserved, and simulations can be run until the two fragments are well separated (up to $\simeq$ 30 fm between the fragments in [367]). At that point, the excitation energy of the fragment is simply the difference between the computed value and the ground-state binding energy. In addition, the TKE can be computed directly as the relative kinetic energy of the two moving fragments, rather than through the Coulomb energy proxy. This approach was first

outlined in [368] and applied in [374] in the context of TDHF theory. With the inclusion of pairing in full TDHFB calculations, estimates of TKE and fragment excitation energy in the low-energy fission of nuclei such as ^{240}Pu became possible [355] up to percent precision. Results for the most likely fission suggest the two fragments do not have the same temperature.

7. Conclusion

In spite of its applications in nuclear engineering and its essential role in answering fundamental science questions about the stability of superheavy elements or the formation of heavy elements in the Cosmos, the phenomenon of fission remains shrouded in mysteries. In terms of sheer complexity, it has few rivals as it compounds the challenges of any quantum many-body theory with those of open quantum systems, nuclear forces and out-of-equilibrium processes. From a nuclear theory perspective, fission is a deep and unforgiving probe into many properties of atomic nuclei: small errors in computing nuclear deformation properties can lead to orders of magnitude discrepancies on actual observables.

In this article, we attempted to give as thorough a review on fission theories as possible. We highlighted that there are, broadly speaking, three main phases in the process: the probability for a nucleus to fission, the large-amplitude collective motion leading to the production of primary fragments and the deexcitation of these fragments after they are formed. The first phase requires the tools of reaction theory to account for the competition between fission *per se* and every other decay channel. Even though most of the theoretical formalism was developed between the 1950's and the early 1980's, lack of proper nuclear structure inputs has been the major bottleneck and progress, while real, has been relatively slow. In contrast, it is fair to say that the description of large-amplitude nuclear collective dynamics has seen the most spectacular progress in the last two decades. This was largely caused by the possibility to perform large-scale, precise energy density functional calculations with realistic energy functionals on supercomputers. The last phase of the fission process, the prompt and delayed emission of particles from the fragments, is described by the same methods of nuclear reaction theory as the entrance channel. In recent years, several codes have been published to perform complete simulations of fission events and thereby connect with transport codes used in technological applications.

Looking ahead, we see many opportunities to bridge these three phases of fission into a single, consistent theoretical framework. For example, the recent studies on the number of particles, excitation energy or spin distribution of the fission fragments that were discussed in Section 6 have shown that one can start replacing phenomenological inputs of deexcitation models with microscopic predictions based on actual simulations of fission dynamics. Similarly, both the statistical and R-matrix formalisms for fission cross sections summarized in Secs. 3.2.2 and 3.2.3 rely, most generally, on nuclear structure theory inputs that could be computed with more advanced models than used until now. This global theoretical framework that we envision is bound to be based on the EDF approach, at least in the foreseeable future: large-amplitude collective motion, γ emission or absorption and β decay are naturally described within this framework. It is reasonable to think that formal developments and computational advances should soon enable the calculation of the complete sets of nuclear wave functions with good quantum numbers needed to describe

the entrance channel. Putting together all these ingredients will without a doubt require considerable effort, but is also the promise of a bright future for fission theory.

Acknowledgments

The authors would like to thank O. Litaize, N. Pillet, J. Randrup, P. Romain, P. Tamagno and I. Thompson for reading parts of the manuscript and making relevant suggestions. This work was supported in part by the NUCLEI SciDAC-4 collaboration DE-SC001822 and was performed under the auspices of the U.S. Department of Energy by Lawrence Livermore National Laboratory under Contract DE-AC52-07NA27344. Computing support came from the Lawrence Livermore National Laboratory (LLNL) Institutional Computing Grand Challenge program.

References

hahn1938ueber [1] O. Hahn, F. Strassmann, Über die Entstehung von Radiumisotopen aus Uran durch Bestrahlen mit schnellen und verlangsamten Neutronen, Naturwiss. 26 (46) (1938) 755. doi:10.1007/BF01774197.

hahn1939ueber [2] O. Hahn, F. Strassmann, Über den Nachweis und das Verhalten der bei der Bestrahlung des Urans mittels Neutronen entstehenden Erdalkalimetalle, Naturwiss. 27 (1) (1939) 11. doi:10.1007/BF01488241.

939disintegration [3] L. Meitner, O. R. Frisch, Disintegration of Uranium by Neutrons: A New Type of Nuclear Reactions, Nature 143 (1939) 239. doi:10.1038/143239a0.

ohr1939mechanism [4] N. Bohr, J. A. Wheeler, The mechanism of nuclear fission, Phys. Rev. 56 (5) (1939) 426. doi:10.1103/PhysRev.56.426.

erov1940discovery [5] G. Flerov, K. Petrzhak, Спонтанное деление ядер урана, J. Phys. U.S.S.R. 3 (1940) 275.

er1946spontaneous [6] G. Scharff-Goldhaber, G. S. Klaiber, Spontaneous Emission of Neutrons from Uranium, Phys. Rev. 70 (3-4) (1946) 229. doi:10.1103/PhysRev.70.229.2.

mills1995fission [7] R. W. Mills, Fission product yield evaluation, Ph.D. thesis, University of Birmingham (1995).

ontaneousfission [8] R. Smolańczuk, J. Skalski, A. Sobiczewski, Spontaneous-fission half-lives of deformed superheavy nuclei, Phys. Rev. C 52 (4) (1995) 1871. doi:10.1103/PhysRevC.52.1871.

ann2000discovery [9] S. Hofmann, G. Münzenberg, The discovery of the heaviest elements, Rev. Mod. Phys. 72 (3) (2000) 733. doi:10.1103/RevModPhys.72.733.

er2001superheavy [10] J.-F. Berger, L. Bitaud, J. Dechargé, M. Girod, K. Dietrich, Superheavy, hyperheavy and bubble nuclei, Nucl. Phys. A 685 (1–4) (2001) 1. doi:10.1016/S0375-9474(01)00524-3.

2004systematics [11] T. Bürvenich, M. Bender, J. Maruhn, P.-G. Reinhard, Systematics of fission barriers in superheavy elements, Phys. Rev. C 69 (1) (2004) 014307. doi:10.1103/PhysRevC.69.014307.

elorz2009fission [12] N. Schindzielorz, J. Erler, P. Klüpfel, P.-G. Reinhard, G. Hager, Fission of super-heavy nuclei explored with Skyrme forces, Int. J. Mod. Phys. E 18 (2009) 773. doi:10.1142/S0218301309012860.

pei2009fission [13] J. C. Pei, W. Nazarewicz, J. A. Sheikh, A. K. Kerman, Fission Barriers of Compound Superheavy Nuclei, Phys. Rev. Lett. 102 (19) (2009) 192501. doi:10.1103/PhysRevLett.102.192501.

kh2009systematic [14] J. A. Sheikh, W. Nazarewicz, J. C. Pei, Systematic study of fission barriers of excited superheavy nuclei, Phys. Rev. C 80 (1) (2009) 011302. doi:10.1103/PhysRevC.80.011302.

warda2012fission [15] M. Warda, J. L. Egido, Fission half-lives of superheavy nuclei in a microscopic approach, Phys. Rev. C 86 (1) (2012) 014322. doi:10.1103/PhysRevC.86.014322.

k2013spontaneous [16] A. Staszczak, A. Baran, W. Nazarewicz, Spontaneous fission modes and lifetimes of superheavy elements in the nuclear density functional theory, Phys. Rev. C 87 (2) (2013) 024320. doi:10.1103/PhysRevC.87.024320.

baran2015fission [17] A. Baran, M. Kowal, P.-G. Reinhard, L. M. Robledo, A. Staszczak, M. Warda, Fission barriers and probabilities of spontaneous fission for elements with Z≥100, Nucl. Phys. A 944 (2015) 442. doi:10.1016/j.nuclphysa.2015.06.002.

warda2018cluster [18] M. Warda, A. Zdeb, L. M. Robledo, Cluster radioactivity in superheavy nuclei, Phys. Rev. C 98 (4) (2018) 041602(R). doi:10.1103/PhysRevC.98.041602.

ni2019colloquium [19] S. A. Giuliani, Z. Matheson, W. Nazarewicz, E. Olsen, P.-G. Reinhard, J. Sadhukhan, B. Schuetrumpf, N. Schunck, P. Schwerdtfeger, Colloquium: Superheavy elements: Oganesson and beyond, Rev. Mod. Phys. 91 (1) (2019) 011001. doi:10.1103/RevModPhys.91.011001.

erler2012fission [20] J. Erler, K. Langanke, H. P. Loens, G. Martínez-Pinedo, P.-G. Reinhard, Fission properties for r-process nuclei, Phys. Rev. C 85 (2) (2012) 025802. doi:10.1103/PhysRevC.85.025802.

nov2013influence [21] I. V. Panov, I. Y. Korneev, G. Martinez-Pinedo, F.-K. Thielemann, Influence of spontaneous fission rates on the yields of superheavy elements in the r-process, Astron. Lett. 39 (3) (2013) 150. doi:10.1134/S1063773713030043.

iani2018fission [22] S. A. Giuliani, G. Martínez-Pinedo, L. M. Robledo, Fission properties of superheavy nuclei for r-process calculations, Phys. Rev. C 97 (3) (2018) 034323. doi:10.1103/PhysRevC.97.034323.

umpower2018beta [23] M. R. Mumpower, T. Kawano, T. M. Sprouse, N. Vassh, E. M. Holmbeck, R. Surman, P. Möller, β-delayed Fission in r-process Nucleosynthesis, Astrophys. J. 869 (1) (2018) 14. doi:10.3847/1538-4357/aaeaca.

berti2006nuclear [24] G. Aliberti, G. Palmiotti, M. Salvatores, T. K. Kim, T. A. Taiwo, M. Anitescu, I. Kodeli, E. Sartori, J. C. Bosq, J. Tommasi, Nuclear data sensitivity, uncertainty and target accuracy assessment for future nuclear systems, Ann. Nuc. En. 33 (8) (2006) 700. doi:10.1016/j.anucene.2006.02.003.

tori2013nuclear [25] E. Sartori, Nuclear data for radioactive waste management, Annals of Nuclear Energy 62 (2013) 579. doi:10.1016/j.anucene.2013.02.003.

risto2020chapter [26] M. J. Kristo, Chapter 13 - Nuclear forensics, in: M. F. L'Annunziata (Ed.), Handbook of Radioactivity Analysis: Volume 2 (Fourth Edition), Academic Press, 2020, pp. 921–951. doi:10.1016/B978-0-12-814395-7.00013-1.

plompen2020joint [27] A. J. M. Plompen, O. Cabellos, C. De Saint Jean, M. Fleming, A. Algora, M. Angelone, P. Archier, E. Bauge, O. Bersillon, A. Blokhin, F. Cantargi, A. Chebboubi, C. Diez, H. Duarte, E. Dupont, J. Dyrda, B. Erasmus, L. Fiorito, U. Fischer, D. Flammini, D. Foligno, M. R. Gilbert, J. R. Granada, W. Haeck, F.-J. Hambsch, P. Helgesson, S. Hilaire, I. Hill, M. Hursin, R. Ichou, R. Jacqmin, B. Jansky, C. Jouanne, M. A. Kellett, D. H. Kim, H. Kim, I. Kodeli, A. J. Koning, A. Y. Konobeyev, S. Kopecky, B. Kos, A. Krasa, L. C. Leal, N. Leclaire, P. Leconte, Y. O. Lee, H. Leeb, O. Litaize, M. Majerle, J. Marquez Damian, F. Michel-Sendis, R. W. Mills, B. Morillon, G. Noguere, M. Pecchia, S. Pelloni, P. Pereslavtsev, R. J. Perry, D. Rochman, A. Roehrmoser, P. Romain, P. Romojaro, D. Roubtsov, P. Sauvan, P. Schillebeeckx, K. H. Schmidt, O. Serot, S. Simakov, I. Sirakov, H. Sjostrand, A. Stankovskiy, J. C. Sublet, P. Tamagno, A. Trkov, S. van der Marck, F. Alvarez-Velarde, R. Villari, T. C. Ware, K. Yokoyama, G. Zerovnik, The joint evaluated fission and fusion nuclear data library, JEFF-3.3, Eur. Phys. J. A 56 (7) (2020) 181. doi:10.1140/epja/s10050-020-00141-9.

brown2018endf [28] D. A. Brown, M. B. Chadwick, R. Capote, A. C. Kahler, A. Trkov, M. W. Herman, A. A. Sonzogni, Y. Danon, A. D. Carlson, M. Dunn, D. L. Smith, G. M. Hale, G. Arbanas, R. Arcilla, C. R. Bates, B. Beck, B. Becker, F. Brown, R. J. Casperson, J. Conlin, D. E. Cullen, M.-A. Descalle, R. Firestone, T. Gaines, K. H. Guber, A. I. Hawari, J. Holmes, T. D. Johnson, T. Kawano, B. C. Kiedrowski, A. J. Koning, S. Kopecky, L. Leal, J. P. Lestone, C. Lubitz, J. I. Márquez Damián, C. M. Mattoon, E. A. McCutchan, S. Mughabghab, P. Navratil, D. Neudecker, G. P. A. Nobre, G. Noguere, M. Paris, M. T. Pigni, A. J. Plompen, B. Pritychenko, V. G. Pronyaev, D. Roubtsov, D. Rochman, P. Romano, P. Schillebeeckx, S. Simakov, M. Sin, I. Sirakov, B. Sleaford, V. Sobes, E. S. Soukhovitskii, I. Stetcu, P. Talou, I. Thompson, S. van der Marck, L. Welser-Sherrill, D. Wiarda, M. White, J. L. Wormald, R. Q. Wright, M. Zerkle, G. Žerovnik, Y. Zhu, ENDF/B-VIII.0: The 8th Major Release of the Nuclear Reaction Data Library with CIELO-project Cross Sections, New Standards and Thermal Scattering Data, Nucl. Data Sheets 148 (2018) 1. doi:10.1016/j.nds.2018.02.001.

evaluated [29] Evaluated and Compiled Nuclear Structure Data, http://www.nndc.bnl.gov/ensdf/.

power2020primary [30] M. R. Mumpower, P. Jaffke, M. Verriere, J. Randrup, Primary fission fragment mass yields across the chart of nuclides, Phys. Rev. C 101 (5) (2020) 054607. doi:10.1103/PhysRevC.101.054607.

2016microscopic [31] N. Schunck, L. M. Robledo, Microscopic theory of nuclear fission: A review, Rep. Prog. Phys. 79 (11) (2016) 116301. doi:10.1088/0034-4885/79/11/116301.

bender2020future [32] M. Bender, R. Bernard, G. Bertsch, S. Chiba, J. Dobaczewski, N. Dubray, S. A. Giuliani, K. Hagino, D. Lacroix, Z. Li, P. Magierski, J. Maruhn, W. Nazarewicz, J. Pei, S. Péru, N. Pillet, J. Randrup, D. Regnier, P.-G. Reinhard,

L. M. Robledo, W. Ryssens, J. Sadhukhan, G. Scamps, N. Schunck, C. Simenel, J. Skalski, I. Stetcu, P. Stevenson, S. Umar, M. Verriere, D. Vretenar, M. Warda, S. Åberg, Future of nuclear fission theory, J. Phys. G: Nucl. Part. Phys. 47 (11) (2020) 113002. doi:10.1088/1361-6471/abab4f.

deh2019combining [33] M. I. Radaideh, T. Kozlowski, Combining simulations and data with deep learning and uncertainty quantification for advanced energy modeling, Int. J. Energ. Res. 43 (14) (2019) 7866–7890. doi:10.1002/er.4698.

ker2020enhancing [34] D. Neudecker, M. Grosskopf, M. Herman, W. Haeck, P. Grechanuk, S. Vander Wiel, M. Rising, A. Kahler, N. Sly, P. Talou, Enhancing nuclear data validation analysis by using machine learning, Nucl. Data Sheets 167 (2020) 36–60. doi:https://doi.org/10.1016/j.nds.2020.07.002.

ll2020evaluating [35] B. J. Whewell, M. Grosskopf, D. Neudecker, Evaluating ^{239}Pu(n,f) cross sections via machine learning using experimental data, covariances, and measurement features, Nucl. Inst. Meth. Phys. Res. A 978 (2020) 164305. doi:https://doi.org/10.1016/j.nima.2020.164305.

krappe2012theory [36] H. Krappe, K. Pomorski, Theory of Nuclear Fission, Springer, 2012.

s2019microscopic [37] W. Younes, D. M. Gogny, J.-F. Berger, A Microscopic Theory of Fission Dynamics Based on the Generator Coordinate Method, Lecture Notes in Physics, Springer International Publishing, 2019.

2021introduction [38] W. Younes, W. D. Loveland, An Introduction to Nuclear Fission, Springer, 2021. doi:https://doi.org/10.1007/978-3-030-84592-6.

reyev2017nuclear [39] A. N. Andreyev, K. Nishio, K.-H. Schmidt, Nuclear fission: A review of experimental advances and phenomenology, Rep. Prog. Phys. 81 (1) (2017) 016301. doi:10.1088/1361-6633/aa82eb.

chmidt2018review [40] K.-H. Schmidt, B. Jurado, Review on the progress in nuclear fission - experimental methods and theoretical descriptions, Rep. Prog. Phys. 81 (10) (2018) 106301. doi:10.1088/1361-6633/aacfa7.

nix1965studies [41] J. R. Nix, W. J. Swiatecki, Studies in the liquid-drop theory of nuclear fission, Nucl. Phys. 71 (1) (1965) 1. doi:10.1016/0029-5582(65)90038-6.

nix1969further [42] J. R. Nix, Further studies in the liquid-drop theory on nuclear fission, Nucl. Phys. A 130 (2) (1969) 241. doi:10.1016/0375-9474(69)90730-1.

beun2008fission [43] J. Beun, G. C. McLaughlin, R. Surman, W. R. Hix, Fission cycling in a supernova r-process, Phys. Rev. C 77 (3) (2008) 035804. doi:10.1103/PhysRevC.77.035804.

goriely2013new [44] S. Goriely, J.-L. Sida, J.-F. Lemaître, S. Panebianco, N. Dubray, S. Hilaire, A. Bauswein, H.-T. Janka, New Fission Fragment Distributions and r-Process Origin of the Rare-Earth Elements, Phys. Rev. Lett. 111 (24) (2013) 242502. doi:10.1103/PhysRevLett.111.242502.

mpower2016impact [45] M. R. Mumpower, R. Surman, G. C. McLaughlin, A. Aprahamian, The impact of individual nuclear properties on r-process nucleosynthesis, Prog. Part. Nucl. Phys. 86 (2016) 86. doi:10.1016/j.ppnp.2015.09.001.

sch2020astromers [46] G. W. Misch, S. K. Ghorui, P. Banerjee, Y. Sun, M. R. Mumpower, Astromers: Nuclear Isomers in Astrophysics, Astrophys. J. Supp. Ser. 252 (1) (2020) 2. doi:10.3847/1538-4365/abc41d.

cowan2021origin [47] J. J. Cowan, C. Sneden, J. E. Lawler, A. Aprahamian, M. Wiescher, K. Langanke, G. Martínez-Pinedo, F.-K. Thielemann, Origin of the heaviest elements: The rapid neutron-capture process, Rev. Mod. Phys. 93 (1) (2021) 015002. doi:10.1103/RevModPhys.93.015002.

tion2011reactor [48] G. Mention, M. Fechner, T. Lasserre, T. A. Mueller, D. Lhuillier, M. Cribier, A. Letourneau, Reactor antineutrino anomaly, Phys. Rev. D 83 (7) (2011) 073006. doi:10.1103/PhysRevD.83.073006.

ller2011improved [49] T. A. Mueller, D. Lhuillier, M. Fallot, A. Letourneau, S. Cormon, M. Fechner, L. Giot, T. Lasserre, J. Martino, G. Mention, A. Porta, F. Yermia, Improved predictions of reactor antineutrino spectra, Phys. Rev. C 83 (5) (2011) 054615. doi:10.1103/PhysRevC.83.054615.

zogni2015nuclear [50] A. A. Sonzogni, T. D. Johnson, E. A. McCutchan, Nuclear structure insights into reactor antineutrino spectra, Phys. Rev. C 91 (1) (2015) 011301. doi:10.1103/PhysRevC.91.011301.

ni2017dissecting [51] A. A. Sonzogni, E. A. McCutchan, A. C. Hayes, Dissecting Reactor Antineutrino Flux Calculations, Phys. Rev. Lett. 119 (11) (2017) 112501. doi:10.1103/PhysRevLett.119.112501.

gni2018revealing [52] A. A. Sonzogni, M. Nino, E. A. McCutchan, Revealing fine structure in the antineutrino spectra from a nuclear reactor, Phys. Rev. C 98 (1) (2018) 014323. doi:10.1103/PhysRevC.98.014323.

llaboration2021 [53] PROSPECT Collaboration, M. Andriamirado, A. B. Balantekin, H. R. Band, C. D. Bass, D. E. Bergeron, D. Berish, N. S. Bowden, J. P. Brodsky, C. D. Bryan, T. Classen, A. J. Conant, G. Deichert, M. V. Diwan, M. J. Dolinski, A. Erickson, B. T. Foust, J. K. Gaison, A. Galindo-Uribarri, C. E. Gilbert, B. W. Goddard, B. T. Hackett, S. Hans, A. B. Hansell, K. M. Heeger, D. E. Jaffe, X. Ji, D. C. Jones, O. Kyzylova, C. E. Lane, T. J. Langford, J. LaRosa, B. R. Littlejohn, X. Lu, J. Maricic, M. P. Mendenhall, A. M. Meyer, R. Milincic, I. Mitchell, P. E. Mueller, H. P. Mumm, J. Napolitano, C. Nave, R. Neilson, J. A. Nikkel, D. Norcini, S. Nour, J. L. Palomino, D. A. Pushin, X. Qian, E. Romero-Romero, R. Rosero, P. T. Surukuchi, M. A. Tyra, R. L. Varner, D. Venegas-Vargas, P. B. Weatherly, C. White, J. Wilhelmi, A. Woolverton, M. Yeh, A. Zhang, C. Zhang, X. Zhang, Improved short-baseline neutrino oscillation search and energy spectrum measurement with the PROSPECT experiment at HFIR, Phys. Rev. D 103 (3) (2021) 032001. doi:10.1103/PhysRevD.103.032001.

ani2021bayesian [54] A. Ashtari Esfahani, M. Betancourt, Z. Bogorad, S. Böser, N. Buzinsky, R. Cervantes, C. Claessens, L. de Viveiros, M. Fertl, J. A. Formaggio, L. Gladstone, M. Grando, M. Guigue, J. Hartse, K. M. Heeger, X. Huyan, J. Johnston, A. M. Jones, K. Kazkaz, B. H. LaRoque, A. Lindman, R. Mohiuddin, B. Monreal, J. A. Nikkel, E. Novitski, N. S. Oblath, M. Ottiger, W. Pettus, R. G. H. Robertson, G. Rybka, L. Saldaña, M. Schram, V. Sibille, P. L. Slocum, Y.-H. Sun, P. T. Surukuchi, J. R. Tedeschi, A. B. Telles, M. Thomas, T. Thümmler, L. Tvrznikova, B. A. VanDevender, T. E. Weiss, T. Wendler, E. Zayas, A. Ziegler, Bayesian analysis of a future

β decay experiment's sensitivity to neutrino mass scale and ordering, Phys. Rev. C 103 (6) (2021) 065501. doi:10.1103/PhysRevC.103.065501.

laboration2021a [55] PROSPECT Collaboration, M. Andriamirado, A. B. Balantekin, H. R. Band, C. D. Bass, D. E. Bergeron, N. S. Bowden, C. D. Bryan, T. Classen, A. J. Conant, G. Deichert, M. V. Diwan, M. J. Dolinski, A. Erickson, B. T. Foust, J. K. Gaison, A. Galindo-Uribarri, C. E. Gilbert, S. Hans, A. B. Hansell, K. M. Heeger, B. Heffron, D. E. Jaffe, S. Jayakumar, X. Ji, D. C. Jones, J. Koblanski, O. Kyzylova, C. E. Lane, T. J. Langford, J. LaRosa, B. R. Littlejohn, X. Lu, J. Maricic, M. P. Mendenhall, A. M. Meyer, R. Milincic, P. E. Mueller, H. P. Mumm, J. Napolitano, R. Neilson, J. A. Nikkel, S. Nour, J. L. Palomino, D. A. Pushin, X. Qian, R. Rosero, P. T. Surukuchi, M. A. Tyra, R. L. Varner, D. Venegas-Vargas, P. B. Weatherly, C. White, J. Wilhelmi, A. Woolverton, M. Yeh, C. Zhang, X. Zhang, C. V. Cappiello, Limits on sub-GeV dark matter from the PROSPECT reactor antineutrino experiment, Phys. Rev. D 104 (1) (2021) 012009. doi:10.1103/PhysRevD.104.012009.

lgac2016induced [56] A. Bulgac, P. Magierski, K. J. Roche, I. Stetcu, Induced Fission of ^{240}Pu within a Real-Time Microscopic Framework, Phys. Rev. Lett. 116 (12) (2016) 122504. doi:10.1103/PhysRevLett.116.122504.

aize2015fission [57] O. Litaize, O. Serot, L. Berge, Fission modelling with FIFRELIN, Eur. Phys. J. A 51 (12) (2015) 177. doi:10.1140/epja/i2015-15177-9.

bohr1998nuclear [58] A. Bohr, B. Mottelson, Nuclear Structure, Vol. I, Single-Particle Motion, World Scientific, 1998. doi:10.1142/3530.

ring2004nuclear [59] P. Ring, P. Schuck, The Nuclear Many-Body Problem, Texts and Monographs in Physics, Springer, 2004.

arrett2013initio [60] B. R. Barrett, P. Navrátil, J. P. Vary, Ab initio no core shell model, Prog. Part. Nucl. Phys. 69 (2013) 131. doi:10.1016/j.ppnp.2012.10.003.

2019nonempirical [61] S. R. Stroberg, H. Hergert, S. K. Bogner, J. D. Holt, Nonempirical Interactions for the Nuclear Shell Model: An Update, Annu. Rev. Nucl. Part. Sci. 69 (1) (2019) 307. doi:10.1146/annurev-nucl-101917-021120.

4coupledcluster [62] G. Hagen, T. Papenbrock, M. Hjorth-Jensen, D. J. Dean, Coupled-cluster computations of atomic nuclei, Rep. Prog. Phys. 77 (9) (2014) 096302. doi:10.1088/0034-4885/77/9/096302.

lson2015quantum [63] J. Carlson, S. Gandolfi, F. Pederiva, S. C. Pieper, R. Schiavilla, K. E. Schmidt, R. B. Wiringa, Quantum Monte Carlo methods for nuclear physics, Rev. Mod. Phys. 87 (3) (2015) 1067. doi:10.1103/RevModPhys.87.1067.

gert2016inmedium [64] H. Hergert, S. K. Bogner, T. D. Morris, A. Schwenk, K. Tsukiyama, The In-Medium Similarity Renormalization Group: A novel ab initio method for nuclei, Phys. Rep. 621 (Supplement C) (2016) 165. doi:10.1016/j.physrep.2015.12.007.

[65] J. Rainwater, Nuclear Energy Level Argument for a Spheroidal Nuclear Model, Phys. Rev. 79 (3) (1950) 432. doi:10.1103/PhysRev.79.432.

[66] A. Bohr, Nuclear Magnetic Moments and Atomic Hyperfine Structure, Phys. Rev. 81 (3) (1951) 331. doi:10.1103/PhysRev.81.331.

[67] J. Rainwater, Background for the spheroidal nuclear model proposal, Rev. Mod. Phys. 48 (3) (1976) 385. doi:10.1103/RevModPhys.48.385.

[68] N. Schunck, Energy Density Functional Methods for Atomic Nuclei., IOP Expanding Physics, IOP Publishing, Bristol, UK, 2019.

[69] M. Brack, J. Damgaard, A. S. Jensen, H. C. Pauli, V. M. Strutinsky, C. Y. Wong, Funny hills: The shell-correction approach to nuclear shell effects and its applications to the fission process, Rev. Mod. Phys. 44 (2) (1972) 320. doi:10.1103/RevModPhys.44.320.

[70] M. Bolsterli, E. O. Fiset, J. R. Nix, J. L. Norton, New Calculation of Fission Barriers for Heavy and Superheavy Nuclei, Phys. Rev. C 5 (3) (1972) 1050. doi:10.1103/PhysRevC.5.1050.

[71] P. Möller, J. R. Nix, W. D. Myers, W. J. Swiatecki, Nuclear Ground-State Masses and Deformations, Atom. Data Nuc. Data Tab. 59 (2) (1995) 185. doi:10.1006/adnd.1995.1002.

[72] P. Möller, J. R. Nix, K. L. Kratz, Nuclear Properties for Astrophysical and Radioactive Ion Beam Applications, Atom. Data Nuc. Data Tab. 66 (2) (1997) 131. doi:10.1016/0375-9474(69)90691-5.

[73] P. Möller, R. Bengtsson, B. G. Carlsson, P. Olivius, T. Ichikawa, Global Calculations of Ground-State Axial Shape Asymmetry of Nuclei, Phys. Rev. Lett. 97 (16) (2006) 162502. doi:10.1103/PhysRevLett.97.162502.

[74] L. Bonneau, P. Quentin, P. Möller, Global microscopic calculations of ground-state spins and parities for odd-mass nuclei, Phys. Rev. C 76 (2) (2007) 024320. doi:10.1103/PhysRevC.76.024320.

[75] P. Möller, A. J. Sierk, T. Ichikawa, H. Sagawa, Nuclear ground-state masses and deformations: FRDM (2012), Atom. Data Nuc. Data Tab. 109 (2016) 1. doi:10.1016/j.adt.2015.10.002.

[76] P.-O. Löwdin, Quantum Theory of Many-Particle Systems. I. Physical Interpretations by Means of Density Matrices, Natural Spin-Orbitals, and Convergence Problems in the Method of Configurational Interaction, Phys. Rev. 97 (6) (1955) 1474. doi:10.1103/PhysRev.97.1474.

[77] P.-O. Löwdin, Quantum Theory of Many-Particle Systems. II. Study of the Ordinary Hartree-Fock Approximation, Phys. Rev. 97 (6) (1955) 1490. doi:10.1103/PhysRev.97.1490.

[78] P.-O. Löwdin, Quantum Theory of Many-Particle Systems. III. Extension of the Hartree-Fock Scheme to Include Degenerate Systems and Correlation Effects, Phys. Rev. 97 (6) (1955) 1509. doi:10.1103/PhysRev.97.1509.

[79] W. Kohn, L. J. Sham, Self-Consistent Equations Including Exchange and Correlation Effects, Phys. Rev. 140 (4A) (1965) A1133. doi:10.1103/PhysRev.140.A1133.

[80] W. Nazarewicz, Microscopic origin of nuclear deformations, Nucl. Phys. A 574 (1) (1994) 27. doi:10.1016/0375-9474(94)90037-X.

[81] H. Flocard, P. Quentin, D. Vautherin, M. Veneroni, A. K. Kerman, Self-consistent calculation of the fission barrier of ^{240}Pu, Nucl. Phys. A 231 (1) (1974) 176. doi:10.1016/0375-9474(74)90300-5.

[82] J. W. Negele, S. E. Koonin, P. Möller, J. R. Nix, A. J. Sierk, Dynamics of induced fission, Phys. Rev. C 17 (3) (1978) 1098. doi:10.1103/PhysRevC.17.1098.

[83] W. D. Myers, W. J. Swiatecki, Average nuclear properties, Ann. Phys. 55 (3) (1969) 395. doi:10.1016/0003-4916(69)90202-4.

[84] W. D. Myers, W. J. Swiatecki, The nuclear droplet model for arbitrary shapes, Ann. Phys. 84 (1-2) (1974) 186. doi:10.1016/0003-4916(74)90299-1.

[85] J. Treiner, H. Krivine, Semi-classical nuclear properties from effective interactions, Ann. Phys. 170 (2) (1986) 406. doi:10.1016/0003-4916(86)90098-9.

[86] P.-G. Reinhard, M. Bender, W. Nazarewicz, T. Vertse, From finite nuclei to the nuclear liquid drop: Leptodermous expansion based on self-consistent mean-field theory, Phys. Rev. C 73 (1) (2006) 014309. doi:10.1103/PhysRevC.73.014309.

[87] N. Nikolov, N. Schunck, W. Nazarewicz, M. Bender, J. Pei, Surface symmetry energy of nuclear energy density functionals, Phys. Rev. C 83 (3) (2011) 034305. doi:10.1103/PhysRevC.83.034305.

[88] W. D. Myers, W. J. Swiatecki, Nuclear masses and deformations, Nucl. Phys. 81 (2) (1966) 1. doi:10.1016/S0029-5582(66)80001-9.

[89] V. M. Strutinsky, Shell effects in nuclear masses and deformation energies, Nucl. Phys. A 95 (2) (1967) 420. doi:10.1016/0375-9474(67)90510-6.

[90] V. M. Strutinsky, "Shells" in deformed nuclei, Nucl. Phys. A 122 (1) (1968) 1. doi:10.1016/0375-9474(68)90699-4.

[91] T. Vertse, A. T. Kruppa, R. J. Liotta, W. Nazarewicz, N. Sandulescu, T. R. Werner, Shell corrections for finite depth potentials: Particle continuum effects, Phys. Rev. C 57 (6) (1998) 3089. doi:10.1103/PhysRevC.57.3089.

[92] A. T. Kruppa, Calculation of the continuum level density, Phys. Lett. B 431 (3) (1998) 237. doi:10.1016/S0370-2693(98)00573-5.

vertse2000shell [93] T. Vertse, A. T. Kruppa, W. Nazarewicz, Shell corrections for finite-depth deformed potentials: Green's function oscillator expansion method, Phys. Rev. C 61 (6) (2000) 064317. doi:10.1103/PhysRevC.61.064317.

rski2004particle [94] K. Pomorski, Particle number conserving shell-correction method, Phys. Rev. C 70 (4) (2004) 044306. doi:10.1103/PhysRevC.70.044306.

v1962spontaneous [95] S. Polikanov, V. Druin, V. Karnaukhov, V. Mikheev, A. Pleve, N. Skobelev, V. Subbotin, G. Terakopyan, V. Fomichev, Spontaneous Fission with an Anomalously Short Period .1., Soviet Physics Jetp-Ussr 15 (6) (1962) 1016–1021.

977spontaneously [96] R. Vandenbosch, Spontaneously Fissioning Isomers, Annu. Rev. Nucl. Part. Sci. 27 (1977) 1–35. doi:10.1146/annurev.ns.27.120177.000245.

brink2005nuclear [97] D. Brink, R. Broglia (Eds.), Nuclear Superfluidity - Pairing in Finite Systems, Cambridge University Press, 2005.

l1972statistical [98] L. G. Moretto, Statistical description of deformation in excited nuclei and disappearance of shell effects with excitation energy, Nucl. Phys. A 182 (3) (1972) 641. doi:10.1016/0375-9474(72)90543-X.

jensen1973shell [99] A. S. Jensen, J. Damgaard, Shell effects in a paired nucleus for finite excitation energies, Nucl. Phys. A 203 (3) (1973) 578. doi:10.1016/0375-9474(73)90365-5.

981microscopic [100] M. Diebel, K. Albrecht, R. W. Hasse, Microscopic calculations of fission barriers and critical angular momenta for excited heavy nuclear systems, Nucl. Phys. A 355 (1) (1981) 66. doi:10.1016/0375-9474(81)90132-9.

gt1983highspin [101] M. J. A. de Voigt, J. Dudek, Z. Szymański, High-spin phenomena in atomic nuclei, Rev. Mod. Phys. 55 (4) (1983) 949. doi:10.1103/RevModPhys.55.949.

a1985rotational [102] T. Bengtsson, I. Ragnarsson, Rotational bands and particle-hole excitations at very high spin, Nucl. Phys. A 436 (1) (1985) 14. doi:10.1016/0375-9474(85)90541-X.

dek1988pairing [103] J. Dudek, B. Herskind, W. Nazarewicz, Z. Szymanski, T. R. Werner, Pairing, temperature, and deformed-shell effects on the properties of superdeformed ^{152}Dy nucleus, Phys. Rev. C 38 (2) (1988) 940. doi:10.1103/PhysRevC.38.940.

erner1995shape [104] T. R. Werner, J. Dudek, Shape Coexistence Effects of Super- and Hyperdeformed Configurations in Rotating Nuclei II. Nuclei with 42≤Z≤56 and 74≤Z≤92, Atom. Data Nuc. Data Tab. 59 (1) (1995) 1. doi:10.1006/adnd.1995.1001.

2018temperature [105] F. A. Ivanyuk, C. Ishizuka, M. D. Usang, S. Chiba, Temperature dependence of shell corrections, Phys. Rev. C 97 (5) (2018) 054331. doi:10.1103/PhysRevC.97.054331.

sson1995shapes [106] S. G. Nilsson, I. Ragnarsson, Shapes and Shells in Nuclear Structure, Cambridge University Press, 1995. doi:10.1017/CBO9780511563973.

1971asymmetric [107] V. V. Pashkevich, On the asymmetric deformation of fissioning nuclei, Nucl. Phys. A 169 (2) (1971) 275. doi:10.1016/0375-9474(71)90884-0.

hr1998nucleara [108] A. Bohr, B. Mottelson, Nuclear Structure, Vol. II, Nuclear Deformations, World Scientific, 1998. doi:10.1142/3530.

81hexadecapole [109] S. G. Rohoziński, A. Sobiczewski, Hexadecapole Nuclear Potential for Non-Axial Shapes, Acta Phys. Pol. B 12 (10) (1981) 1001.

arametrization [110] S. G. Rohoziński, Parametrization of nonaxial deformations in rotational nuclei, Phys. Rev. C 56 (1) (1997) 165. doi:10.1103/PhysRevC.56.165.

i2015universal [111] K. Pomorski, B. Nerlo-Pomorska, J. Bartel, C. Schmitt, Universal, Low-dimensional Shape Parametrization of Fissioning Nuclei, Acta Phys. Pol. B Proc. Suppl. 8 (3) (2015) 667. doi:10.5506/APhysPolBSupp.8.667.

ski2016solving [112] A. Dobrowolski, K. Pomorski, J. Bartel, Solving the eigenvalue problem of the nuclear Yukawa-folded mean-field Hamiltonian, Comput. Phys. Commun. 199 (2016) 118. doi:10.1016/j.cpc.2015.09.020.

2021properties [113] P. Jachimowicz, M. Kowal, J. Skalski, Properties of heaviest nuclei with $98 \leq Z \leq 126$ and $134 \leq N \leq 192$, Atom. Data Nuc. Data Tab. 138 (2021) 101393. doi:10.1016/j.adt.2020.101393.

ler2001nuclear [114] P. Möller, D. G. Madland, A. J. Sierk, A. Iwamoto, Nuclear fission modes and fragment mass asymmetries in a five-dimensional deformation space, Nature 409 (2001) 785. doi:10.1038/35057204.

amps2019effect [115] G. Scamps, C. Simenel, Effect of shell structure on the fission of sub-lead nuclei, Phys. Rev. C 100 (4) (2019) 041602. doi:10.1103/PhysRevC.100.041602.

amps2018impact [116] G. Scamps, C. Simenel, Impact of pear-shaped fission fragments on mass-asymmetric fission in actinides, Nature 564 (7736) (2018) 382. doi:10.1038/s41586-018-0780-0.

972calculation [117] J. R. Nix, Calculation of Fission Barriers for Heavy and Superheavy Nuclei, Annu. Rev. Nucl. Sci. 22 (1) (1972) 65. doi:10.1146/annurev.ns.22.120172.000433.

sson1972fission [118] S. E. Larsson, I. Ragnarsson, S. G. Nilsson, Fission barriers and the inclusion of axial asymmetry, Phys. Lett. B 38 (5) (1972) 269. doi:10.1016/0370-2693(72)90243-2.

moller1989new [119] P. Möller, J. R. Nix, W. J. Swiatecki, New developments in the calculation of heavy-element fission barriers, Nucl. Phys. A 492 (3) (1989) 349. doi:10.1016/0375-9474(89)90403-X.

09heavyelement [120] P. Möller, A. J. Sierk, T. Ichikawa, A. Iwamoto, R. Bengtsson, H. Uhrenholt, S. Åberg, Heavy-element fission barriers, Phys. Rev. C 79 (6) (2009) 064304. doi:10.1103/PhysRevC.79.064304.

[121] M. Kowal, P. Jachimowicz, A. Sobiczewski, Fission barriers for even-even superheavy nuclei, Phys. Rev. C 82 (1) (2010) 014303. doi:10.1103/PhysRevC.82.014303.

[122] P. Jachimowicz, M. Kowal, J. Skalski, Secondary fission barriers in even-even actinide nuclei, Phys. Rev. C 85 (3) (2012) 034305. doi:10.1103/PhysRevC.85.034305.

[123] P. Jachimowicz, M. Kowal, J. Skalski, Eight-dimensional calculations of the third barrier in ^{232}Th, Phys. Rev. C 87 (4) (2013) 044308. doi:10.1103/PhysRevC.87.044308.

[124] P. Jachimowicz, M. Kowal, J. Skalski, Adiabatic fission barriers in superheavy nuclei, Phys. Rev. C 95 (1) (2017) 014303. doi:10.1103/PhysRevC.95.014303.

[125] P. Jachimowicz, M. Kowal, J. Skalski, Static fission properties of actinide nuclei, Phys. Rev. C 101 (1) (2020) 014311. doi:10.1103/PhysRevC.101.014311.

[126] M. Baldo, L. M. Robledo, P. Schuck, X. Viñas, Barcelona-Catania-Paris-Madrid functional with a realistic effective mass, Phys. Rev. C 95 (1) (2017) 014318. doi:10.1103/PhysRevC.95.014318.

[127] S. Goriely, S. Hilaire, A. J. Koning, M. Sin, R. Capote, Towards a prediction of fission cross sections on the basis of microscopic nuclear inputs, Phys. Rev. C 79 (2) (2009) 024612. doi:10.1103/PhysRevC.79.024612.

[128] D. J. Thouless, Stability conditions and nuclear rotations in the Hartree-Fock theory, Nucl. Phys. 21 (1960) 225. doi:10.1016/0029-5582(60)90048-1.

[129] J. G. Valatin, Generalized Hartree-Fock Method, Phys. Rev. 122 (4) (1961) 1012. doi:10.1103/PhysRev.122.1012.

[130] P. Hohenberg, W. Kohn, Inhomogeneous Electron Gas, Phys. Rev. 136 (3B) (1964) B864. doi:10.1103/PhysRev.136.B864.

[131] T. H. R. Skyrme, The effective nuclear potential, Nucl. Phys. 9 (4) (1959) 615. doi:10.1016/0029-5582(58)90345-6.

[132] J. Dechargé, D. Gogny, Hartree-Fock-Bogolyubov calculations with the D1 effective interaction on spherical nuclei, Phys. Rev. C 21 (4) (1980) 1568. doi:10.1103/PhysRevC.21.1568.

[133] M. Bender, P.-H. Heenen, P.-G. Reinhard, Self-consistent mean-field models for nuclear structure, Rev. Mod. Phys. 75 (1) (2003) 121. doi:10.1103/RevModPhys.75.121.

[134] S. A. Fayans, S. V. Tolokonnikov, E. L. Trykov, D. Zawischa, Isotope shifts within the energy-density functional approach with density dependent pairing, Phys. Lett. B 338 (1) (1994) 1. doi:10.1016/0370-2693(94)91334-X.

[135] M. Baldo, P. Schuck, X. Viñas, Kohn-Sham density functional inspired approach to nuclear binding, Phys. Lett. B 663 (5) (2008) 390. doi:10.1016/j.physletb.2008.04.013.

[136] M. Baldo, L. M. Robledo, P. Schuck, X. Viñas, New Kohn-Sham density functional based on microscopic nuclear and neutron matter equations of state, Phys. Rev. C 87 (6) (2013) 064305. doi:10.1103/PhysRevC.87.064305.

[137] A. Bulgac, M. M. Forbes, S. Jin, R. N. Perez, N. Schunck, Minimal nuclear energy density functional, Phys. Rev. C 97 (4) (2018) 044313. doi:10.1103/PhysRevC.97.044313.

[138] J. Sadoudi, M. Bender, K. Bennaceur, D. Davesne, R. Jodon, T. Duguet, Skyrme pseudo-potential-based EDF parametrization for spuriousity-free MR EDF calculations, Phys. Scr. T154 (2013) 014013. doi:10.1088/0031-8949/2013/T154/014013.

[139] J. Sadoudi, T. Duguet, J. Meyer, M. Bender, Skyrme functional from a three-body pseudopotential of second order in gradients: Formalism for central terms, Phys. Rev. C 88 (6) (2013) 064326. doi:10.1103/PhysRevC.88.064326.

[140] H.-J. Mang, The self-consistent single-particle model in nuclear physics, Phys. Rep. 18 (6) (1975) 325. doi:10.1016/0370-1573(75)90012-5.

[141] D. Lacroix, B. Avez, C. Simenel, Quantum Many-Body Dynamics: Applications to Nuclear Reactions, VDM Verlag, 2010.

[142] A. Bulgac, Time-Dependent Density Functional Theory and the Real-Time Dynamics of Fermi Superfluids, Annu. Rev. Nucl. Part. Sci. 63 (1) (2013) 97. doi:10.1146/annurev-nucl-102212-170631.

[143] T. Duguet, The Nuclear Energy Density Functional Formalism, in: C. Scheidenberger, M. Pfützner (Eds.), The Euroschool on Exotic Beams, Vol. IV, Vol. 879, Springer Berlin Heidelberg, Berlin, Heidelberg, 2014, p. 293.

[144] T. Nakatsukasa, K. Matsuyanagi, M. Matsuo, K. Yabana, Time-dependent density-functional description of nuclear dynamics, Rev. Mod. Phys. 88 (4) (2016) 045004. doi:10.1103/RevModPhys.88.045004.

[145] J. R. Stone, P.-G. Reinhard, The Skyrme interaction in finite nuclei and nuclear matter, Prog. Part. Nucl. Phys. 58 (2) (2007) 587. doi:10.1016/j.ppnp.2006.07.001.

[146] L. M. Robledo, T. R. Rodríguez, R. R. Rodríguez-Guzmán, Mean field and beyond description of nuclear structure with the Gogny force: A review, J. Phys. G: Nucl. Part. Phys. 46 (1) (2019) 013001. doi:10.1088/1361-6471/aadebd.

[147] P. Ring, Relativistic mean field theory in finite nuclei, Prog. Part. Nucl. Phys. 37 (1996) 193. doi:10.1016/0146-6410(96)00054-3.

11relativistic [148] T. Nikšić, D. Vretenar, P. Ring, Relativistic nuclear energy density functionals: Mean-field and beyond, Prog. Part. Nucl. Phys. 66 (3) (2011) 519. doi:10.1016/j.ppnp.2011.01.055.

rtel1982better [149] J. Bartel, P. Quentin, M. Brack, C. Guet, H.-B. Håkansson, Towards a better parametrisation of Skyrme-like effective forces: A critical study of the SkM force, Nucl. Phys. A 386 (1) (1982) 79. doi:10.1016/0375-9474(82)90403-1.

nen2012nuclear [150] M. Kortelainen, J. McDonnell, W. Nazarewicz, P.-G. Reinhard, J. Sarich, N. Schunck, M. V. Stoitsov, S. M. Wild, Nuclear energy density optimization: Large deformations, Phys. Rev. C 85 (2) (2012) 024304. doi:10.1103/PhysRevC.85.024304.

1timedependent [151] J. F. Berger, M. Girod, D. Gogny, Time-dependent quantum collective dynamics applied to nuclear fission, Comput. Phys. Commun. 63 (1) (1991) 365. doi:10.1016/0010-4655(91)90263-K.

ksic2008finite [152] T. Nikšić, D. Vretenar, G. A. Lalazissis, P. Ring, Finite- to zero-range relativistic mean-field interactions, Phys. Rev. C 77 (3) (2008) 034302. doi:10.1103/PhysRevC.77.034302.

azissis2005new [153] G. A. Lalazissis, T. Nikšić, D. Vretenar, P. Ring, New relativistic mean-field interaction with density-dependent meson-nucleon couplings, Phys. Rev. C 71 (2) (2005) 024312. doi:10.1103/PhysRevC.71.024312.

zhao2010new [154] P. W. Zhao, Z. P. Li, J. M. Yao, J. Meng, New parametrization for the nuclear covariant energy density functional with a point-coupling interaction, Phys. Rev. C 82 (5) (2010) 054319. doi:10.1103/PhysRevC.82.054319.

nsitydependent [155] R. R. Chasman, Density-dependent delta interactions and actinide pairing matrix elements, Phys. Rev. C 14 (5) (1976) 1935. doi:10.1103/PhysRevC.14.1935.

n2009separable [156] Y. Tian, Z.-Y. Ma, P. Ring, Separable pairing force for relativistic quasiparticle random-phase approximation, Phys. Rev. C 79 (6) (2009) 064301. doi:10.1103/PhysRevC.79.064301.

08nonempirical [157] T. Duguet, T. Lesinski, Non-empirical pairing functional, Eur. Phys. J. A 156 (1) (2008) 207. doi:10.1140/epjst/e2008-00618-x.

09nonempirical [158] T. Lesinski, T. Duguet, K. Bennaceur, J. Meyer, Non-empirical pairing energy density functional: First order in the nuclear plus Coulomb two-body interaction, Eur. Phys. J. A 40 (2) (2009) 121. doi:10.1140/epja/i2009-10780-y.

09nonempirical [159] K. Hebeler, T. Duguet, T. Lesinski, A. Schwenk, Non-empirical pairing energy functional in nuclear matter and finite nuclei, Phys. Rev. C 80 (4) (2009) 044321. doi:10.1103/PhysRevC.80.044321.

enormalization [160] A. Bulgac, Y. Yu, Renormalization of the Hartree-Fock-Bogoliubov Equations in the Case of a Zero Range Pairing Interaction, Phys. Rev. Lett. 88 (4) (2002) 042504. doi:10.1103/PhysRevLett.88.042504.

bulgac2002local [161] A. Bulgac, Local density approximation for systems with pairing correlations, Phys. Rev. C 65 (5) (2002) 051305(R). doi:10.1103/PhysRevC.65.051305.

ewski2000point [162] J. Dobaczewski, J. Dudek, S. G. Rohoziński, T. R. Werner, Point symmetries in the Hartree-Fock approach. I. Densities, shapes, and currents, Phys. Rev. C 62 (1) (2000) 014310. doi:10.1103/PhysRevC.62.014310.

wski2000pointa [163] J. Dobaczewski, J. Dudek, S. G. Rohoziński, T. R. Werner, Point symmetries in the Hartree-Fock approach. II. Symmetry-breaking schemes, Phys. Rev. C 62 (1) (2000) 014311. doi:10.1103/PhysRevC.62.014311.

selfconsistent [164] S. G. Rohoziński, J. Dobaczewski, W. Nazarewicz, Self-consistent symmetries in the proton-neutron Hartree-Fock-Bogoliubov approach, Phys. Rev. C 81 (1) (2010) 014313. doi:10.1103/PhysRevC.81.014313.

1981strutinsky [165] M. Brack, P. Quentin, The Strutinsky method and its foundation from the Hartree-Fock-Bogoliubov approximation at finite temperature, Nucl. Phys. A 361 (1) (1981) 35. doi:10.1016/0375-9474(81)90470-X.

rich1988quantum [166] D. Varshalovich, A. Moskalev, V. Khersonskii, Quantum Theory of Angular Momentum, World Scientific, Singapore, 1988.

014description [167] N. Schunck, D. Duke, H. Carr, A. Knoll, Description of induced nuclear fission with Skyrme energy functionals: Static potential energy surfaces and fission fragment properties, Phys. Rev. C 90 (5) (2014) 054305. doi:10.1103/PhysRevC.90.054305.

atorcoordinate [168] C. Wa Wong, Generator-coordinate methods in nuclear physics, Phys. Rep. 15 (5) (1975) 283. doi:10.1016/0370-1573(75)90036-8.

1957collective [169] J. J. Griffin, J. A. Wheeler, Collective Motions in Nuclei by the Method of Generator Coordinates, Phys. Rev. 108 (2) (1957) 311. doi:10.1103/PhysRev.108.311.

kh2021symmetry [170] J. A. Sheikh, J. Dobaczewski, P. Ring, L. M. Robledo, C. Yannouleas, Symmetry restoration in mean-field approaches, J. Phys. G: Nucl. Part. Phys. 48 (2021) 123001. doi:https://doi.org/10.1088/1361-6471/ac288a.

arityprojected [171] J. L. Egido, L. M. Robledo, Parity-projected calculations on octupole deformed nuclei, Nucl. Phys. A 524 (1) (1991) 65. doi:10.1016/0375-9474(91)90016-Y.

no2001particle [172] M. Anguiano, J. L. Egido, L. M. Robledo, Particle number projection with effective forces, Nucl. Phys. A 696 (3–4) (2001) 467. doi:10.1016/S0375-9474(01)01219-2.

particlenumber [173] J. Dobaczewski, M. V. Stoitsov, W. Nazarewicz, P.-G. Reinhard, Particle-number projection and the density functional theory, Phys. Rev. C 76 (5) (2007) 054315. doi:10.1103/PhysRevC.76.054315.

[174] B. Bally, M. Bender, Projection on particle number and angular momentum: Example of triaxial Bogoliubov quasiparticle states, Phys. Rev. C 103 (2) (2021) 024315. doi:10.1103/PhysRevC.103.024315.

[175] J. L. Egido, State-of-the-art of beyond mean field theories with nuclear density functionals, Phys. Scr. 91 (7) (2016) 073003. doi:10.1088/0031-8949/91/7/073003.

[176] D. M. Brink, A. Weiguny, The generator coordinate theory of collective motion, Nucl. Phys. A 120 (1) (1968) 59. doi:10.1016/0375-9474(68)90059-6.

[177] P.-G. Reinhard, K. Goeke, The generator coordinate method and quantised collective motion in nuclear systems, Rep. Prog. Phys. 50 (1) (1987) 1. doi:10.1088/0034-4885/50/1/001.

[178] S. G. Rohoziński, Gaussian overlap approximation for the quadrupole collective states, J. Phys. G: Nucl. Part. Phys. 39 (9) (2012) 095104. doi:10.1088/0954-3899/39/9/095104.

[179] S. G. Rohoziński, On the Gaussian overlap approximation for the collective excitations of odd nuclei, J. Phys. G: Nucl. Part. Phys. 42 (2) (2015) 025109. doi:10.1088/0954-3899/42/2/025109.

[180] K. Matsuyanagi, M. Matsuo, T. Nakatsukasa, K. Yoshida, N. Hinohara, K. Sato, Microscopic derivation of the Bohr-Mottelson collective Hamiltonian and its application to quadrupole shape dynamics, Phys. Scr. 91 (6) (2016) 063014. doi:10.1088/0031-8949/91/6/063014.

[181] S. Trentalange, S. E. Koonin, A. J. Sierk, Shape parametrization for liquid-drop studies, Phys. Rev. C 22 (3) (1980) 1159. doi:10.1103/PhysRevC.22.1159.

[182] W. Younes, D. Gogny, Nuclear Scission and Quantum Localization, Phys. Rev. Lett. 107 (13) (2011) 132501. doi:10.1103/PhysRevLett.107.132501.

[183] N. Dubray, H. Goutte, J.-P. Delaroche, Structure properties of ^{226}Th and ^{256,258,260}Fm fission fragments: Mean-field analysis with the Gogny force, Phys. Rev. C 77 (1) (2008) 014310. doi:10.1103/PhysRevC.77.014310.

[184] U. Brosa, S. Grossmann, A. Müller, Nuclear scission, Phys. Rep. 197 (4) (1990) 167. doi:10.1016/0370-1573(90)90114-H.

[185] M. Rizea, N. Carjan, Dynamical scission model, Nucl. Phys. A 909 (2013) 50. doi:10.1016/j.nuclphysa.2013.04.014.

[186] M. Warda, A. Zdeb, Fission fragment mass yield deduced from density distribution in the pre-scission configuration, Phys. Scr. 90 (11) (2015) 114003. doi:10.1088/0031-8949/90/11/114003.

[187] K. T. R. Davies, R. A. Managan, J. R. Nix, A. J. Sierk, Rupture of the neck in nuclear fission, Phys. Rev. C 16 (5) (1977) 1890. doi:10.1103/PhysRevC.16.1890.

[188] G. F. Bertsch, W. Younes, L. M. Robledo, Scission dynamics with K partitions, Phys. Rev. C 97 (6) (2018) 064619. doi:10.1103/PhysRevC.97.064619.

[189] G. F. Bertsch, L. M. Robledo, Decay widths at the scission point in nuclear fission, Phys. Rev. C 100 (4) (2019) 044606. doi:10.1103/PhysRevC.100.044606.

[190] G. F. Bertsch, W. Younes, L. M. Robledo, Diabatic paths through the scission point in nuclear fission, Phys. Rev. C 100 (2) (2019) 024607. doi:10.1103/PhysRevC.100.024607.

[191] P. Fong, Fission Dynamics and the Statistical Theory, Phys. Rev. 135 (6B) (1964) B1338. doi:10.1103/PhysRev.135.B1338.

[192] B. D. Wilkins, E. P. Steinberg, R. R. Chasman, Scission-point model of nuclear fission based on deformed-shell effects, Phys. Rev. C 14 (5) (1976) 1832. doi:10.1103/PhysRevC.14.1832.

[193] P. E. Hodgson, Compound nucleus reactions, Rep. Prog. Phys. 50 (9) (1987) 1171. doi:10.1088/0034-4885/50/9/002.

[194] D. Brink, The compound nucleus at high excitation energy, Nucl. Phys. A 519 (1) (1990) 3. doi:10.1016/0375-9474(90)90611-O.

[195] J. L. Egido, P. Ring, The decay of hot nuclei, J. Phys. G: Nucl. Part. Phys. 19 (1) (1993) 1. doi:10.1088/0954-3899/19/1/002.

[196] C. Simenel, K. Godbey, A. S. Umar, Timescales of Quantum Equilibration, Dissipation and Fluctuation in Nuclear Collisions, Phys. Rev. Lett. 124 (21) (2020) 212504. doi:10.1103/PhysRevLett.124.212504.

[197] J. Tōke, R. Bock, G. X. Dai, A. Gobbi, S. Gralla, K. D. Hildenbrand, J. Kuzminski, W. F. J. Müller, A. Olmi, H. Stelzer, B. B. Back, S. Bjørnholm, Quasi-fission — The mass-drift mode in heavy-ion reactions, Nucl. Phys. A 440 (2) (1985) 327. doi:10.1016/0375-9474(85)90344-6.

[198] E. Merzbacher, Quantum Mechanics, John Wiley and Sons, Inc, 1961.

[199] A. Klein, N. R. Walet, G. Do Dang, Classical theory of collective motion in the large amplitude, small velocity regime, Ann. Phys. 208 (1) (1991) 90. doi:10.1016/0003-4916(91)90343-7.

[200] H. Hofmann, A quantal transport theory for nuclear collective motion: The merits of a locally harmonic approximation, Phys. Rep. 284 (4) (1997) 137. doi:10.1016/S0370-1573(97)00006-9.

[201] G. D. Dang, A. Klein, N. R. Walet, Self-consistent theory of large-amplitude collective motion: Applications to approximate quantization of nonseparable systems and to nuclear physics, Phys. Rep. 335 (3) (2000) 93. doi:10.1016/S0370-1573(99)00119-2.

asa2012density [202] T. Nakatsukasa, Density functional approaches to collective phenomena in nuclei: Time-dependent density functional theory for perturbative and non-perturbative nuclear dynamics, Prog. Theor. Exp. Phys. 2012 (1) (2012) 1A207. doi:10.1093/ptep/pts016.

initeamplitude [203] K. Washiyama, N. Hinohara, T. Nakatsukasa, Finite-amplitude method for collective inertia in spontaneous fission, Phys. Rev. C 103 (1) (2021) 014306. doi:10.1103/PhysRevC.103.014306.

ordinatemethod [204] K. Goeke, P.-G. Reinhard, The generator-coordinate-method with conjugate parameters and the unification of microscopic theories for large amplitude collective motion, Ann. Phys. 124 (2) (1980) 249. doi:10.1016/0003-4916(80)90210-9.

1981quadrupole [205] J. Dobaczewski, J. Skalski, The quadrupole vibrational inertial function in the adiabatic time-dependent Hartree-Fock-Bogolyubov approximation, Nucl. Phys. A 369 (1) (1981) 123. doi:10.1016/0375-9474(81)90010-5.

hara2012effect [206] N. Hinohara, Z. P. Li, T. Nakatsukasa, T. Nikšić, D. Vretenar, Effect of time-odd mean fields on inertial parameters of the quadrupole collective Hamiltonian, Phys. Rev. C 85 (2) (2012) 024323. doi:10.1103/PhysRevC.85.024323.

2011quadrupole [207] A. Baran, J. A. Sheikh, J. Dobaczewski, W. Nazarewicz, A. Staszczak, Quadrupole collective inertia in nuclear fission: Cranking approximation, Phys. Rev. C 84 (5) (2011) 054321. doi:10.1103/PhysRevC.84.054321.

onperturbative [208] S. A. Giuliani, L. M. Robledo, Non-perturbative collective inertias for fission: A comparative study, Phys. Lett. B 787 (2018) 134. doi:10.1016/j.physletb.2018.10.045.

0timedependent [209] J. Zhao, T. Nikšić, D. Vretenar, S.-G. Zhou, Time-dependent generator coordinate method study of fission: Mass parameters, Phys. Rev. C 101 (6) (2020) 064605. doi:10.1103/PhysRevC.101.064605.

013spontaneous [210] J. Sadhukhan, K. Mazurek, A. Baran, J. Dobaczewski, W. Nazarewicz, J. A. Sheikh, Spontaneous fission lifetimes from the minimization of self-consistent collective action, Phys. Rev. C 88 (6) (2013) 064314. doi:10.1103/PhysRevC.88.064314.

hbaeva1999mass [211] E. K. Yuldashbaeva, J. Libert, P. Quentin, M. Girod, Mass parameters for large amplitude collective motion: A perturbative microscopic approach, Phys. Lett. B 461 (1–2) (1999) 1. doi:10.1016/S0370-2693(99)00836-9.

o2000adiabatic [212] M. Matsuo, T. Nakatsukasa, K. Matsuyanagi, Adiabatic Selfconsistent Collective Coordinate Method for Large Amplitude Collective Motion in Nuclei with Pairing Correlations, Prog. Theor. Phys. 103 (5) (2000) 959. doi:10.1143/PTP.103.959.

gaugeinvariant [213] N. Hinohara, T. Nakatsukasa, M. Matsuo, K. Matsuyanagi, Gauge-Invariant Formulation of the Adiabatic Self-Consistent Collective Coordinate Method, Prog. Theor. Phys. 117 (3) (2007) 451. doi:10.1143/PTP.117.451.

ani2013fission [214] S. A. Giuliani, L. M. Robledo, Fission properties of the Barcelona-Catania-Paris-Madrid energy density functional, Phys. Rev. C 88 (2013) 054325. doi:10.1103/PhysRevC.88.054325.

ani2014dynamic [215] S. A. Giuliani, L. M. Robledo, R. Rodríguez-Guzmán, Dynamic versus static fission paths with realistic interactions, Phys. Rev. C 90 (5) (2014) 054311. doi:10.1103/PhysRevC.90.054311.

pairinginduced [216] J. Sadhukhan, J. Dobaczewski, W. Nazarewicz, J. A. Sheikh, A. Baran, Pairing-induced speedup of nuclear spontaneous fission, Phys. Rev. C 90 (6) (2014) 061304. doi:10.1103/PhysRevC.90.061304.

llyconstrained [217] J. Zhao, B.-N. Lu, T. Nikšić, D. Vretenar, S.-G. Zhou, Multidimensionally-constrained relativistic mean-field study of spontaneous fission: Coupling between shape and pairing degrees of freedom, Phys. Rev. C 93 (4) (2016) 044315. doi:10.1103/PhysRevC.93.044315.

015uncertainty [218] J. D. McDonnell, N. Schunck, D. Higdon, J. Sarich, S. M. Wild, W. Nazarewicz, Uncertainty Quantification for Nuclear Density Functional Theory and Information Content of New Measurements, Phys. Rev. Lett. 114 (12) (2015) 122501. doi:10.1103/PhysRevLett.114.122501.

ck2020bayesian [219] N. Schunck, K. R. Quinlan, J. Bernstein, A Bayesian analysis of nuclear deformation properties with Skyrme energy functionals, J. Phys. G: Nucl. Part. Phys. 47 (10) (2020) 104002. doi:10.1088/1361-6471/aba4fa.

ernard2019role [220] R. Bernard, S. A. Giuliani, L. M. Robledo, Role of dynamic pairing correlations in fission dynamics, Phys. Rev. C 99 (6) (2019) 064301. doi:10.1103/PhysRevC.99.064301.

966spontaneous [221] M. G. Urin, D. F. Zaretsky, On the spontaneous fission of nuclei, Nucl. Phys. 75 (1) (1966) 101. doi:10.1016/0029-5582(66)90749-8.

o1972influence [222] L. G. Moretto, S. G. Thompson, J. Routti, R. C. Gatti, Influence of shells and pairing on the fission probabilities of nuclei below radium, Phys. Lett. B 38 (7) (1972) 471. doi:10.1016/0370-2693(72)90519-9.

retto1974large [223] L. G. Moretto, R. P. Babinet, Large superfluidity enhancement in the penetration of the fission barrier, Phys. Lett. B 49 (2) (1974) 147. doi:10.1016/0370-2693(74)90494-8.

gozdz1985mass [224] A. Góźdź, K. Pomorski, M. Brack, E. Werner, The mass parameters for the average mean-field potential, Nucl. Phys. A 442 (1) (1985) 26. doi:10.1016/0375-9474(85)90131-9.

v1987influence [225] Y. A. Lazarev, Influence of Pairing Correlations on the Probability and Dynamics of Tunnelling Through the Barrier in Fission and Fusion of Complex Nuclei, Phys. Scr. 35 (3) (1987) 255. doi:10.1088/0031-8949/35/3/007.

[226] A. Staszczak, S. Piłat, K. Pomorski, Influence of the pairing vibrations on spontaneous fission probability, Nucl. Phys. A 504 (3) (1989) 589. doi:10.1016/0375-9474(89)90559-9.

[227] J. Randrup, S. E. Larsson, P. Möller, S. G. Nilsson, K. Pomorski, A. Sobiczewski, Spontaneous-fission half-lives for even nuclei with $Z \geq 92$, Phys. Rev. C 13 (1) (1976) 229. doi:10.1103/PhysRevC.13.229.

[228] A. Baran, K. Pomorski, A. Lukasiak, A. Sobiczewski, A dynamic analysis of spontaneous-fission half-lives, Nucl. Phys. A 361 (1) (1981) 83. doi:10.1016/0375-9474(81)90471-1.

[229] M. Warda, J. Egido, L. Robledo, Spontaneous fission of Fm isotopes in the HFB framework, Phys. Scr. T125 (2006) 226. doi:10.1088/0031-8949/2006/T125/063.

[230] S. Levit, J. W. Negele, Z. Paltiel, Time-dependent mean-field theory and quantized bound states, Phys. Rev. C 21 (4) (1980) 1603. doi:10.1103/PhysRevC.21.1603.

[231] S. Levit, J. W. Negele, Z. Paltiel, Barrier penetration and spontaneous fission in the time-dependent mean-field approximation, Phys. Rev. C 22 (5) (1980) 1979. doi:10.1103/PhysRevC.22.1979.

[232] G. Puddu, J. W. Negele, Solution of the mean field equations for spontaneous fission, Phys. Rev. C 35 (3) (1987) 1007. doi:10.1103/PhysRevC.35.1007.

[233] S. Levit, Variational approach to tunneling dynamics. Application to hot superfluid Fermi systems. Spontaneous and induced fission, Phys. Lett. B 813 (2021) 136042. doi:10.1016/j.physletb.2020.136042.

[234] J. Skalski, Nuclear fission with mean-field instantons, Phys. Rev. C 77 (6) (2008) 064610. doi:10.1103/PhysRevC.77.064610.

[235] W. Brodziński, J. Skalski, Instanton-motivated study of spontaneous fission of odd-A nuclei, Phys. Rev. C 102 (5) (2020) 054603. doi:10.1103/PhysRevC.102.054603.

[236] G. Scamps, K. Hagino, Multidimensional fission model with a complex absorbing potential, Phys. Rev. C 91 (4) (2015) 044606. doi:10.1103/PhysRevC.91.044606.

[237] K. Hagino, G. F. Bertsch, Microscopic model for spontaneous fission: Validity of the adiabatic approximation, Phys. Rev. C 101 (6) (2020) 064317. doi:10.1103/PhysRevC.101.064317.

[238] K. Hagino, G. F. Bertsch, Least action and the maximum-coupling approximations in the theory of spontaneous fission, Phys. Rev. C 102 (2) (2020) 024316. doi:10.1103/PhysRevC.102.024316.

[239] H. J. Rose, G. A. Jones, A new kind of natural radioactivity, Nature 307 (5948) (1984) 245. doi:10.1038/307245a0.

[240] D. N. Poenaru, Y. Nagame, R. A. Gherghescu, W. Greiner, Systematics of cluster decay modes, Phys. Rev. C 65 (5) (2002) 054308. doi:10.1103/PhysRevC.65.054308.

[241] D. N. Poenaru, R. A. Gherghescu, W. Greiner, Potential energy surfaces for cluster emitting nuclei, Phys. Rev. C 73 (1) (2006) 014608. doi:10.1103/PhysRevC.73.014608.

[242] M. Mirea, Time-dependent pairing equations for seniority-one nuclear systems, Phys. Rev. C 78 (4) (2008) 044618. doi:10.1103/PhysRevC.78.044618.

[243] M. Warda, L. M. Robledo, Microscopic description of cluster radioactivity in actinide nuclei, Phys. Rev. C 84 (4) (2011) 044608. doi:10.1103/PhysRevC.84.044608.

[244] Z. Matheson, S. A. Giuliani, W. Nazarewicz, J. Sadhukhan, N. Schunck, Cluster radioactivity of $^{294}_{118}\mathrm{Og}_{176}$, Phys. Rev. C 99 (4) (2019) 041304. doi:10.1103/PhysRevC.99.041304.

[245] R. Bonetti, M. B. Chadwick, P. E. Hodgson, B. V. Carlson, M. S. Hussein, The Feshbach-Kerman-Koonin multistep compound reaction theory, Phys. Rep. 202 (4) (1991) 171–231. doi:10.1016/0370-1573(91)90105-U.

[246] G. F. Bertsch, P. F. Bortignon, R. A. Broglia, Damping of nuclear excitations, Rev. Mod. Phys. 55 (1) (1983) 287. doi:10.1103/RevModPhys.55.287.

[247] B. Lauritzen, T. Døssing, R. A. Broglia, Damping of rotational motion, Nucl. Phys. A 457 (1) (1986) 61. doi:10/bww3dp.

[248] M. Matsuo, T. Døssing, B. Herskind, S. Frauendorf, Poisson and Porter-Thomas fluctuations in off-yrast rotational transitions, Nucl. Phys. A 564 (3) (1993) 345. doi:10/dh4k8r.

[249] T. Døssing, B. Herskind, S. Leoni, A. Bracco, R. A. Broglia, M. Matsuo, E. Vigezzi, Fluctuation analysis of rotational spectra, Phys. Rep. 268 (1) (1996) 1. doi:10/dq7gx6.

[250] M. Matsuo, K. Yoshida, T. Døssing, E. Vigezzi, R. A. Broglia, Microscopic structure of rotational damping, Nucl. Phys. A 649 (1) (1999) 379. doi:10/fn8vkb.

[251] N. Otuka, E. Dupont, V. Semkova, B. Pritychenko, A. I. Blokhin, M. Aikawa, S. Babykina, M. Bossant, G. Chen, S. Dunaeva, R. A. Forrest, T. Fukahori, N. Furutachi, S. Ganesan, Z. Ge, O. O. Gritzay, M. Herman, S. Hlavač, K. Katō, B. Lalremruata, Y. O. Lee, A. Makinaga, K. Matsumoto, M. Mikhaylyukova, G. Pikulina, V. G. Pronyaev, A. Saxena, O. Schwerer, S. P. Simakov, N. Soppera, R. Suzuki, S. Takács, X. Tao, S. Taova, F. Tárkányi, V. V. Varlamov, J. Wang, S. C. Yang, V. Zerkin, Y. Zhuang, Towards a More Complete and Accurate Experimental Nuclear Reaction Data Library (EXFOR): International Collaboration Between Nuclear Reaction Data Centres (NRDC), Nucl. Data Sheets 120 (2014) 272. doi:10.1016/j.nds.2014.07.065.

[252] V. V. Zerkin, B. Pritychenko, The experimental nuclear reaction data (EXFOR): Extended computer database and Web retrieval system, Nucl. Instrum. Methods in Phys. Res. A 888 (2018) 31. doi:10.1016/j.nima.2018.01.045.

[253] F. Tovesson, T. S. Hill, Cross Sections for ^{239}Pu(n,f) and ^{241}Pu(n,f) in the Range E_n = 0.01 eV to 200 MeV, Nucl. Sci. Eng. 165 (2) (2010) 224. doi:10.13182/NSE09-41.

[254] M. B. Chadwick, M. Herman, P. Obložinský, M. E. Dunn, Y. Danon, A. C. Kahler, D. L. Smith, B. Pritychenko, G. Arbanas, R. Arcilla, R. Brewer, D. A. Brown, R. Capote, A. D. Carlson, Y. S. Cho, H. Derrien, K. Guber, G. M. Hale, S. Hoblit, S. Holloway, T. D. Johnson, T. Kawano, B. C. Kiedrowski, H. Kim, S. Kunieda, N. M. Larson, L. Leal, J. P. Lestone, R. C. Little, E. A. McCutchan, R. E. MacFarlane, M. MacInnes, C. M. Mattoon, R. D. McKnight, S. F. Mughabghab, G. P. A. Nobre, G. Palmiotti, A. Palumbo, M. T. Pigni, V. G. Pronyaev, R. O. Sayer, A. A. Sonzogni, N. C. Summers, P. Talou, I. J. Thompson, A. Trkov, R. L. Vogt, S. C. van der Marck, A. Wallner, M. C. White, D. Wiarda, P. G. Young, ENDF/B-VII.1 Nuclear Data for Science and Technology: Cross Sections, Covariances, Fission Product Yields and Decay Data, Nucl. Data Sheets 112 (12) (2011) 2887. doi:10.1016/j.nds.2011.11.002.

[255] A. J. Koning, D. Rochman, Modern Nuclear Data Evaluation with the TALYS Code System, Nuclear Data Sheets 113 (12) (2012) 2841. doi:10.1016/j.nds.2012.11.002.

[256] D. L. Smith, N. Otuka, Experimental Nuclear Reaction Data Uncertainties: Basic Concepts and Documentation, Nucl. Data Sheets 113 (12) (2012) 3006. doi:10.1016/j.nds.2012.11.004.

[257] D. A. Brown, M. Herman, S. Hoblit, E. A. McCutchan, G. P. A. Nobre, B. Pritychenko, A. A. Sonzogni, Uncertainty quantification in the Nuclear Data Program, J. Phys. G: Nucl. Part. Phys. 42 (3) (2015) 034020. doi:10.1088/0954-3899/42/3/034020.

[258] P. Talou, T. Kawano, M. B. Chadwick, D. Neudecker, M. E. Rising, Uncertainties in nuclear fission data, J. Phys. G: Nucl. Part. Phys. 42 (3) (2015) 034025. doi:10.1088/0954-3899/42/3/034025.

[259] H. A. Kramers, Brownian motion in a field of force and the diffusion model of chemical reactions, Phys. 7 (4) (1940) 284. doi:10.1016/S0031-8914(40)90098-2.

[260] Y. Abe, S. Ayik, P.-G. Reinhard, E. Suraud, On stochastic approaches of nuclear dynamics, Phys. Rep. 275 (2–3) (1996) 49. doi:10.1016/0370-1573(96)00003-8.

[261] H. Risken, The Fokker-Planck Equation - Methods of Solution and Applications, Springer, 1989. doi:10.10071978-3-642-61544-3.

[262] P. Hänggi, P. Talkner, M. Brokovec, Reaction-rate theory: Fifty years after Kramers, Rev. Mod. Phys. 62 (2) (1990) 251. doi:10.1103/RevModPhys.62.251.

[263] H. Hofmann, The Physics of Warm Nuclei: With Analogies to Mesoscopic Systems, Oxford Studies in Nuclear Physics, Oxford University Press, Oxford, 2008. doi:10.1093/acprof:oso/9780198504016.001.0001.

[264] P. Grangé, H. A. Weidenmüller, Fission probability and the nuclear friction constant, Phys. Lett. B 96 (1) (1980) 26. doi:10.1016/0370-2693(80)90204-X.

[265] P. Grangé, L. Jun-Qing, H. A. Weidenmüller, Induced nuclear fission viewed as a diffusion process: Transients, Phys. Rev. C 27 (5) (1983) 2063. doi:10.1103/PhysRevC.27.2063.

[266] Z. Jing-Shang, H. A. Weidenmüller, Generalization of Kramers's formula: Fission over a multidimensional potential barrier, Phys. Rev. C 28 (5) (1983) 2190. doi:10.1103/PhysRevC.28.2190.

[267] P. Grange, Effects of transients on particle emission prior to fission in a transport description of the fission process, Nucl. Phys. A 428 (1984) 37. doi:10.1016/0375-9474(84)90241-0.

[268] H. A. Weidenmüller, Z. Jing-Shang, Stationary diffusion over a multidimensional potential barrier: A generalization of Kramers' formula, J. Stat. Phys. 34 (1-2) (1984) 191. doi:10.1007/BF01770354.

[269] D. M. Brink, L. F. Canto, The decay rate in a multi-dimensional fission problem, J. Phys. G: Nucl. Phys. 12 (6) (1986) L147. doi:10.1088/0305-4616/12/6/004.

[270] P. N. Nadtochy, A. Kelić, K.-H. Schmidt, Fission rate in multi-dimensional Langevin calculations, Phys. Rev. C 75 (6) (2007) 064614. doi:10.1103/PhysRevC.75.064614.

[271] I. I. Gontchar, R. A. Kuzyakin, Integral Kramers formula for the fission rate versus dynamical modeling: The case of deformation-dependent temperature, Phys. Rev. C 84 (1) (2011) 014617. doi:10.1103/PhysRevC.84.014617.

[272] D. Boilley, E. Suraud, A. Yasuhisa, S. Ayik, Nuclear fission with a Langevin equation, Nucl. Phys. A 556 (1) (1993) 67. doi:10.1016/0375-9474(93)90238-S.

[273] T. Wada, N. Carjan, Y. Abe, Multi-dimensional Langevin approach to fission dynamics, Nucl. Phys. A 538 (1992) 283. doi:10.1016/0375-9474(92)90778-I.

[274] I. I. Gontchar, P. Fröbrich, Nuclear fission: Combining the dynamical Langevin equation with the statistical model, Nucl. Phys. A 551 (3) (1993) 495. doi:10.1016/0375-9474(93)90459-B.

[275] P. Fröbrich, G. R. Tillack, Path-integral derivation for the rate of stationary diffusion over a multidimensional barrier, Nucl. Phys. A 540 (1) (1992) 353. doi:10.1016/0375-9474(92)90209-3.

[276] P. Fröbrich, I. I. Gontchar, N. D. Mavlitov, Langevin fluctuation-dissipation dynamics of hot nuclei: Prescission neutron multiplicities and fission probabilities, Nucl. Phys. A 556 (2) (1993) 281. doi:10.1016/0375-9474(93)90352-X.

[277] V. V. Sargsyan, Y. V. Palchikov, Z. Kanokov, G. G. Adamian, N. V. Antonenko, Fission rate and transient time with a quantum master equation, Phys. Rev. C 76 (6) (2007) 064604. doi:10.1103/PhysRevC.76.064604.

[278] S. V. Radionov, V. M. Kolomietz, Non-Markovian fission rate within the Kramers model, Phys. Rev. C 92 (2) (2015) 024311. doi:10.1103/PhysRevC.92.024311.

[279] W. Hauser, H. Feshbach, The Inelastic Scattering of Neutrons, Phys. Rev. 87 (2) (1952) 366. doi:10.1103/PhysRev.87.366.

[280] N. Bohr, Neutron capture and nuclear constitution, Nature 137 (1936) 344. doi:10.1038/137344a0.

[281] V. Weisskopf, Statistics and Nuclear Reactions, Phys. Rev. 52 (1937) 295. doi:10.1103/PhysRev.52.295.

[282] H. A. Bethe, Nuclear Physics B. Nuclear Dynamics, Theoretical, Rev. Mod. Phys. 9 (2) (1937) 69. doi:10.1103/RevModPhys.9.69.

[283] V. F. Weisskopf, D. H. Ewing, On the Yield of Nuclear Reactions with Heavy Elements, Phys. Rev. 57 (6) (1940) 472. doi:10.1103/PhysRev.57.472.

[284] J. Blatt, W. Weisskopf, Theoretical Nuclear Physics, Springer, New York, NY, 1979.

[285] P. A. Moldauer, Theory of Average Neutron Reaction Cross Sections in the Resonance Region, Phys. Rev. 123 (3) (1961) 968. doi:10.1103/PhysRev.123.968.

[286] C. Mahaux, H. A. Weidenmuller, Recent Developments in Compound-Nucleus Theory, Annu. Rev. Nucl. Part. Sci. 29 (1) (1979) 1. doi:10.1146/annurev.ns.29.120179.000245.

[287] C. A. Engelbrecht, H. A. Weidenmüller, Hauser-Feshbach Theory and Ericson Fluctuations in the Presence of Direct Reactions, Phys. Rev. C 8 (3) (1973) 859–862. doi:10.1103/PhysRevC.8.859.

[288] M. Kawai, A. K. Kerman, K. W. McVoy, Modification of Hauser-Feshbach calculations by direct-reaction channel coupling, Ann. Phys. 75 (1) (1973) 156. doi:10.1016/0003-4916(73)90465-X.

[289] D. Agassi, H. A. Weidenmüller, G. Mantzouranis, The statistical theory of nuclear reactions for strongly overlapping resonances as a theory of transport phenomena, Phys. Rep. 22 (3) (1975) 145. doi:10.1016/0370-1573(75)90028-9.

[290] P. Talou, I. Stetcu, P. Jaffke, M. E. Rising, A. E. Lovell, T. Kawano, Fission fragment decay simulations with the CGMF code, Comput. Phys. Commun. 269 (2021) 108087. doi:10.1016/j.cpc.2021.108087.

[291] S. Bjørnholm, J. E. Lynn, The double-humped fission barrier, Rev. Mod. Phys. 52 (4) (1980) 725. doi:10.1103/RevModPhys.52.725.

[292] E. Wigner, The transition state method, Trans. Faraday Soc. 34 (0) (1938) 29. doi:10.1039/TF9383400029.

[293] A. J. Koning, S. Hilaire, S. Goriely, Talys 1.95 User Manual.

[294] D. L. Hill, J. A. Wheeler, Nuclear Constitution and the Interpretation of Fission Phenomena, Phys. Rev. 89 (5) (1953) 1102. doi:10.1103/PhysRev.89.1102.

[295] A. J. Sierk, Macroscopic model of rotating nuclei, Phys. Rev. C 33 (6) (1986) 2039–2053. doi:10.1103/PhysRevC.33.2039.

[296] A. Mamdouh, J. M. Pearson, M. Rayet, F. Tondeur, Fission barriers of neutron-rich and superheavy nuclei calculated with the ETFSI method, Nucl. Phys. A 679 (3) (2001) 337–358. doi:10.1016/S0375-9474(00)00358-4.

[297] V. Y. Denisov, I. Y. Sedykh, Calculation of the fission width of an excited nucleus with the fission barrier dependent on excitation energy, Phys. Rev. C 98 (2) (2018) 024601. doi:10.1103/PhysRevC.98.024601.

[298] P. Tamagno, Challenging fission cross section simulation with long standing macro-microscopic model of nucleus potential energy surface, Ph.D. thesis (2015).

[299] J. D. Cramer, J. R. Nix, Exact Calculation of the Penetrability Through Two-Peaked Fission Barriers, Phys. Rev. C 2 (3) (1970) 1048–1057. doi:10.1103/PhysRevC.2.1048.

[300] J. N. Leboeuf, R. C. Sharma, F-matrix calculation of penetrability through double-hump fission barriers, Nucl. Phys. A 208 (3) (1973) 514. doi:10.1016/0375-9474(73)90671-4.

[301] M. Sin, R. Capote, M. W. Herman, A. Trkov, Extended optical model for fission, Phys. Rev. C 93 (3) (2016) 034605. doi:10.1103/PhysRevC.93.034605.

[302] G. Vladuca, M. Sin, A. Tudora, PROBFIS — A program for subbarrier prompt and isomeric fission probabilities calculations for even-even nuclei, Comput. Phys. Commun. 83 (2) (1994) 266. doi:10.1016/0010-4655(94)90054-X.

[303] H. Weigmann, An interpretation of the structure of subthreshold fission cross section of ^{240}Pu, Z. Physik 214 (1) (1968) 7. doi:10.1007/BF01380080.

[304] S. Bjørnholm, V. M. Strutinsky, Intermediate states in fission, Nucl. Phys. A 136 (1) (1969) 1. doi:10.1016/0375-9474(69)90035-9.

[305] H. Feshbach, A. K. Kerman, R. H. Lemmer, Intermediate structure and doorway states in nuclear reactions, Ann. Phys. 41 (2) (1967) 230. doi:10.1016/0003-4916(67)90235-7.

[306] J. E. Lynn, B. B. Back, Sub-barrier fission probability for a double-humped barrier, J. Phys. A: Math. Nucl. Gen. 7 (3) (1974) 395. doi:10.1088/0305-4470/7/3/011.

[307] P. D. Goldstone, P. Paul, Doorway-state approach to the calculation of fission widths, Phys. Rev. C 18 (4) (1978) 1733. doi:10.1103/PhysRevC.18.1733.

ane1958rmatrix [308] A. M. Lane, R. G. Thomas, R-Matrix Theory of Nuclear Reactions, Rev. Mod. Phys. 30 (2) (1958) 257. doi:10.1103/RevModPhys.30.257.

ont2010rmatrix [309] P. Descouvemont, D. Baye, The R-matrix theory, Rep. Prog. Phys. 73 (3) (2010) 036301. doi:10.1088/0034-4885/73/3/036301.

jean2021conrad [310] C. D. S. Jean, P. Tamagno, P. Archier, G. Noguere, CONRAD – a code for nuclear data modeling and evaluation, EPJ Nuclear Sci. Technol. 7 (2021) 10. doi:10.1051/epjn/2021011.

rson2008updated [311] N. M. Larson, Updated User's Guide for Sammy: Multilevel R-Matrix Fits to Neutron Data Using Bayes' Equations, Tech. Rep. ORNL/TM-9179/R8, Oak Ridge National Lab. (ORNL), Oak Ridge, TN (United States) (2008). doi:10.2172/941054.

nn1968structure [312] J. E. Lynn, Structure Effects in Fission, in: Nuclear Structure: Dubna Symposium 1968, International Atomic Energy Agency (IAEA), Dubna, 1968, p. 463.

nn1969structure [313] J. E. Lynn, Structure phenomena in near-barrier fission reactions, in: Physics and Chemistry of Fission, International Atomic Energy Agency (IAEA), Vienna, 1969, p. 249.

ynn1973fission [314] J. E. Lynn, Fission in nuclear reaction theory, J. Phys. A: Math. Nucl. Gen. 6 (4) (1973) 542. doi:10.1088/0305-4470/6/4/018.

975doorwaystate [315] A. Vitturi, F. Zardi, Doorway-state description of fission intermediate structure, Riv. Nuovo Cim. 5 (4) (1975) 648. doi:10.1007/BF02747510.

20investigation [316] A. Stamatopoulos, A. Tsinganis, N. Colonna, M. Kokkoris, R. Vlastou, M. Diakaki, P. Žugec, P. Schillebeeckx, F. Gunsing, M. Sabaté-Gilarte, M. Barbagallo, O. Aberle, J. Andrzejewski, L. Audouin, V. Bécares, M. Bacak, J. Balibrea, S. Barros, F. Bečvář, C. Beinrucker, F. Belloni, E. Berthoumieux, J. Billowes, D. Bosnar, M. Brugger, M. Caamaño, S. Lo Meo, F. Calviño, M. Calviani, D. Cano-Ott, F. Cerutti, E. Chiaveri, G. Cortés, M. A. Cortés-Giraldo, L. Cosentino, L. A. Damone, K. Deo, C. Domingo-Pardo, R. Dressler, E. Dupont, I. Durán, B. Fernández-Domínguez, A. Ferrari, P. Ferreira, P. Finocchiaro, R. J. W. Frost, V. Furman, K. Göbel, A. R. García, I. Gheorghe, T. Glodariu, I. F. Gonçalves, E. González-Romero, A. Goverdovski, E. Griesmayer, C. Guerrero, H. Harada, T. Heftrich, S. Heinitz, A. Hernández-Prieto, J. Heyse, D. G. Jenkins, E. Jericha, F. Käppeler, Y. Kadi, T. Katabuchi, P. Kavrigin, V. Ketlerov, V. Khryachkov, A. Kimura, N. Kivel, I. Knapova, M. Krtička, E. Leal-Cidoncha, C. Lederer, H. Leeb, J. Lerendegui-Marco, M. Licata, R. Losito, D. Macina, J. Marganiec, T. Martínez, C. Massimi, P. Mastinu, M. Mastromarco, F. Matteucci, E. Mendoza, A. Mengoni, P. M. Milazzo, F. Mingrone, M. Mirea, S. Montesano, A. Musumarra, R. Nolte, F. R. Palomo-Pinto, C. Paradela, N. Patronis, A. Pavlik, J. Perkowski, A. Plompen, J. I. Porras, J. Praena, J. M. Quesada, T. Rauscher, R. Reifarth, A. Riego-Perez, M. Robles, C. Rubbia, J. A. Ryan, A. Saxena, S. Schmidt, D. Schumann, P. Sedyshev, A. G. Smith, S. V. Suryanarayana, G. Tagliente, J. L. Tain, A. Tarifeño Saldivia, L. Tassan-Got, S. Valenta, G. Vannini, V. Variale, P. Vaz, A. Ventura, V. Vlachoudis, A. Wallner, S. Warren, M. Weigand, C. Weiss, T. Wright,

Investigation of the ^{240}Pu(n,f) reaction at the nTOF/EAR2 facility in the 9 meV–6 MeV range, Phys. Rev. C 102 (2020) 014616. doi:10.1103/PhysRevC.102.014616.

son2009neutron [317] F. Tovesson, T. S. Hill, M. Mocko, J. D. Baker, C. A. McGrath, Neutron induced fission of ^{240,242}Pu from 1 eV to 200 MeV, Phys. Rev. C 79 (2009) 014613. doi:10.1103/PhysRevC.79.014613.

land2013rmatrix [318] O. Bouland, J. E. Lynn, P. Talou, R-matrix analysis and prediction of low-energy neutron-induced fission cross sections for a range of Pu isotopes, Phys. Rev. C 88 (5) (2013) 054612. doi:10.1103/PhysRevC.88.054612.

ck1974strength [319] B. B. Back, Strength function for fission in the two humped barrier model, Nucl. Phys. A 228 (2) (1974) 323. doi:10.1016/0375-9474(74)90436-9.

land1997rmatrix [320] O. Bouland, H. Derrien, N. M. Larson, L. C. Leal, R-Matrix Analysis of the ^{240}Pu Neutron Cross Sections in the Thermal to 5700-eV Energy Range, Nucl. Sci. Eng. 127 (2) (1997) 105–129. doi:10.13182/NSE127-105.

eal1999rmatrix [321] L. C. Leal, H. Derrien, N. M. Larson, R. Q. Wright, R-Matrix Analysis of ^{235}U Neutron Transmission and Cross-Section Measurements in the 0- to 2.25-keV Energy Range, Nucl. Sci. Eng. 131 (2) (1999) 230–253. doi:10.13182/NSE99-A2031.

land2014impact [322] O. Bouland, J. E. Lynn, P. Talou, The Impact of Intermediate Structure on the Average Fission Cross Sections, Nucl. Data Sheets 118 (2014) 211. doi:10.1016/j.nds.2014.04.039.

019reexamining [323] O. Bouland, Reexamining fission-probability data using $\mathcal{R}$-matrix Monte Carlo simulations: Beyond the surrogate-reaction method, Phys. Rev. C 100 (6) (2019) 064611. doi:10.1103/PhysRevC.100.064611.

0timedependent [324] M. Verriere, D. Regnier, The Time-Dependent Generator Coordinate Method in Nuclear Physics, Front. Phys. 8 (2020) 1. doi:10.3389/fphy.2020.00233.

asca2016energy [325] H. Pasca, A. V. Andreev, G. G. Adamian, N. V. Antonenko, Y. Kim, Energy dependence of mass, charge, isotopic, and energ distributions in neutron-induced fission of ^{235}U and ^{239}Pu, Phys. Rev. C 93 (5) (2016) 054602. doi:10.1103/PhysRevC.93.054602.

emaitre2015new [326] J.-F. Lemaître, S. Panebianco, J.-L. Sida, S. Hilaire, S. Heinrich, New statistical scission-point model to predict fission fragment observables, Phys. Rev. C 92 (3) (2015) 034617. doi:10.1103/PhysRevC.92.034617.

aitre2019fully [327] J.-F. Lemaître, S. Goriely, S. Hilaire, J.-L. Sida, Fully microscopic scission-point model to predict fission fragment observables, Phys. Rev. C 99 (3) (2019) 034612. doi:10.1103/PhysRevC.99.034612.

018transitions [328] H. Paşca, A. V. Andreev, G. G. Adamian, N. V. Antonenko, Transitions between symmetric and asymmetric modes in the region of heavy actinides, Nucl. Phys. A 969 (2018) 226. doi:10.1016/j.nuclphysa.2017.10.001.

sca2018induced [329] H. Paşca, A. V. Andreev, G. G. Adamian, N. V. Antonenko, Induced fission modes of Fermium and Nobelium isotopes, Nucl. Phys. A 977 (2018) 1. doi:10.1016/j.nuclphysa.2018.05.008.

21simultaneous [330] H. Paşca, A. V. Andreev, G. G. Adamian, N. V. Antonenko, Simultaneous description of charge, mass, total kinetic energy, and neutron multiplicity distributions in fission of Th and U isotopes, Phys. Rev. C 104 (1) (2021) 014604. doi:10.1103/PhysRevC.104.014604.

asca2019change [331] H. Paşca, A. V. Andreev, G. G. Adamian, N. V. Antonenko, Change of the shape of mass and charge distributions in fission of Cf isotopes with excitation energy, Phys. Rev. C 99 (6) (2019) 064611. doi:10.1103/PhysRevC.99.064611.

ch1998langevin [332] P. Fröbrich, I. I. Gontchar, Langevin description of fusion, deep-inelastic collisions and heavy-ion-induced fission, Phys. Rep. 292 (3-4) (1998) 131. doi:10.1016/S0370-1573(97)00042-2.

cki1978onebody [333] J. Blocki, Y. Boneh, J. R. Nix, J. Randrup, M. Robel, A. J. Sierk, W. J. Swiatecki, One-body dissipation and the super-viscidity of nuclei, Ann. Phys. 113 (2) (1978) 330. doi:10.1016/0003-4916(78)90208-7.

984dissipative [334] J. Randrup, W. J. Swiatecki, Dissipative resistance against changes in the mass asymmetry degree of freedom in nuclear dynamics: The completed wall-and-window formula, Nucl. Phys. A 429 (1) (1984) 105. doi:10.1016/0375-9474(84)90151-9.

rk2017langevin [335] A. J. Sierk, Langevin model of low-energy fission, Phys. Rev. C 96 (3) (2017) 034603. doi:10.1103/PhysRevC.96.034603.

016microscopic [336] J. Sadhukhan, W. Nazarewicz, N. Schunck, Microscopic modeling of mass and charge distributions in the spontaneous fission of ^{240}Pu, Phys. Rev. C 93 (1) (2016) 011304. doi:10.1103/PhysRevC.93.011304.

n2017formation [337] J. Sadhukhan, C. Zhang, W. Nazarewicz, N. Schunck, Formation and distribution of fragments in the spontaneous fission of ^{240}Pu, Phys. Rev. C 96 (6) (2017) 061301. doi:10.1103/PhysRevC.96.061301.

n2020efficient [338] J. Sadhukhan, S. A. Giuliani, Z. Matheson, W. Nazarewicz, Efficient method for estimation of fission fragment yields of r-process nuclei, Phys. Rev. C 101 (6) (2020) 065803. doi:10.1103/PhysRevC.101.065803.

020microscopic [339] J. Sadhukhan, Microscopic Theory for Spontaneous Fission, Front. Phys. 8 (2020) 567171. doi:10.3389/fphy.2020.567171.

ang2016effects [340] M. D. Usang, F. A. Ivanyuk, C. Ishizuka, S. Chiba, Effects of microscopic transport coefficients on fission observables calculated by the Langevin equation, Phys. Rev. C 94 (4) (2016) 044602. doi:10.1103/PhysRevC.94.044602.

015independent [341] Y. Aritomo, S. Chiba, K. Nishio, Independent fission yields studied based on Langevin equation, Prog. Nucl. Energy 85 (2015) 568. doi:10.1016/j.pnucene.2015.08.004.

[342] K. Pomorski, A. Dobrowolski, R. Han, B. Nerlo-Pomorska, M. Warda, Z. Xiao, Y. Chen, L. Liu, J.-L. Tian, Mass yields of fission fragments of Pt to Ra isotopes, Phys. Rev. C 101 (6) (2020) 064602. doi:10.1103/PhysRevC.101.064602.

[343] M. D. Usang, F. A. Ivanyuk, C. Ishizuka, S. Chiba, Analysis of the total kinetic energy of fission fragments with the Langevin equation, Phys. Rev. C 96 (6) (2017) 064617. doi:10.1103/PhysRevC.96.064617.

[344] L.-L. Liu, Y.-J. Chen, X.-Z. Wu, Z.-X. Li, Z.-G. Ge, K. Pomorski, Analysis of nuclear fission properties with the Langevin approach in Fourier shape parametrization, Phys. Rev. C 103 (4) (2021) 044601. doi:10.1103/PhysRevC.103.044601.

[345] M. Albertsson, B. G. Carlsson, T. Døssing, P. Möller, J. Randrup, S. Åberg, Calculated fission-fragment mass yields and average total kinetic energies of heavy and superheavy nuclei, Eur. Phys. J. A 56 (2) (2020) 46. doi:10.1140/epja/s10050-020-00036-9.

[346] S. Tanaka, Y. Aritomo, Y. Miyamoto, K. Hirose, K. Nishio, Effects of multichance fission on isotope dependence of fission fragment mass distributions at high energies, Phys. Rev. C 100 (6) (2019) 064605. doi:10.1103/PhysRevC.100.064605.

[347] J. Randrup, P. Möller, Brownian Shape Motion on Five-Dimensional Potential-Energy Surfaces: Nuclear Fission-Fragment Mass Distributions, Phys. Rev. Lett. 106 (13) (2011) 132503. doi:10.1103/PhysRevLett.106.132503.

[348] J. Randrup, P. Möller, A. J. Sierk, Fission-fragment mass distributions from strongly damped shape evolution, Phys. Rev. C 84 (3) (2011) 034613. doi:10.1103/PhysRevC.84.034613.

[349] P. Möller, J. Randrup, A. J. Sierk, Calculated fission yields of neutron-deficient mercury isotopes, Phys. Rev. C 85 (2) (2012) 024306. doi:10.1103/PhysRevC.85.024306.

[350] J. Randrup, P. Möller, Energy dependence of fission-fragment mass distributions from strongly damped shape evolution, Phys. Rev. C 88 (6) (2013) 064606. doi:10.1103/PhysRevC.88.064606.

[351] P. Möller, J. Randrup, Calculated fission-fragment yield systematics in the region $74 \leq Z \leq 94$ and $90 \leq N \leq 150$, Phys. Rev. C 91 (4) (2015) 044316. doi:10.1103/PhysRevC.91.044316.

[352] A. V. Ignatyuk, I. N. Mikhailov, L. H. Molina, R. G. Nazmitdinov, K. Pomorsky, The shape of the heated fast-rotating nuclei, Nucl. Phys. A 346 (1–2) (1980) 191. doi:10.1016/0375-9474(80)90497-2.

[353] N. Schunck, J. Dudek, B. Herskind, Nuclear hyperdeformation and the Jacobi shape transition, Phys. Rev. C 75 (5) (2007) 054304. doi:10.1103/PhysRevC.75.054304.

[354] D. E. Ward, B. G. Carlsson, T. Døssing, P. Möller, J. Randrup, S. Åberg, Nuclear shape evolution based on microscopic level densities, Phys. Rev. C 95 (2) (2017) 024618. doi:10.1103/PhysRevC.95.024618.

gac2019fission [355] A. Bulgac, S. Jin, K. J. Roche, N. Schunck, I. Stetcu, Fission dynamics of ^{240}Pu from saddle to scission and beyond, Phys. Rev. C 100 (3) (2019) 034615. doi:10.1103/PhysRevC.100.034615.

erk1980fission [356] A. J. Sierk, J. R. Nix, Fission in a wall-and-window one-body-dissipation model, Phys. Rev. C 21 (3) (1980) 982. doi:10.1103/PhysRevC.21.982.

tte1980fission [357] G. Schütte, P. Möller, J. R. Nix, A. J. Sierk, Fission with microscopic energy dissipation, Z. Phys. A 297 (4) (1980) 289. doi:10.1007/BF01422786.

yuk1999pairing [358] F. A. Ivanyuk, H. Hofmann, Pairing and shell effects in the transport coefficients of collective motion, Nucl. Phys. A 657 (1) (1999) 19. doi:10.1016/S0375-9474(99)00324-3.

ann2001nuclear [359] H. Hofmann, F. A. Ivanyuk, C. Rummel, S. Yamaji, Nuclear fission: The "onset of dissipation" from a microscopic point of view, Phys. Rev. C 64 (5) (2001) 054316. doi:10.1103/PhysRevC.64.054316.

2015collective [360] Y. Tanimura, D. Lacroix, G. Scamps, Collective aspects deduced from time-dependent microscopic mean-field with pairing: Application to the fission process, Phys. Rev. C 92 (3) (2015) 034601. doi:10.1103/PhysRevC.92.034601.

el2018heavyion [361] C. Simenel, A. S. Umar, Heavy-ion collisions and fission dynamics with the time-dependent Hartree–Fock theory and its extensions, Prog. Part. Nucl. Phys. 103 (2018) 19. doi:10.1016/j.ppnp.2018.07.002.

5timedependent [362] R. Balian, M. Véneroni, Time-dependent variational principle for the expectation value of an observable: Mean-field applications, Ann. Phys. 164 (2) (1985) 334. doi:10.1016/0003-4916(85)90020-X.

zot1985quantum [363] J.-P. Blaizot, G. Ripka, Quantum Theory of Finite Systems, The MIT Press, Cambridge, 1985.

lian1988static [364] R. Balian, M. Véneroni, Static and dynamic variational principles for expectation values of observables, Ann. Phys. 187 (1) (1988) 29. doi:10.1016/0003-4916(88)90280-1.

92correlations [365] R. Balian, M. Véneroni, Correlations and fluctuations in static and dynamic mean-field approaches, Ann. Phys. 216 (2) (1992) 351. doi:10.1016/0003-4916(92)90181-K.

gac2020nuclear [366] A. Bulgac, S. Jin, I. Stetcu, Nuclear Fission Dynamics: Past, Present, Needs, and Future, Front. Phys. 8 (2020) 63. doi:10.3389/fphy.2020.00063.

gac2021fission [367] A. Bulgac, I. Abdurrahman, S. Jin, K. Godbey, N. Schunck, I. Stetcu, Fission Fragment Intrinsic Spins and Their Correlations, Phys. Rev. Lett. 126 (14) (2021) 142502. doi:10.1103/PhysRevLett.126.142502.

el2014formation [368] C. Simenel, A. S. Umar, Formation and dynamics of fission fragments, Phys. Rev. C 89 (3) (2014) 031601(R). doi:10.1103/PhysRevC.89.031601.

ancic2020shape [369] M. Pancic, Y. Qiang, J. Pei, P. Stevenson, Shape Evolutions in Fission Dynamics Within Time-Dependent Hartree-Fock Approach, Front. Phys. 8 (2020) 351. doi:10.3389/fphy.2020.00351.

maruhn2014tdhf [370] J. A. Maruhn, P.-G. Reinhard, P. D. Stevenson, A. S. Umar, The TDHF code Sky3D, Comput. Phys. Commun. 185 (7) (2014) 2195. doi:10.1016/j.cpc.2014.04.008.

etrumpf2018tdhf [371] B. Schuetrumpf, P. G. Reinhard, P. D. Stevenson, A. S. Umar, J. A. Maruhn, The TDHF code Sky3D Version 1.1, Comput. Phys. Commun. 229 (2018) 211–213. doi:10.1016/j.cpc.2018.03.012.

jin2021lise [372] S. Jin, K. J. Roche, I. Stetcu, I. Abdurrahman, A. Bulgac, The LISE package: Solvers for static and time-dependent superfluid local density approximation equations in three dimensions, Comput. Phys. Commun. 269 (2021) 108130. doi:10.1016/j.cpc.2021.108130.

2015superfluid [373] G. Scamps, C. Simenel, D. Lacroix, Superfluid dynamics of ^{258}Fm fission, Phys. Rev. C 92 (1) (2015) 011602. doi:10.1103/PhysRevC.92.011602.

lard2015fission [374] P. Goddard, P. Stevenson, A. Rios, Fission dynamics within time-dependent Hartree-Fock: Deformation-induced fission, Phys. Rev. C 92 (5) (2015) 054610. doi:10.1103/PhysRevC.92.054610.

lard2016fission [375] P. Goddard, P. Stevenson, A. Rios, Fission dynamics within time-dependent Hartree-Fock. II. Boost-induced fission, Phys. Rev. C 93 (1) (2016) 014620. doi:10.1103/PhysRevC.93.014620.

le1982meanfield [376] J. W. Negele, The mean-field theory of nuclear structure and dynamics, Rev. Mod. Phys. 54 (4) (1982) 913. doi:10.1103/RevModPhys.54.913.

984fluctuations [377] R. Balian, M. Vénéroni, Fluctuations in a time-dependent mean-field approach, Phys. Lett. B 136 (5–6) (1984) 301. doi:10.1016/0370-2693(84)92008-2.

2008stochastic [378] S. Ayik, A stochastic mean-field approach for nuclear dynamics, Phys. Lett. B 658 (4) (2008) 174. doi:10.1016/j.physletb.2007.09.072.

2014stochastic [379] D. Lacroix, S. Ayik, Stochastic quantum dynamics beyond mean field, Eur. Phys. J. A 50 (6) (2014) 95. doi:10.1140/epja/i2014-14095-8.

017microscopic [380] Y. Tanimura, D. Lacroix, S. Ayik, Microscopic Phase-Space Exploration Modeling of ^{258}Fm Spontaneous Fission, Phys. Rev. Lett. 118 (15) (2017) 152501. doi:10.1103/PhysRevLett.118.152501.

gac2019unitary [381] A. Bulgac, S. Jin, I. Stetcu, Unitary evolution with fluctuations and dissipation, Phys. Rev. C 100 (1) (2019) 014615. doi:10.1103/PhysRevC.100.014615.

1timedependent [382] R. Balian, M. Vénéroni, Time-Dependent Variational Principle for Predicting the Expectation Value of an Observable, Phys. Rev. Lett. 47 (19) (1981) 1353–1356. doi:10.1103/PhysRevLett.47.1353.

kizawa2019tdhf [383] K. Sekizawa, TDHF Theory and Its Extensions for the Multinucleon Transfer Reaction: A Mini Review, Front. Phys. 7. doi:10.3389/fphy.2019.00020.

einhard1983time [384] P. G. Reinhard, R. Y. Cusson, K. Goeke, Time evolution of coherent ground-state correlations and the TDHF approach, Nucl. Phys. A 398 (1) (1983) 141. doi:10.1016/0375-9474(83)90653-X.

[385] D. Regnier, D. Lacroix, Microscopic description of pair transfer between two superfluid Fermi systems. II. Quantum mixing of time-dependent Hartree-Fock-Bogolyubov trajectories, Phys. Rev. C 99 (6) (2019) 064615. doi:10.1103/PhysRevC.99.064615.

[386] W. Cassing, W. Nörenberg, On the role of memory effects for dissipation and diffusion in slow collective nuclear motion, Nucl. Phys. A 401 (3) (1983) 467. doi:10.1016/0375-9474(83)90361-5.

[387] M. Baranger, M. Veneroni, An adiabatic time-dependent Hartree-Fock theory of collective motion in finite systems, Ann. Phys. 114 (1) (1978) 123. doi:10.1016/0003-4916(78)90265-8.

[388] G. Holzwarth, Four approaches to the function of inertia in a solvable model, Nucl. Phys. A 207 (3) (1973) 545. doi:10.1016/0375-9474(73)90861-0.

[389] D. M. Brink, M. J. Giannoni, M. Veneroni, Derivation of an adiabatic time-dependent Hartree-Fock formalism from a variational principle, Nucl. Phys. A 258 (2) (1976) 237. doi:10.1016/0375-9474(76)90004-X.

[390] F. Villars, Adiabatic time-dependent Hartree-Fock theory in nuclear physics, Nucl. Phys. A 285 (2) (1977) 269. doi:10.1016/0375-9474(77)90253-6.

[391] S. J. Krieger, K. Goeke, Application of the adiabatic, time-dependent Hartree-Bogolyubov approximation to a solvable model, Nucl. Phys. A 234 (2) (1974) 269. doi:10.1016/0375-9474(74)90562-4.

[392] H. Goutte, J.-F. Berger, P. Casoli, D. Gogny, Microscopic approach of fission dynamics applied to fragment kinetic energy and mass distributions in ^{238}U, Phys. Rev. C 71 (2) (2005) 024316. doi:10.1103/PhysRevC.71.024316.

[393] D. Regnier, N. Dubray, N. Schunck, M. Verrière, Fission fragment charge and mass distributions in ^{239}Pu(n,f) in the adiabatic nuclear energy density functional theory, Phys. Rev. C 93 (5) (2016) 054611. doi:10.1103/PhysRevC.93.054611.

[394] A. Zdeb, A. Dobrowolski, M. Warda, Fission dynamics of ^{252}Cf, Phys. Rev. C 95 (5) (2017) 054608. doi:10.1103/PhysRevC.95.054608.

[395] J. F. Berger, M. Girod, D. Gogny, Microscopic analysis of collective dynamics in low energy fission, Nucl. Phys. A 428 (1984) 23. doi:10.1016/0375-9474(84)90240-9.

[396] D. Regnier, M. Verrière, N. Dubray, N. Schunck, FELIX-1.0: A finite element solver for the time dependent generator coordinate method with the Gaussian overlap approximation, Comput. Phys. Commun. 200 (2016) 350. doi:10.1016/j.cpc.2015.11.013.

[397] D. Regnier, N. Dubray, M. Verrière, N. Schunck, FELIX-2.0: New version of the finite element solver for the time dependent generator coordinate method with the Gaussian overlap approximation, Comput. Phys. Commun. 225 (2018) 180. doi:10.1016/j.cpc.2017.12.007.

es2012fragment [398] W. Younes, D. Gogny, Fragment Yields Calculated in a Time-Dependent Microscopic Theory of Fission, Tech. Rep. LLNL-TR-586678, Lawrence Livermore National Laboratory (LLNL), Livermore, CA (2012).

017microscopic [399] H. Tao, J. Zhao, Z. P. Li, T. Nikšić, D. Vretenar, Microscopic study of induced fission dynamics of ^{226}Th with covariant energy density functionals, Phys. Rev. C 96 (2) (2017) 024319. doi:10.1103/PhysRevC.96.024319.

019microscopic [400] J. Zhao, T. Nikšić, D. Vretenar, S.-G. Zhou, Microscopic self-consistent description of induced fission dynamics: Finite-temperature effects, Phys. Rev. C 99 (1) (2019) 014618. doi:10.1103/PhysRevC.99.014618.

2019asymmetric [401] D. Regnier, N. Dubray, N. Schunck, From asymmetric to symmetric fission in the fermium isotopes within the time-dependent generator-coordinate-method formalism, Phys. Rev. C 99 (2) (2019) 024611. doi:10.1103/PhysRevC.99.024611.

9timedependent [402] J. Zhao, J. Xiang, Z.-P. Li, T. Nikšić, D. Vretenar, S.-G. Zhou, Time-dependent generator-coordinate-method study of mass-asymmetric fission of actinides, Phys. Rev. C 99 (5) (2019) 054613. doi:10.1103/PhysRevC.99.054613.

021microscopic [403] M. Verriere, N. Schunck, D. Regnier, Microscopic calculation of fission product yields with particle-number projection, Phys. Rev. C 103 (5) (2021) 054602. doi:10.1103/PhysRevC.103.054602.

1984comparison [404] C. Wagemans, E. Allaert, A. Deruytter, R. Barthélémy, P. Schillebeeckx, Comparison of the energy and mass characteristics of the ^{239}Pu(n$_{\mathrm{th}}$,f) and the ^{240}Pu(sf) fragments, Phys. Rev. C 30 (1) (1984) 218. doi:10.1103/PhysRevC.30.218.

t1986precision [405] P. Geltenbort, F. Gönnenwein, A. Oed, Precision measurements of mean kinetic energy release in thermal-neutron-induced fission of ^{233}U, ^{235}U and ^{239}Pu, Radiat. Eff. 93 (1-4) (1986) 57. doi:10.1080/00337578608207429.

992comparative [406] P. Schillebeeckx, C. Wagemans, A. J. Deruytter, R. Barthélémy, Comparative study of the fragments' mass and energy characteristics in the spontaneous fussion of ^{238}Pu, ^{240}Pu and ^{242}Pu and in the thermal-neutron-induced fission of ^{239}Pu, Nucl. Phys. A 545 (3) (1992) 623. doi:10.1016/0375-9474(92)90296-V.

995measurement [407] K. Nishio, Y. Nakagome, I. Kanno, I. Kimura, Measurement of Fragment Mass Dependent Kinetic Energy and Neutron Multiplicity for Thermal Neutron Induced Fission of Plutonium-239, J. Nucl. Sci. Technol. 32 (5) (1995) 404. doi:10.1080/18811248.1995.9731725.

00simultaneous [408] C. Tsuchiya, Y. Nakagome, H. Yamana, H. Moriyama, K. Nishi, I. Kanno, K. Shin, I. Kimura, Simultaneous Measurement of Prompt Neutrons and Fission Fragments for ^{239}Pu(n$_{\mathrm{th}}$,f), J. Nucl. Sci. Technol. 37 (11) (2000) 941. doi:10.1080/18811248.2000.9714976.

er1984fragment [409] R. Müller, A. A. Naqvi, F. Käppeler, F. Dickmann, Fragment velocities, energies, and masses from fast neutron induced fission of ^{235}U, Phys. Rev. C 29 (3) (1984) 885. doi:10.1103/PhysRevC.29.885.

simon1990pulse [410] G. Simon, J. Trochon, F. Brisard, C. Signarbieux, Pulse height defect in an ionization chamber investigated by cold fission measurements, Nucl. Instrum. Methods in Phys. Res. A 286 (1) (1990) 220. doi:10.1016/0168-9002(90)90224-T.

6investigation [411] S. Zeynalov, V. I. Furman, F. J. Hambsch, M. Florec, V. Y. Konovalov, V. A. Khryachkov, Y. S. Zamyatnin, Investigation of mass-TKE distributions of fission fragments from the U-235(n,f)- reaction in resonances, in: Proceedings of the 13th International Seminar on Interaction of Neutrons with Nuclei (ISINN-13) - Neutron Spectroscopy, Nuclear Structure, Related Topics, Vol. 13, Joint Institute for Nuclear Research, 2006, pp. 351–359.

ano2010fission [412] C. Romano, Y. Danon, R. Block, J. Thompson, E. Blain, E. Bond, Fission fragment mass and energy distributions as a function of incident neutron energy measured in a lead slowing-down spectrometer, Phys. Rev. C 81 (1) (2010) 014607. doi:10.1103/PhysRevC.81.014607.

021microscopic [413] J. Zhao, T. Nikšić, D. Vretenar, Microscopic self-consistent description of induced fission: Dynamical pairing degree of freedom, Phys. Rev. C 104 (4) (2021) 044612. doi:10.1103/PhysRevC.104.044612.

a2021generator [414] N. Hizawa, K. Hagino, K. Yoshida, Generator coordinate method with a conjugate momentum: Application to particle number projection, Phys. Rev. C 103 (3) (2021) 034313. doi:10.1103/PhysRevC.103.034313.

ere2017fission [415] M. Verrière, N. Dubray, N. Schunck, D. Regnier, P. Dossantos-Uzarralde, Fission description: First steps towards a full resolution of the time-dependent Hill-Wheeler equation, EPJ Web Conf. 146 (2017) 04034. doi:10.1051/epjconf/201714604034.

y2012numerical [416] N. Dubray, D. Regnier, Numerical search of discontinuities in self-consistent potential energy surfaces, Comput. Phys. Commun. 183 (10) (2012) 2035. doi:10.1016/j.cpc.2012.05.001.

u2021smoothing [417] N.-W. T. Lau, R. N. Bernard, C. Simenel, Smoothing of 1D and 2D discontinuities in potential energy surfaces, arXiv:2111.06513.

011microscopic [418] R. Bernard, H. Goutte, D. Gogny, W. Younes, Microscopic and nonadiabatic Schrödinger equation derived from the generator coordinate method based on zero- and two-quasiparticle states, Phys. Rev. C 84 (4) (2011) 044308. doi:10.1103/PhysRevC.84.044308.

010microscopic [419] K. Dietrich, J.-J. Niez, J.-F. Berger, Microscopic transport theory of nuclear processes, Nucl. Phys. A 832 (3) (2010) 249. doi:10.1016/j.nuclphysa.2009.11.004.

ard1978concept [420] P.-G. Reinhard, K. Goeke, The concept of a collective path and its range of validity, Nucl. Phys. A 312 (1) (1978) 121. doi:10.1016/0375-9474(78)90579-1.

reedimensional [421] K. Goeke, F. Grümmer, P.-G. Reinhard, Three-dimensional nuclear dynamics in the quantized ATDHF approach, Ann. Phys. 150 (2) (1983) 504. doi:10.1016/0003-4916(83)90025-8.

008microscopic [422] N. Hinohara, T. Nakatsukasa, M. Matsuo, K. Matsuyanagi, Microscopic Derivation of Collective Hamiltonian by Means of the Adiabatic Self-Consistent Collective Coordinate Method: Shape Mixing in Low-Lying States of ^{68}Se and ^{72}Kr, Prog. Theor. Phys. 119 (1) (2008) 59. doi:10.1143/PTP.119.59.

lpern1971three [423] I. Halpern, Three Fragment Fission, Annu. Rev. Nucl. Sci. 21 (1) (1971) 245. doi:10.1146/annurev.ns.21.120171.001333.

d1989lowenergy [424] J. P. Theobald, P. Heeg, M. Mutterer, Low-energy ternary fission, Nuclear Physics A 502 (1989) 343. doi:10.1016/0375-9474(89)90674-X.

jan1976origine [425] N. Cârjan, Sur l'origine des alphas de scission, J. Phys. France 37 (11) (1976) 1279. doi:10.1051/jphys:0197600370110127900.

aru2001nuclear [426] D. N. Poenaru, W. Greiner, J. H. Hamilton, A. V. Ramayya, Nuclear molecules in ternary fission, APH N.S., Heavy Ion Physics 14 (1) (2001) 285. doi:10.1556/APH.14.2001.1-4.27.

021calculation [427] V. Y. Denisov, I. Y. Sedykh, Calculation of fission fragment characteristics for the reactions $n_{th}+^{235}$u and $n_{14\ MeV}+^{235}$u, Eur. Phys. J. A 57 (4) (2021) 129. doi:10.1140/epja/s10050-021-00433-8.

ura1987dynamic [428] O. Tanimura, T. Fliessbach, Dynamic model for alpha particle emission during fission, Z. Phys. A 328 (4) (1987) 475. doi:10.1007/BF01289634.

fer1995quantum [429] R. Schafer, T. Fliessbach, Quantum mechanical treatment of alpha-particle emission during fission, J. Phys. G: Nucl. Part. Phys. 21 (6) (1995) 861. doi:10.1088/0954-3899/21/6/013.

nya1988dynamic [430] V. A. Rubchenya, S. G. Yavshits, Dynamic treatment of ternary fission, Z. Phys. A 329 (2) (1988) 217. doi:10.1007/BF01283778.

ne2004combined [431] J. P. Lestone, Combined statistical and dynamical model of ternary nuclear fission, Phys. Rev. C 70 (2) (2004) 021601. doi:10.1103/PhysRevC.70.021601.

7comprehensive [432] A. Tudora, F. J. Hambsch, Comprehensive overview of the Point-by-Point model of prompt emission in fission, Eur. Phys. J. A 53 (8) (2017) 159. doi:10.1140/epja/i2017-12347-9.

shman1996monte [433] G. Fishman, Monte Carlo, corrected Edition, Springer, 1996.

idt2016general [434] K.-H. Schmidt, B. Jurado, C. Amouroux, C. Schmitt, General Description of Fission Observables: GEF Model Code, Nucl. Data Sheets 131 (2016) 107. doi:10.1016/j.nds.2015.12.009.

eke2015fission [435] J. M. Verbeke, J. Randrup, R. Vogt, Fission Reaction Event Yield Algorithm, FREYA - For event-by-event simulation of fission, Comput. Phys. Commun. 191 (2015) 178. doi:10.1016/j.cpc.2015.02.002.

967deexcitation [436] J. R. Grover, J. Gilat, De-Excitation of Highly Excited Nuclei, Phys. Rev. 157 (4) (1967) 802–813. doi:10.1103/PhysRev.157.802.

1967dissipation [437] J. R. Grover, J. Gilat, Dissipation of Energy and Angular Momentum by Emission of Neutrons and Gamma Rays, Phys. Rev. 157 (4) (1967) 814–823. doi:10.1103/PhysRev.157.814.

rer1967emission [438] J. R. Grover, J. Gilat, Emission of Alpha Particles from Nuclei Having Large Angular Momenta, Phys. Rev. 157 (4) (1967) 823–831. doi:10.1103/PhysRev.157.823.

omas1967angular [439] T. D. Thomas, J. R. Grover, Angular Momentum Effects in the Gamma-Ray De-Excitation of Fission Fragments, Phys. Rev. 159 (4) (1967) 980–984. doi:10.1103/PhysRev.159.980.

npen2006summary [440] A. Plompen, A. Carlson, H. Henriksson, A. Ignatyuk, R. Jacqmin, R. McKnight, G. Rimpault, M. Salvatores, Summary record of the WPEC Subgroup C meeting on the High Priority Request List (HPRL).
URL http://www.oecd-nea.org/dbdata/hprl/Documentation/HPRL-minutes_3May06.pdf

dnea2006nuclear [441] OECD-NEA, Nuclear Data High Priority Request List (Req. ID: H.3 and H.4).
URL http://www.oecd-nea.org/dbdata/hprl/hprlview.pl?ID=421

emaire2006monte [442] S. Lemaire, P. Talou, T. Kawano, M. B. Chadwick, D. G. Madland, Monte Carlo approach to sequential γ-ray emission from fission fragments, Phys. Rev. C 73 (1) (2006) 014602. doi:10.1103/PhysRevC.73.014602.

no2021influence [443] T. Kawano, S. Okumura, A. E. Lovell, I. Stetcu, P. Talou, Influence of nonstatistical properties in nuclear structure on emission of prompt fission neutrons, Phys. Rev. C 104 (1) (2021) 014611. doi:10.1103/PhysRevC.104.014611.

l2021extension [444] A. E. Lovell, T. Kawano, S. Okumura, I. Stetcu, M. R. Mumpower, P. Talou, Extension of the Hauser-Feshbach fission fragment decay model to multichance fission, Phys. Rev. C 103 (1) (2021) 014615. doi:10.1103/PhysRevC.103.014615.

2017microscopic [445] K. Sekizawa, Microscopic description of production cross sections including deexcitation effects, Phys. Rev. C 96 (1) (2017) 014615. doi:10.1103/PhysRevC.96.014615.

oning2008talys1 [446] A. J. Koning, S. Hilaire, M. C. Duijvestijn, TALYS-1.0, in: Proceedings of the International Conference on Nuclear Data for Science and Technology, EDP Sciences, Nice, France, 2008, p. 211. doi:10.1051/ndata:07767.

erman2007empire [447] M. Herman, R. Capote, B. V. Carlson, P. Obložinský, M. Sin, A. Trkov, H. Wienke, V. Zerkin, EMPIRE: Nuclear Reaction Model Code System for Data Evaluation, Nucl. Data Sheets 108 (12) (2007) 2655. doi:10.1016/j.nds.2007.11.003.

eutronfragment [448] J. P. Lestone, Neutron-fragment and Neutron-neutron Correlations in Low-energy Fission, Nucl. Data Sheets 131 (2016) 357–376. doi:10.1016/j.nds.2015.12.007.

leman1967prompt [449] J. W. Boldeman, A. W. Dalton, Prompt Nu-bar measurements for thermal neutron fusion, Tech. Rep. AAEC/E-172, Australian Atomic Energy Commission Research Establishment, Lucas Heights (Australia) (1967).

8nuclearcharge [450] A. C. Wahl, Nuclear-charge distribution and delayed-neutron yields for thermal-neutron-induced fission of ^{235}U, ^{233}U, and ^{239}Pu and for spontaneous fission of ^{252}Cf, Atom. Data Nucl. Data Tab. 39 (1) (1988) 1–156. doi:10.1016/0092-640X(88)90016-2.

12eventbyevent [451] R. Vogt, J. Randrup, D. A. Brown, M. A. Descalle, W. E. Ormand, Event-by-event evaluation of the prompt fission neutron spectrum from ^{239}Pu(n,f), Phys. Rev. C 85 (2) (2012) 024608. doi:10.1103/PhysRevC.85.024608.

00relativistic [452] K.-H. Schmidt, S. Steinhäuser, C. Böckstiegel, A. Grewe, A. Heinz, A. R. Junghans, J. Benlliure, H.-G. Clerc, M. de Jong, J. Müller, M. Pfützner, B. Voss, Relativistic radioactive beams: A new access to nuclear-fission studies, Nucl. Phys. A 665 (3) (2000) 221. doi:10.1016/S0375-9474(99)00384-X.

vassh2019using [453] N. Vassh, R. Vogt, R. Surman, J. Randrup, T. M. Sprouse, M. R. Mumpower, P. Jaffke, D. Shaw, E. M. Holmbeck, Y. Zhu, G. C. McLaughlin, Using excitation-energy dependent fission yields to identify key fissioning nuclei in r-process nucleosynthesis, J. Phys. G: Nucl. Part. Phys. 46 (6) (2019) 065202. doi:10.1088/1361-6471/ab0bea.

ssh2020probing [454] N. Vassh, M. Mumpower, T. Sprouse, R. Surman, R. Vogt, Probing the fission properties of neutron-rich actinides with the astrophysical r process, EPJ Web Conf. 242 (2020) 04002. doi:10.1051/epjconf/202024204002.

t2020employing [455] R. Vogt, J. Randrup, N. Vassh, T. Sprouse, R. Surman, Employing FREYA for fission product yield evaluations, EPJ Web Conf. 242 (2020) 03002. doi:10.1051/epjconf/202024203002.

huang2021ame [456] W. J. Huang, M. Wang, F. G. Kondev, G. Audi, S. Naimi, The AME 2020 atomic mass evaluation (I). Evaluation of input data, and adjustment procedures, Chinese Phys. C 45 (3) (2021) 030002. doi:10.1088/1674-1137/abddb0.

wang2021ame [457] M. Wang, W. J. Huang, F. G. Kondev, G. Audi, S. Naimi, The AME 2020 atomic mass evaluation (II). Tables, graphs and references, Chinese Phys. C 45 (3) (2021) 030003. doi:10.1088/1674-1137/abddaf.

005proceedings [458] N. Varapai, F.-J. Hambsch, S. Oberstedt, O. Serot, G. Barreau, N. Kornilov, S. Zeinalov, Proceedings of the International Workshop on Nuclear Fission and Fission Product Spectroscopy, in: International Workshop on Nuclear Fission and Fission Product Spectroscopy, 2005, p. 369.

9timedependent [459] N. Carjan, M. Rizea, Time-dependent decay rate and angular distribution of the scission neutrons by a dynamical approach, Int. J. Mod. Phys. E 28 (11) (2019) 1950103. doi:10.1142/S0218301319501039.

[460] N. Carjan, M. Rizea, Structures in the energy distribution of the scission neutrons: Finite neutron-number effect, Phys. Rev. C 99 (3) (2019) 034613. doi:10.1103/PhysRevC.99.034613.

[461] N. Carjan, M. Rizea, Similarities between calculated scission-neutron properties and experimental data on prompt fission neutrons, Phys. Lett. B 747 (2015) 178–181. doi:10.1016/j.physletb.2015.05.050.

[462] R. Capote, N. Carjan, S. Chiba, Scission neutrons for U, Pu, Cm, and Cf isotopes: Relative multiplicities calculated in the sudden limit, Phys. Rev. C 93 (2) (2016) 024609. doi:10.1103/PhysRevC.93.024609.

[463] C. Bloch, Theory of Nuclear Level Density, Phys. Rev. 93 (5) (1954) 1094. doi:10.1103/PhysRev.93.1094.

[464] D. G. Madland, T. R. England, The Influence of Isomeric States on Independent Fission Product Yields, Nucl. Sci. Eng. 64 (4) (1977) 859. doi:10.13182/NSE77-A14501.

[465] G. F. Bertsch, T. Kawano, L. M. Robledo, Angular momentum of fission fragments, Phys. Rev. C 99 (3) (2019) 034603. doi:10.1103/PhysRevC.99.034603.

[466] R. Capote, M. Herman, P. Obložinský, P. G. Young, S. Goriely, T. Belgya, A. V. Ignatyuk, A. J. Koning, S. Hilaire, V. A. Plujko, M. Avrigeanu, O. Bersillon, M. B. Chadwick, T. Fukahori, Z. Ge, Y. Han, S. Kailas, J. Kopecky, V. M. Maslov, G. Reffo, M. Sin, E. Soukhovitskii, P. Talou, RIPL – Reference Input Parameter Library for Calculation of Nuclear Reactions and Nuclear Data Evaluations, Nucl. Data Sheets 110 (12) (2009) 3107. doi:10.1016/j.nds.2009.10.004.

[467] O. Litaize, O. Serot, Investigation of phenomenological models for the monte carlo simulation of the prompt fission neutron and γ emission, Phys. Rev. C 82 (5) (2010) 054616. doi:10.1103/PhysRevC.82.054616.

[468] P. Tamagno, O. Litaize, Impact of nuclear inertia momenta on fission observables, EPJ Web Conf. 193 (2018) 01004. doi:10.1051/epjconf/201819301004.

[469] R. Vogt, J. Randrup, Angular momentum effects in fission, Phys. Rev. C 103 (1) (2021) 014610. doi:10.1103/PhysRevC.103.014610.

[470] J. Randrup, R. Vogt, Refined treatment of angular momentum in the event-by-event fission model FREYA, Phys. Rev. C 89 (4) (2014) 044601. doi:10.1103/PhysRevC.89.044601.

[471] D. Regnier, Contribution à l'étude des gammas prompts de fission, These de doctorat (2013).

[472] A. Oberstedt, R. Billnert, A. Gatera, A. Göök, S. Oberstedt, Prompt fission gamma rays and their angular distributions, EPJ Web Conf. 193 (2018) 03005. doi:10.1051/epjconf/201819303005.

[473] R. Billnert, F.-J. Hambsch, A. Oberstedt, S. Oberstedt, New prompt spectral gamma-ray data from the reaction ^{252}Cf(sf) and its implication on present evaluated nuclear data files, Phys. Rev. C 87 (2) (2013) 024601. doi:10.1103/PhysRevC.87.024601.

ans1991nuclear [474] C. Wagemans, The Nuclear Fission Process, CRC Press, Inc, United States, 1991.

doe [475] DOE Fundamentals Handbook, Nuclear Physics and Reactor Theory.
URL https://www.standards.doe.gov/standards-documents/1000/1019-bhdbk-1993-v1

etcu2013isomer [476] I. Stetcu, P. Talou, T. Kawano, M. Jandel, Isomer production ratios and the angular momentum distribution of fission fragments, Phys. Rev. C 88 (4) (2013) 044603. doi:10.1103/PhysRevC.88.044603.

tcu2014angular [477] I. Stetcu, P. Talou, T. Kawano, M. Jandel, Angular Momentum Distribution of Fission Fragments, Nucl. Data Sheets 118 (2014) 230. doi:10.1016/j.nds.2014.04.044.

ou2016latetime [478] P. Talou, T. Kawano, I. Stetcu, J. P. Lestone, E. McKigney, M. B. Chadwick, Late-time emission of prompt fission γ rays, Phys. Rev. C 94 (6) (2016) 064613. doi:10.1103/PhysRevC.94.064613.

984statistical [479] H. A. Weidenmüller, Statistical theory of nuclear reactions and the Gaussian orthogonal ensemble, Ann. Phys. 158 (1) (1984) 120–141. doi:10.1016/0003-4916(84)90241-0.

90applicat [480] P. O. Hansen, B. Jonson, A. Richter, Applications of statistical nuclear physics to nuclear spectroscopy, Nucl. Phys. A 518 (1) (1990) 13–34. doi:10.1016/0375-9474(90)90532-Q.

gas1988aspects [481] O. Bohigas, H. A. Weidenmuller, Aspects of Chaos in Nuclear Physics, Ann. Rev. Nucl. Part. Sci. 38 (1) (1988) 421–453. doi:10.1146/annurev.ns.38.120188.002225.

56fluctuations [482] C. E. Porter, R. G. Thomas, Fluctuations of Nuclear Reaction Widths, Phys. Rev. 104 (2) (1956) 483. doi:10.1103/PhysRev.104.483.

66fluctuations [483] T. Ericson, T. Mayer-Kuckuk, Fluctuations in Nuclear Reactions, Ann. Rev. Nucl. Sci. 16 (1) (1966) 183–206. doi:10.1146/annurev.ns.16.120166.001151.

th2018measured [484] M. J. Marcath, R. C. Haight, R. Vogt, M. Devlin, P. Talou, I. Stetcu, J. Randrup, P. F. Schuster, S. D. Clarke, S. A. Pozzi, Measured and simulated ^{252}Cf prompt neutron-photon competition, Phys. Rev. C 97 (4) (2018) 044622. doi:10.1103/PhysRevC.97.044622.

2002largescale [485] S. Goriely, E. Khan, Large-scale QRPA calculation of E1-strength and its impact on the neutron capture cross section, Nucl. Phys. A 706 (1) (2002) 217. doi:10.1016/S0375-9474(02)00860-6.

004microscopic [486] S. Goriely, E. Khan, M. Samyn, Microscopic HFB + QRPA predictions of dipole strength for astrophysics applications, Nucl. Phys. A 739 (3) (2004) 331. doi:10.1016/j.nuclphysa.2004.04.105.

7quasipart [487] S. Hilaire, S. Goriely, S. Péru, F. Lechaftois, I. Deloncle, M. Martini, Quasiparticle random phase approximation predictions of the gamma-ray strength functions using the Gogny force, EPJ Web Conf. 146 (2017) 05013. doi:10.1051/epjconf/201714605013.

[488] P. Axel, Electric dipole Ground-State Transition Width Strength Function and 8-MeV Photon Interaction, Phys. Rev. 126 (1962) 671.

[489] D. Regnier, O. Litaize, O. Serot, An improved numerical method to compute neutron/gamma deexcitation cascades starting from a high spin state, Comput. Phys. Commun. 201 (2016) 19–28. doi:10.1016/j.cpc.2015.12.007.

[490] R. Vogt, J. Randrup, Improved modeling of photon observables with the event-by-event fission model FREYA, Phys. Rev. C 96 (6) (2017) 064620. doi:10.1103/PhysRevC.96.064620.

[491] I. Stetcu, P. Talou, T. Kawano, M. Jandel, Properties of prompt-fission γ rays, Phys. Rev. C 90 (2) (2014) 024617. doi:10.1103/PhysRevC.90.024617.

[492] P. Talou, T. Kawano, I. Stetcu, Prompt Fission Neutrons and γ Rays, Nucl. Data Sheets 118 (2014) 195–198. doi:10.1016/j.nds.2014.04.035.

[493] P. Talou, R. Vogt, J. Randrup, M. E. Rising, S. A. Pozzi, J. Verbeke, M. T. Andrews, S. D. Clarke, P. Jaffke, M. Jandel, T. Kawano, M. J. Marcath, K. Meierbachtol, L. Nakae, G. Rusev, A. Sood, I. Stetcu, C. Walker, Correlated prompt fission data in transport simulations, Eur. Phys. J. A 54 (1) (2018) 9. doi:10.1140/epja/i2018-12455-0.

[494] R. Capote, Y.-J. Chen, F.-J. Hambsch, N. V. Kornilov, J. P. Lestone, O. Litaize, B. Morillon, D. Neudecker, S. Oberstedt, T. Ohsawa, N. Otuka, V. G. Pronyaev, A. Saxena, O. Serot, O. A. Shcherbakov, N.-C. Shu, D. L. Smith, P. Talou, A. Trkov, A. C. Tudora, R. Vogt, A. S. Vorobyev, Prompt Fission Neutron Spectra of Actinides, Nucl. Data Sheets 131 (2016) 1. doi:10.1016/j.nds.2015.12.002.

[495] L. Thulliez, O. Litaize, O. Serot, A. Chebboubi, Neutron and γ multiplicities as a function of incident neutron energy for the ^{237}Np(n,f) reaction, Phys. Rev. C 100 (4) (2019) 044616. doi:10.1103/PhysRevC.100.044616.

[496] I. Stetcu, A. E. Lovell, P. Talou, T. Kawano, S. Marin, S. A. Pozzi, A. Bulgac, Angular Momentum Removal by Neutron and Gamma-Ray Emissions during Fission Fragment Decays, Phys. Rev. Lett. 127 (22) (2021) 222502. doi:10.1103/PhysRevLett.127.222502.

[497] S. Okumura, T. Kawano, P. Jaffke, P. Talou, S. Chiba, ^{235}U(n,f) independent fission product yield and isomeric ratio calculated with the statistical Hauser–Feshbach theory, J. Nucl. Sci. Technol. 55 (9) (2018) 1009. doi:10.1080/00223131.2018.1467288.

[498] E. Privas, L. Chabert, Reflector features and physics consideration issued from the Jules Horowitz Reactor design analyses, EPJ Nuclear Sci. Technol. 4 (2018) 18. doi:10.1051/epjn/2018040.

2020evaluation [499] I. Stetcu, M. B. Chadwick, T. Kawano, P. Talou, R. Capote, A. Trkov, Evaluation of the Prompt Fission Gamma Properties for Neutron Induced Fission of ^{235,238}U and ^{239}Pu, Nucl. Data Sheets 163 (2020) 261. doi:10.1016/j.nds.2019.12.007.

all2007nuclear [500] J. M. Hall, S. Asztalos, P. Biltoft, J. Church, M. A. Descalle, T. Luu, D. Manatt, G. Mauger, E. Norman, D. Petersen, J. Pruet, S. Prussin, D. Slaughter, The Nuclear Car Wash: Neutron interrogation of cargo containers to detect hidden SNM, Nucl. Instr. Meth. Phys. Res. B: Beam Int. Mat. Atoms 261 (1) (2007) 337–340. doi:10.1016/j.nimb.2007.04.263.

den2007portable [501] P. A. Hausladen, P. R. Bingham, J. S. Neal, J. A. Mullens, J. T. Mihalczo, Portable fast-neutron radiography with the nuclear materials identification system for fissile material transfers, Nucl. Instr. Meth. Phys. Res. B: Beam Int. Mat. Atoms 261 (1) (2007) 387–390. doi:10.1016/j.nimb.2007.04.206.

20correlations [502] A. E. Lovell, P. Talou, I. Stetcu, K. J. Kelly, Correlations between fission fragment and neutron anisotropies in neutron-induced fission, Phys. Rev. C 102 (2) (2020) 024621. doi:10.1103/PhysRevC.102.024621.

werner2018mcnp [503] C. J. Werner, J. S. Bull, C. J. Solomon, F. B. Brown, G. W. McKinney, M. E. Rising, D. A. Dixon, R. L. Martz, H. G. Hughes, L. J. Cox, A. J. Zukaitis, J. C. Armstrong, R. A. Forster, L. Casswell, MCNP Version 6.2 Release Notes, Tech. Rep. LA-UR-18-20808, Los Alamos National Lab. (LANL), Los Alamos, NM (United States) (2018). doi:10.2172/1419730.

it2016fifrelin [504] O. Petit, C. Jouanne, O. Litaize, O. Serot, A. Chebboubi, Y. Pénéliau, FIFRELIN – TRIPOLI-4® coupling for Monte Carlo simulations with a fission model. Application to shielding calculations, in: 13th International Conference on Radiation Shielding (ICRS-13) & 19th Topical Meeting of the Radiation Protection & Shielding Division of the American Nuclear Society -2016 (RPSD-2016), Vol. 153, 2016, p. 06003. doi:10.1051/epjconf/201715306003.

2018correlated [505] J. M. Verbeke, O. Petit, O. Litaize, A. Chebboubi, Correlated Production and Analog Transport of Fission Neutrons and Photons Using Fission Models FREYA, FIFRELIN, and the Monte Carlo Code TRIPOLI-4, IEEE Trans. Nucl. Sci. 65 (9) (2018) 2471–2478. doi:10.1109/TNS.2018.2825646.

nski1973prompt [506] V. V. Verbinski, H. Weber, R. E. Sund, Prompt Gamma Rays from ^{235}U(n,f), ^{239}Pu(n,f), and Spontaneous Fission of ^{252}Cf, Phys. Rev. C 7 (3) (1973) 1173. doi:10.1103/PhysRevC.7.1173.

2018dependence [507] A. Chyzh, P. Jaffke, C. Y. Wu, R. A. Henderson, P. Talou, I. Stetcu, J. Henderson, M. Q. Buckner, S. A. Sheets, R. Hughes, B. Wang, J. L. Ullmann, S. Mosby, T. A. Bredeweg, A. C. Hayes-Sterbenz, J. M. O'Donnell, Dependence of the prompt fission γ-ray spectrum on the entrance channel of compound nucleus: Spontaneous vs. neutron-induced fission, Phys. Lett. B 782 (2018) 652–656. doi:10.1016/j.physletb.2018.06.006.

kii2019effects [508] H. Makii, K. Nishio, K. Hirose, R. Orlandi, R. Léguillon, T. Ogawa, T. Soldner, U. Köster, A. Pollitt, F.-J. Hambsch, I. Tsekhanovich, M. Aïche, S. Czajkowski, L. Mathieu, C. M. Petrache, A. Astier, S. Guo, T. Ohtsuki,

S. Sekimoto, K. Takamiya, R. J. W. Frost, T. Kawano, Effects of the nuclear structure of fission fragments on the high-energy prompt fission gamma-ray spectrum in ^{235}U(n_{th},f), Phys. Rev. C 100 (4) (2019) 044610. doi:10.1103/PhysRevC.100.044610.

an2019improved [509] H. Almazán, L. Bernard, A. Blanchet, A. Bonhomme, C. Buck, A. Chebboubi, P. del Amo Sanchez, I. El Atmani, J. Haser, F. Kandzia, S. Kox, L. Labit, J. Lamblin, A. Letourneau, D. Lhuillier, M. Lindner, O. Litaize, T. Materna, A. Minotti, H. Pessard, J. S. Réal, C. Roca, T. Salagnac, V. Savu, S. Schoppmann, V. Sergeyeva, T. Soldner, A. Stutz, L. Thulliez, M. Vialat, Improved STEREO simulation with a new gamma ray spectrum of excited gadolinium isotopes using FIFRELIN, Eur. Phys. J. A 55 (10) (2019) 183. doi:10.1140/epja/i2019-12886-y.

021calibration [510] L. Thulliez, D. Lhuillier, F. Cappella, N. Casali, R. Cerulli, A. Chalil, A. Chebboubi, E. Dumonteil, A. Erhart, A. Giuliani, F. Gunsing, E. Jericha, M. Kaznacheeva, A. Kinast, A. Langenkämper, T. Lasserre, A. Letourneau, O. Litaize, P. de Marcillac, S. Marnieros, T. Materna, B. Mauri, E. Mazzucato, C. Nones, T. Ortmann, L. Pattavina, D. V. Poda, R. Rogly, N. Schermer, O. Serot, G. Soum, L. Stodolsky, R. Strauss, M. Vignati, M. Vivier, V. Wagner, A. Wex, Calibration of nuclear recoils at the 100 eV scale using neutron capture, J. Inst. 16 (07) (2021) P07032. doi:10.1088/1748-0221/16/07/P07032.

mura2019prompt [511] S. Okumura, T. Kawano, S. Chiba, Prompt and Delayed Neutron Emissions and Fission Product Yield Calculations with Hauser-Feshbach Statistical Decay Theory and Summation Calculation Method, in: O. Serot, A. Chebboubi (Eds.), 5th International Workshop on Nuclear Data Evaluation for Reactor Applications (Wonder-2018), Vol. 211, E D P Sciences, 2019, p. 04005. doi:10.1051/epjconf/201921104005.

goutte2004mass [512] H. Goutte, P. Casoli, J.-F. Berger, Mass and kinetic energy distributions of fission fragments using the time dependent generator coordinate method, Nucl. Phys. A 734 (2004) 217. doi:10.1016/j.nuclphysa.2004.01.038.

09microscopica [513] W. Younes, D. Gogny, Microscopic calculation of ^{240}Pu scission with a finite-range effective force, Phys. Rev. C 80 (5) (2009) 054313. doi:10.1103/PhysRevC.80.054313.

015description [514] N. Schunck, D. Duke, H. Carr, Description of induced nuclear fission with Skyrme energy functionals. II. Finite temperature effects, Phys. Rev. C 91 (3) (2015) 034327. doi:10.1103/PhysRevC.91.034327.

el2010particle [515] C. Simenel, Particle Transfer Reactions with the Time-Dependent Hartree-Fock Theory Using a Particle Number Projection Technique, Phys. Rev. Lett. 105 (19) (2010) 192701. doi:10.1103/PhysRevLett.105.192701.

iere2019number [516] M. Verrière, N. Schunck, T. Kawano, Number of particles in fission fragments, Phys. Rev. C 100 (2) (2019) 024612. doi:10.1103/PhysRevC.100.024612.

21improvements [517] M. Verriere, M. R. Mumpower, Improvements to the macroscopic-microscopic approach of nuclear fission, Phys. Rev. C 103 (3) (2021) 034617. doi:10.1103/PhysRevC.103.034617.

[518] C. Schmitt, P. Möller, On the isotopic composition of fission fragments, Phys. Lett. B 812 (2021) 136017. doi:10.1016/j.physletb.2020.136017.

[519] P. Möller, T. Ichikawa, A method to calculate fission-fragment yields Y(Z,N) versus proton and neutron number in the Brownian shape-motion model: Application to calculations of U and Pu charge yields, Eur. Phys. J. A 51 (12) (2015) 173. doi:10.1140/epja/i2015-15173-1.

[520] A. C. Wahl, Systematics of Fission-Product Yields, Tech. Rep. LA-13928, Los Alamos National Laboratory (2002).

[521] A. Ruben, H. Märten, Fission neutron multiplicity versus fragment mass and kinetic energy, Z. Phys. A 337 (2) (1990) 237. doi:10.1007/BF01294300.

[522] P. A. Butler, W. Nazarewicz, Intrinsic reflection asymmetry in atomic nuclei, Rev. Mod. Phys. 68 (2) (1996) 349. doi:10.1103/RevModPhys.68.349.

[523] P. Marević, N. Schunck, J. Randrup, R. Vogt, Angular momentum of fission fragments from microscopic theory, Phys. Rev. C 104 (2) (2021) L021601. doi:10.1103/PhysRevC.104.L021601.

[524] A. Bulgac, I. Abdurrahman, K. Godbey, I. Stetcu, Fragment intrinsic spins and fragments' relative orbital angular momentum in nuclear fission, Phys. Rev. Lett. 128 (2022) 022501. doi:10.1103/PhysRevLett.128.022501.

[525] J. N. Wilson, D. Thisse, M. Lebois, N. Jovančević, D. Gjestvang, R. Canavan, M. Rudigier, D. Étasse, R.-B. Gerst, L. Gaudefroy, E. Adamska, P. Adsley, A. Algora, M. Babo, K. Belvedere, J. Benito, G. Benzoni, A. Blazhev, A. Boso, S. Bottoni, M. Bunce, R. Chakma, N. Cieplicka-Oryńczak, S. Courtin, M. L. Cortés, P. Davies, C. Delafosse, M. Fallot, B. Fornal, L. Fraile, A. Gottardo, V. Guadilla, G. Häfner, K. Hauschild, M. Heine, C. Henrich, I. Homm, F. Ibrahim, Ł. W. Iskra, P. Ivanov, S. Jazrawi, A. Korgul, P. Koseoglou, T. Kröll, T. Kurtukian-Nieto, L. Le Meur, S. Leoni, J. Ljungvall, A. Lopez-Martens, R. Lozeva, I. Matea, K. Miernik, J. Nemer, S. Oberstedt, W. Paulsen, M. Piersa, Y. Popovitch, C. Porzio, L. Qi, D. Ralet, P. H. Regan, K. Rezynkina, V. Sánchez-Tembleque, S. Siem, C. Schmitt, P.-A. Söderström, C. Sürder, G. Tocabens, V. Vedia, D. Verney, N. Warr, B. Wasilewska, J. Wiederhold, M. Yavahchova, F. Zeiser, S. Ziliani, Angular momentum generation in nuclear fission, Nature 590 (7847) (2021) 566. doi:10.1038/s41586-021-03304-w.

[526] J. Randrup, R. Vogt, Generation of Fragment Angular Momentum in Fission, Phys. Rev. Lett. 127 (6) (2021) 062502. doi:10.1103/PhysRevLett.127.062502.

[527] U. Brosa, S. Grossmann, In the exit channel of nuclear fission, Z. Phys. A 310 (3) (1983) 177. doi:10.1007/BF01415223.

[528] K. Davies, Effect of viscosity on the dynamics of fission, Phys. Rev. C 13 (6) (1976) 2385. doi:10.1103/PhysRevC.13.2385.

madland1982new [529] D. G. Madland, J. R. Nix, New Calculation of Prompt Fission Neutron Spectra and Average Prompt Neutron Multiplicities, Nucl. Sci. Eng. 81 (2) (1982) 213. doi:10.13182/NSE82-5.

representation [530] Takaaki Ohsawa, Representation of fission neutron spectrum by non-equitemperature Madland-Nix model, Tech. Rep. INDC(NDS)-251, International Atomic Energy Agency (IAEA) (1991).

idt2010entropy [531] K.-H. Schmidt, B. Jurado, Entropy Driven Excitation Energy Sorting in Superfluid Fission Dynamics, Phys. Rev. Lett. 104 (21) (2010) 212501. doi:10.1103/PhysRevLett.104.212501.

hmidt2011final [532] K.-H. Schmidt, B. Jurado, Final excitation energy of fission fragments, Phys. Rev. C 83 (6) (2011) 061601(R). doi:10.1103/PhysRevC.83.061601.

ou2011advanced [533] P. Talou, B. Becker, T. Kawano, M. B. Chadwick, Y. Danon, Advanced Monte Carlo modeling of prompt fission neutrons for thermal and fast neutron-induced fission reactions on ^{239}Pu, Phys. Rev. C 83 (6) (2011) 064612. doi:10.1103/PhysRevC.83.064612.

2020excitation [534] M. Albertsson, B. G. Carlsson, T. Døssing, P. Möller, J. Randrup, S. Åberg, Excitation energy partition in fission, Phys. Lett. B 803 (2020) 135276. doi:10.1016/j.physletb.2020.135276.

021correlation [535] M. Albertsson, B. G. Carlsson, T. Døssing, P. Möller, J. Randrup, S. Åberg, Correlation studies of fission-fragment neutron multiplicities, Phys. Rev. C 103 (1) (2021) 014609. doi:10.1103/PhysRevC.103.014609.